MANEUVERING CONTROL AND CONFIGURATION ADAPTATION OF A BIOLOGICALLY INSPIRED MORPHING AIRCRAFT

By

MUJAHID ABDULRAHIM

A DISSERTATION PRESENTED TO THE GRADUATE SCHOOL
OF THE UNIVERSITY OF FLORIDA IN PARTIAL FULFILLMENT
OF THE REQUIREMENTS FOR THE DEGREE OF
DOCTOR OF PHILOSOPHY

UNIVERSITY OF FLORIDA

2007

In the Name of Allah, the Most Gracious, the Most Merciful

To those with whom I am hopelessly infatuated.

Chapter 1, Introduction, is dedicated to my parents, Arifa Garman and Abdulhamid Abdulrahim, who first to introduce me to the world of creativity by encouraging me to design, build, and explore all things mechanical.

Chapter 2, Literature Review, is dedicated to my mother, Arifa Garman, for spending untold hours teaching me how to read and appreciate a good book.

Chapter 3, Biological Inspiration, is dedicated to my wife, Tasneem Koleilat, who is as enamored with biology as I am with airplanes.

Chapter 4, Dynamics, is dedicated to my brother, Obaida Abdul-rahim, who was my first co-pilot and will always be the one I choose whenever I need a long drive.

Chapter 5, Maneuvering Control, is dedicated to my sister, Raja Abdulrahim, with whom I have many adventures in both vehicular and conversational maneuvering.

Chapter 6, Optimal Control, is also dedicated to my mother, who gently reminded me of the verse “God loves a servant, who when he performs an action, perfects it”.

ACKNOWLEDGMENTS

Thank you to my advisor, my committee, my colleagues, and my family. All have been quite supportive in ways that make me feel as though I uphold the fine values of the scientific method, even during times when the MATLAB *rand* function produces cleaner data and *Windows Paint* produces crisper images.

Thank you to Dr. David Bloomquist, for being my undergraduate honors advisor, for taking my flying all over the US in the Cessna "N337P" Skymaster, and for mentoring me on an untold number of research projects. Hopefully he will one day forgive me for crashing the Telemaster.

Thank you to Dr. Peter Ifju, who invited me to work in his research lab even before I started freshman classes. Working with Dr. Ifju on the MAV competition team and research projects was truly a delightful experience. Maybe one day our patent will be approved.

Thank you to my advisor, Dr. Rick Lind, for showing me the wonderful, yet often violently-turbulent world of flight dynamics. Under his guidance and direction, I have partly satiated my ongoing passion for conducting meaningful, significant, and delightful research. Perhaps one day I will be respected as a scientist.

A final thank you to Adam Watkins, Daniel "Tex" Grant, Joe Kehoe, and Ryan Causey for being very bemusing colleagues. It is doubtful that any of us would have survived the PhD program without our communal gum-olympics, frosty-times, and helicopter-breaks.

TABLE OF CONTENTS

LIST OF TABLES

LIST OF FIGURES

Abstract of Dissertation Presented to the Graduate School
of the University of Florida in Partial Fulfillment of the
Requirements for the Degree of Doctor of Philosophy

MANEUVERING CONTROL AND CONFIGURATION ADAPTATION OF A BIOLOGICALLY INSPIRED MORPHING AIRCRAFT

By

Mujahid Abdulrahim

August 2007

Chair: Rick Lind
Major: Aerospace Engineering

Natural flight as a source of inspiration for aircraft design was prominent with early aircraft but became marginalized as aircraft became larger and faster. With recent interest in small unmanned air vehicles, biological inspiration is a possible technology to enhance mission performance of aircraft that are dimensionally similar to gliding birds. Serial wing joints, loosely modeling the avian skeletal structure, are used in the current study to allow significant reconfiguration of the wing shape. The wings are reconfigured to optimize aerodynamic performance and maneuvering metrics related to specific mission tasks. Wing shapes for each mission are determined and related to the seagulls, falcons, albatrosses, and non-migratory African swallows on which the aircraft are based. Variable wing geometry changes the vehicle dynamics, affording versatility in flight behavior but also requiring appropriate compensation to maintain stability and controllability. Time-varying compensation is in the form of a baseline controller which adapts to both the variable vehicle dynamics and to the changing mission requirements. Wing shape is adapted in flight to minimize a cost function which represents energy, temporal, and spatial efficiency. An optimal control architecture unifies the control and adaptation tasks.

CHAPTER 1
INTRODUCTION

1.1 Motivation

Research in some areas of atmospheric sciences is facilitated by the proliferation of unmanned air vehicle (UAV) technology. UAVs are able to safely support high-risk experiments with lower costs relative to a manned flight program. Such experiments can yield highly beneficial results that support further technological advancements. The usefulness of UAVs becomes evident with a cursory survey of disparate fields in science and application. Flight dynamics and control engineers are increasingly turning toward UAVs for testing advanced system identification and control techniques that cannot be safely conducted on a manned vehicle. Wildlife biologists are using UAVs to conduct population surveys on species in remote areas where the cost, noise, and required infrastructure of manned vehicles are excessive. Non-science uses of UAVs include military reconnaissance, police crime-scene investigations, border patrol, and fire fighting.

The widespread use of UAVs underscores a fundamental limitation in the aircraft design process. The wide range of airspeeds, altitudes, and maneuverability requirements encountered in UAV missions can be beyond the design range of the UAV. The result is a flight system that performs at a lower level of maneuverability or efficiency than the operator may desire during certain portions of a mission. The design process of a UAV involves finding a fixed configuration that best compromises between the imagined mission scenarios. Such a compromised design prevents the UAV from operating under varied flight conditions with a constantly high efficiency.

Consider a UAV that is required to engage in a two-part mission consisting of a maximum-endurance persistence phase and a maximum-speed pursuit phase. An aircraft optimized for the former would achieve a high-lift to drag ratio at a specific angle of attack and may feature high-aspect ratio wings. In transitioning to the pursuit phase, the aircraft may operate at an inefficient angle of attack and be subject to undesirable drag and structural flexibility due to the wing design. Furthermore, a fixed aircraft design may be a poor

compromise between the stability and maneuverability requirements of different mission segments. Such a compromise may result in an aircraft that has diluted performance at all extremes of the flight envelope. Figure 1.1 shows a geometry comparison of two UAVs, one designed for endurance and the other for combat engagement.

Figure 1-1. Two dissimilar UAVs designed for disparate tasks, Predator variant (left) and X-45 variant (right)[18]

A possible solution to the limitations of fixed-configuration aircraft is the use of morphing to dramatically vary the vehicle shape for different mission segments. Morphing is envisioned for many types of vehicles that engage in multi-part missions. The technology is particularly attractive for UAVs because possibilities for endurance and maneuverability are greatly expanded over manned vehicles.

The appeal of morphing is that the vehicle design is adapted in flight to achieve different mission objectives. A morphing aircraft might morph into distinct shapes, where each configuration is locally optimal for a particular task of a desired mission. Additionally, shape deformations of morphing aircraft can provide high levels of maneuverability compared to conventional control surfaces.

The substantial benefits of a morphing aircraft come with considerable technological challenges. DARPA and NASA envision future aircraft as having highly reconfigurable, continuous-moldline control systems composed of hundreds or thousands of shape-affecting actuators. Actuator and structural technologies needed to achieve such a goal are still relatively immature and confined to laboratory studies. The compliant shape of a morphing airplane may result in increasingly flexible structures that are prone to

aeroelastic problems or even excessive deformation under aerodynamic loads. Morphing aircraft also pose challenges in the area of sensing and instrumentation due to the large number of sensors required and the effect of the shape change on sensitive measurements such as accelerations, angle of attack, and sideslip.

Perhaps the most under-served area of morphing technology in the literature is the area of dynamics and control. Significant contributions are made in actuators and aeroelasticity while the rigid-body motion and stabilization of morphing aircraft is largely unaddressed. Complications in the vehicle model such as time-dependent dynamics and highly nonlinear, coupled control pose considerable challenges.

Another open area of research addresses the challenge in identifying how to use the morphing effectively to satisfy or improve upon current mission profiles. The possibility of a highly reconfigurable aircraft is quite appealing and poses difficult questions related to how shape-optimization can be performed in-flight and how the vehicle can be made to autonomously morph into different shapes.

As with most other problems in aerospace, morphing developments are usually performed with respect to a specific size and weight application. For instance, a morphing actuator designed for small UAVs is unlikely to be useful for transport-category aircraft. It is with this limitation that the current work proposes to address open areas of research in the application of morphing to small UAVs or Micro Air Vehicles (MAV) that may engage in a broad range of missions.

UAVs are primarily tasked with reconnaissance missions, which require surveillance of targets of interest using a variety of sensors. Large UAVs, such as the Predator, fly for extended periods at high altitudes to provide persistent observation of a broad area[18]. The aircraft operate in far-and-away environments largely free of obstacles and traffic. The data gathered from such operations affords excellent regional awareness, but lacks local detail that may be obscured by buildings and structures.

Small UAVs are uniquely qualified to observe targets which lie within environments populated with buildings, alleys, bridges, and trees. The small size and low speed of the vehicles permits operations within an urban environment, within line-of-sight of targets underneath canopies or otherwise obscured from observation from above. The flight path for a small vehicle depends not only on the location of the target, but also on obstacles which affect visibility and trajectory permissibility. Such a path affords a perspective of the environment which enhances local awareness compared to a remote observer.

A typical mission for a small, urban reconnaissance UAV may involve such disparate segments as cruise, steep descent, obstacle avoidance, target tracking, and high-speed dash. Each phase of the mission may be performed in regions where atmospheric disturbances are very large in comparison to the flight speed, thus requiring significant control power for disturbance rejection. The mission phases are also sufficiently distinct so as to require very different vehicle geometries for successful completion. A current UAV, specifically the AeroVironment Pointer, features a long, slender wing with rudder and elevator control surfaces and no wing-borne control surfaces. Cruise, loiter, and broad surveillance missions are easily performed with such an aircraft but the fixed configuration prevents the vehicle from performing steep descents, aggressive maneuvers, and large airspeed variations. Conversely, a different vehicle designed for high-speed pursuit flight may excel at speed and maneuvering but lack the persistence necessary for loiter tasks.

Operating a UAV in urban environments depends upon the ability to safely perform the required flight path maneuvers and also on contingencies involving loss-of-control incidents. Both the maneuvering and the safety requirements promote a vehicle design which is small, lightweight, and operates at slow speeds. Acceleration forces due to intentional maneuvers or unintended collisions are small, which reduce the risk of damage in the latter case. Flight among buildings and other obstacles favors a small vehicle, which can maneuver through narrow corridors without impinging on the surroundings.

In the size and weight range of interest for small UAVs, the most prominent example of morphing is the various species of gliding birds, such as gulls, vultures, and albatrosses. Of these, the gulls arguably make the most use of wing-shape changes to effect flight path in different maneuvers. All gliding birds have been observed to vary the span, sweep, twist, gull-angle, and wing feather orientation over the course of a flight. The gull-angle appears to have a correlation with the steepness of descent, while different feather orientations likely correspond to aggressive maneuvering or soaring.

Figure 1-2. Different wing shapes used by a gliding gull through joint articulation

The motivation for using biological systems as inspiration for morphing flight vehicles lies in the similarity between the two with respect to size, weight, airspeed range, and operating environment. A Laughing Gull, for instance, has a wingspan of 1 meter, a flying mass of 322 grams, and a cruise airspeed of 13 meters per second. The gull specifications are quite similar to many small UAVs, with the possible exception of mass, which is usually higher on UAVs.

Given the similarities between birds and small UAVs, adapting ideas from biological systems for conventional flight is quite appropriate both in aerodynamic shape and mechanical structure. Significant shape changes on a UAV wing can be accomplished by simplifying the wing skeleton of a bird into a serial joint linkage mechanism. A flexible, membrane wing attached to the linkage allows the aerodynamic surface to smoothly deform into several different positions. The aerodynamic benefits of such a morphable wing are easily accomplished using simple, readily available electro-mechanical actuators. At the small scales of interest to MAVs, the strength of actuators is quite high compared

to structural stiffness or aerodynamic forces; thus, morphing can be achieved without immediate need for advanced actuation and structural technology. Although existing actuators provide a basic level of operation, improved shape-change effectors can be incorporated into the designs to enhance performance. In particular, combined structures and actuators can expand the wing configurability compared to a mechanical solution relying on hinges, bending, and twisting.

1.2 Problem Statement

The design of an aircraft capable of operating in an urban environment involves numerous challenges. The aircraft must have sufficient endurance for moderate-length missions yet must also be maneuverable to avoid collisions with obstacles and navigate through narrow corridors. The UAV is expected to follow a complex trajectory, with each segment having different requirements for endurance, maneuvering, and airspeed. The design requirements for each mission task are often conflicting which motivates the use of wing morphing to change the vehicle shape and performance in flight.

Several smaller challenges exist within the broad problem of a versatile aircraft design. The simplest question is one having morphological considerations. Into what shapes should an aircraft morph in order to achieve the range of performance required by the mission? How should biological-inspiration, taken from gliding birds, be used to influence the wing design and morphing action?

What control strategy is appropriate for an aircraft that may incur large changes in the stability and control over the range of morphing? Is there a relation between the maneuvering rates and the allowable morphing actuation speed? Can stability and controllability be guaranteed for all mission segments?

An additional problem is present in the control of the morphing configurations. How can the vehicle shape adapt efficiently to a complex, unknown trajectory? What metrics can be used in flight to estimate the optimal morphing configuration?

1.3 Dissertation Outline

I present a brief overview of the current research related to morphing aircraft design and dynamics. Discussion of biological flight studies is given to motivate the use of gliding birds as a source of inspiration for aircraft design. Simulation and wind tunnel studies of several morphing vehicles shows the significant performance benefits achievable through shape change. Robust control and adaptation literature are used to build the framework for control of a morphing aircraft.

My research discusses in greater detail the effect of wing and feather motions on the aerodynamics of gliding birds. Disparate wing shapes are compared to observed flight paths to hypothesize the function of each type of morphing. The musculo-skeletal structure of birds is then compared to mechanical components to show how biologically inspired morphing can be implemented on a flight vehicle.

The mission profile is segmented into individual maneuvers. The aerodynamic and dynamic characteristics needed for each maneuver are given. These characteristics provide the metrics for which the vehicle shape may be optimized. The equations of motions are derived for a morphing aircraft, including nonlinear and coupled terms that may become important for certain morphing configurations.

I use a robust-control framework to develop a time-varying controller that is able to compensate for the changing dynamics of the aircraft. Output and actuation weighting are used to specify a desired level of performance for each morphing condition. The different conditions are then linearly interpolated using methods based on linear parameter varying theory. Desired performance is specified by a mission-specific reference model. An adaptive architecture responds to errors in the tracking performance of the aircraft relative to the reference model and adapts controller gains.

I discuss application of optimal control theory to morphing aircraft control and adaptation problem. An indirect method is used initially to demonstrate the effect of morphing parametric dependence on the optimality of trajectory and aircraft shape

solutions. A direct, numerical method demonstrates solutions for the rate trajectory, configuration adaptation, and maneuvering control of the vehicle.

1.4 Contributions

1. Increase maneuverability and endurance for a morphing MAV
2. Identify a desired mission profile to expand range of functionality by using morphing
3. Identify requirements of mission segments on aircraft dynamics and performance
4. Develop morphing micro air vehicle with biologically inspired morphing wings
5. Parameterize flight dynamics with respect to wing morphology
6. Develop closed-loop performance requirements over parameter space
7. Develop design point criteria for linear parameter varying framework
8. Maneuver aircraft using hybrid robust/optimal baseline adaptive controller
9. Develop adaptation algorithm for automatic control of morphing
10. Apply optimal control to rate command, shape adaptation, and maneuvering

CHAPTER 2
LITERATURE REVIEW

The first national programs designed to advance technologies to facilitate morphing aircraft were the AFRL Adaptive Flexible Wing and NASA Aircraft Morphing Programs. In the 1998 NASA paper[95], Wlezien et.al, described programmatic goals related to the use of "smart materials and actuators to improve efficiency, reduce noise, and decrease weight on a conventionally flown aircraft". The scope of the morphing is relatively conservative, considering that the authors primarily intend to apply the technology to a limited class of air vehicles to achieve modest improvements in performance. The paper presents an overview of the disparate technologies needed to implement morphing, including unconventional materials, optimal aerodynamic analysis, aeroelastic modeling, time-varying dynamic modeling, and learning control systems. The authors propose the use of adaptive-predictive controllers that are able to "learn the system dynamics on-line and accommodate changes in the system dynamics".

The NASA morphing initiative has since produced a number of excellent studies[22][95][79] on the aerodynamics and aeroelasticity of configuration morphing but has had a relatively small contribution to understanding the dynamics and control of morphing vehicles. Additionally, none of the concepts presented has matured to point of flight testing on a manned or unmanned air vehicle. The program, although limited, has successfully motivated subsequent progress by many researchers, perhaps including the DARPA Morphing Aircraft Structures program. A paper by Padula summarizes some of the developments after several years of work on the NASA morphing program[67]. The main contributions are cited as multidisciplinary design optimization of the vehicle configuration and advanced flow control. A novel aircraft control system is designed by using distributed shape change devices to achieve maneuvering control for a tailless vehicle.

A more recent DARPA initiative seeks to develop and field morphing technology to enable a broader range of functionality than that envisioned by the NASA program. In particular, the DARPA Morphing Aircraft Structures has specified a goal of morphing

the aircraft geometry such as wingspan, chord, twist, sweep, and planform shape by as much as 50% of the nominal dimension. The gross variations in shape are envisioned for morphing the aircraft between two flight conditions with different airframe geometry requirements. In particular, a wing may morph from a long, slender configuration for cruise to a short, low-aspect ratio planform for high-speed flight. The transition of a wing from the high-aspect ratio, high wing area to a much smaller wing presents considerable structural challenges.

The DARPA morphing program has established goals to bring various shape-change strategies to flight maturity. In particular, three aerospace companies are each pursuing a form of wing morphing that varies a particular aspect of the geometry. The shape-changing mechanism are each based on biological systems or design parameters that afford freedom to change flight condition.

Lockheed Martin is developing a morphing unmanned air vehicle that uses a set of chordwise hinges to extend and retract the wing into a cruise and dash configuration, respectively. The morphing causing significant variations in the wingspan, aspect ratio, wing planform, wing position, and roll control effectiveness. The hinge mechanism opens new challenges in design, as the engineers try to find ways to articulate the joint without opening gaps in the wing surface and causing excessive drag [58].

NextGen Aeronautics is working on a similarly inspired concept of sliding skins to allow the wing to smoothly change in area[46]. The skins appear loosely based on bird feathers, where changing the overlap of adjacent feathers can be used to increase or decrease the wing surface area. For both birds and conventional aircraft, the ability to change wing area affords freedom to optimize aircraft lift-to-drag ratio for different flight conditions. The NextGen concept is able to address some of the concerns raised in the Lockheed design; namely, the sliding skins are able to preserve aerodynamic shape between morphing conditions. Furthermore, the concept is amenable to many possibilities for underlying structure and actuator combinations.

A special case of sliding skin morphing is under consideration by Raytheon, who is developing telescoping wings to vary wing span and aspect ratio. The possible uses of the Raytheon morphing strategy are very similar to the other two DARPA initiatives, where the aircraft transitions from a high-endurance to a high-speed configuration. The telescoping wings are relatively simple compared to some other morphing ideas, but offer benefits across a wide range of operating conditions. Perhaps most notable for civilian aircraft, telescoping wings allow for large wingspans to reduce stall speed and assist pilots in making safe landings. The beneficial characteristics on landing do not hamper cruise operation, where the wing can be retracted to allow for a high cruise airspeed.

The DARPA initiative in general has been an important development in morphing aircraft research. However, because much of the work is conducted in proprietary settings, some of the results are not available to the research community. The programs have proposed to solve many of the challenges facing morphing aircraft development, although promise of a flight demonstration has thus far not been fulfilled.

Morphing represents a dramatic change in design philosophy relative to recent aircraft. The seamless shape changing envisioned for morphing aircraft is in direct contradiction to the stiff, nominally rigid structures found on most modern aircraft. The compromise between flexibility required for shape change and stiffness required for aerodynamic load bearing represents one of the major challenges and perhaps limitations of morphing aircraft. Love et. al [57] of Lockheed have studied the effect of the DARPA-funded folding wing morphing on the ability to withstand loads from different maneuvers. The authors found that the the structural properties vary quite significantly between morphing conditions. They have proposed metrics by which the structures of such vehicles can be assessed in terms of airspeed, maneuvering, and actuator response.

Aircraft morphing presents challenges not only in technological hurdles, but also in accurately representing the result of the shape-change in a design, control, or structural sense. The challenge is illustrated by considering the difference between a conventionally

hinged wing and a freely deformable wing. The geometry of the former can be quite accurately represented by several fixed geometries that are rotated or translated relative to each other. Fowler flaps, for instance, rotate about a hinge point that itself moves aft. Conversely, a morphing wing may have a large number of actuators that allow deformations in span, chord, twist, and camber, where each type of deformation may be non-uniform over the wing. Even in the case of a single actuator that twists a part of the wing, describing such a geometry using conventional means is inadequate. The distribution of twist from the actuation point to the rest of the wing may be represented by a linear distance relationship or may be a complex function of the structure. In either case, accurate representation of the wing geometry requires more than one or two measurements.

Samareh (2000) [79] has proposed a method by which morphing geometries can be represented using techniques from computer graphics. Soft-object animation algorithms are used to parametrically represent the shape perturbation, as opposed to the geometry directly. The framework supports parametric variations in planform, twist, dihedral, thickness, camber, and free-form surfaces. Such a description may be useful in conjunction with conventional metrics to describe morphing wings that are combinations of surface deformations and hinged movements. The biological equivalent is that of a bird wing, which articulates at shoulder, elbow, and wrist joints but also undergoes motion in the muscles, skin, and feathers.

The technique proposed by Samareh can be used to compute grids for both computational fluid dynamics and finite element method codes, each having both high and low fidelity variations. The applicability to both aerodynamic and structural disciplines allows the morphing wing to be studied in a broad sense. Characteristics in other areas, such as control effectiveness, varying dynamics, aerodynamics, and aeroelasticity, can be determined as a direct outcome of the method.

Beyond the national programs, research in morphing is quite diverse in both subject and scope. Individual contributions are usually related to a specific application or discipline, which serve as advancements in the general field of morphing aircraft technology. The innovation in literature is quite impressive. Gano and Renaud [30] in 2002 presented a concept for slowly morphing the airfoil shape of wings over the course of a flight using variable-volume fuel bladders. The proposed morphing has been shown to result in improved range and endurance. The use of passive fuel depletion to change the airfoil from a high-lift to a low-drag configuration illustrates how morphing mechanisms can use innovative effectors to achieve the desired shape change. The paper stresses the importance of advanced optimization techniques to ensure the desired lift-to-drag optimization holds in the presence of uncertainty.

Sanders et. al. [82] have shown through simulation possible benefits of camber or control surface morphing. The 2003 study in the *Journal of Aircraft* showed conformal control surfaces, essentially flaps with no hingeline, are able to achieve a higher lifting force at a lower dynamic pressure than conventional control surfaces. Such results are encouraging for applications to UAVs, where high-lift and large roll control power are desired at relatively low dynamic pressures. The conformal control surfaces are shown to produce a higher maximum roll rate at certain dynamic pressures.

The benefits of such an approach are perhaps mitigated by the increase in nose-down pitching moment occurring with conformal control surfaces. The larger moment produces undesired aeroelastic effects at high dynamic pressures, leading to excessive structural twisting and eventually aileron reversal as dynamic pressure is increased. This limitation is not significant compared to the benefits for slow UAVs, provided that the wing is sufficiently stiff in torsion.

Bae et. al presented a variable-span concept [8] for a cruise missile in order to reduce drag over the airspeed envelope and increase range and endurance. The authors consider both aerodynamic and aeroelastic effects associated with a sliding-wing. In

particular, they showed a decrease in total drag with the wings extended for certain flight condition. As with Sanders work, Bae showed some undesirable aeroelastic characteristics associated with the span morphing. At high dynamic pressures, the wing tip of the extended configuration incurs large static aeroelastic divergence as a result of the increased wing root bending moment.

The variable-span wing has been shown in simulation to have control over the spanwise lift distribution. If combined with a seamless trailing edge effector, such as the model proposed in Ref. [82], the morphing wing would possess a large degree of control over the lift distribution and would be able to achieve the aerodynamic, stability, and stall-progression benefits of a variety of wing planform. Combined morphing mechanisms are somewhat rare in the literature, considering the immaturity of actuators and materials that are able to achieve complex shape changes.

Wind tunnels tests of a morphing aircraft with three degrees of freedom showed significant aerodynamic benefit from span, sweep, and twist morphing [63]. The vehicle uses a telescoping wing to achieve wing span variations of 44%, allowing for increases in lift coefficient relative to the nominal condition. Hinges at the wing root allow the sweep angle to range from 0° to 40° aft, delaying stall and improving pitch stability. The authors have shown that the wing sweep causes a change in both center of gravity position and aerodynamic center position. The aerodynamic center on the wind tunnel vehicle moves aft farther than the center of gravity, thus increasing the magnitude of the longitudinal static margin.

One benefit of the shape-adaptive aircraft is said to be in drag reduction, where three distinct combinations of wingspan and sweep are required to achieve the minimum drag over the full range of lift coefficients. The result is important for mission considerations, where maneuverability and airspeed requirements may change considerably. The paper suggests that a morphing vehicle is appropriate for reducing drag during several portions of a mission.

Valasek et. al published a series of studies on morphing adaptation and trajectory following for an abstracted system[90][85][24]. A variable-geometry vehicle is represented by a blimp-like shape which has various performance capabilities related to the shape. The approach uses reinforcement learning to control the shape adaptation as the vehicle moves through the environment. The vehicle morphs to optimally follow a defined trajectory. Adaptive dynamic inversion is used to control the vehicle and follow trajectory commands. Although the study is physically unrelated to an aircraft, the authors present a unique approach for coupling trajectory requirements and vehicle performance capability. The automatic control of the shape for different environments represents a capability highly sought for a morphing air vehicle.

Optimality in morphing is addressed by Rusnell, who together with colleagues, published studies on the use of a buckle-wing concept to achieve enhanced performance in both cruise and maneuvering flight tasks[76][77]. The morphing aircraft in the study uses a biplane configuration where the top wing conforms to the lower wing to form a single wing in some configurations, and buckles to form a joined-wing biplane in others. Analysis of the Pareto curve is used to compare the optimal configurations of the morphing wing against a conventional wing for the different missions. Vortex-lattice method is used to compute airfoil and planform aerodynamics of the simulated aircraft. The authors suggest that the buckle wing morphing can enhance mission performance relative to an aircraft with fixed configuration.

Boothe et. al[11][12] proposed an approach for disturbance rejection control on a morphing aircraft. Linear input-varying formulation is used to allow the controller to account for the dynamic variations of the morphing, which itself is the control input. The simulated examples include several types of variable wing geometries, including span, chord, and camber varying. Stability lemmas and associated closed-loop simulation responses show that the morphing can be used in some instances to adequately reject

disturbances, although transient effects from the morphing action cause performance limitations.

Bowman[13] studied the mission suitability of morphing and adaptive systems compared to conventional technology. The systems are evaluated on the basis of flight metrics describing the aircraft efficiency and maneuverability in conjunction with logistical issues such as cost, production, and maintenance. Performance for adaptive and conventional vehicles are considered in a multi-role mission scenario, requiring pursuit and engagement tasks. Bowman suggests that the performance of morphing systems is worse than existing capability, except when considering multifunctional structures and decreased dependence on support vehicle, in which case the adaptive systems offer substantial improvement. The cost associated with developing the adaptive vehicle causes poor affordability in general, but the reduced life cycle cost result in long-term gains. The study offers intriguing insight into the ultimate usefulness of a morphing vehicle in the context of a realistic, multi-task mission.

Maneuvers for a morphing aircraft can be computed using optimal control techniques. Trajectories generated for each mission task depend intrinsically on the variable dynamics. Studies relating fighter aircraft agility to allowable flight paths provide a useful architecture on which to develop morphing control techniques[78]. Direct numerical optimization[49][41] can simultaneously optimize the aircraft shape and the trajectory to successfully complete the mission requirements. Aircraft agility and maneuverability for each morphing configuration can be assessed using standard performance metrics[93][61]. These metrics are used within the optimal control framework to morph the aircraft favorably for each task.

The aerodynamic benefits of morphing are usually cited in studies as the leading impetus for shape adaptation, although researchers are also considering morphing for a reduction in actuator energy costs. Johnston et. al have developed a model through which the energy requirements for flight control of a distributed actuation system can be

compared to conventional control surfaces[45]. Their study uses vortex-lattice method and beam theory to analyze the energy required to deform the wing and produce a sufficiently large aerodynamic force. Distributed actuators are shown to have potential improvements in energy requirements by morphing the wing section rather than deflecting a trailing edge flap.

Biological inspiration as a technology for a multi-role aircraft is discussed by Bowman[14] and his co-authors. The varied wing shapes of the bald eagle during soaring, cruising, and steep approach to landing are considered as the basis for aerodynamic evaluation of morphing. Geometric parameters such as planform and airfoil are said to be particularly important for varying the lift and drag characteristics. The variable performance capability of the aircraft is contextualized in an example mission, which describes the role of morphing in the conceptual aircraft design.

Livne recently published survey papers on the state of flexibility, both active and passive, in aircraft design[55][56]. The aeroelastic and aeroservoelastic behavior of conventional and morphing airplanes are described both in terms of design challenges and potential for performance improvement. Livne describes the relation of biological observation to the design of micro air vehicles, in that such small aircraft commonly use flexible and flapping wings in order to achieve flight. Morphing for large aircraft is also discussed, including variable wing sweep on the F-14 and F-111 and the variable wing tip droop of the XB-70. The author contends that a reconfigurable morphing UAV can operate efficiently in a diverse set of operating environments.

A study by Cabell [15] describes applications of morphing to an aircraft subsystem for noise reduction. A variable geometry chevron is used for noise abatement in the nozzle of a turbofan engine. The authors describe both open-loop and closed-loop techniques to adapt the chevron shape to achieve the desired reduction in noise without excessive thrust reduction for a variety of conditions. Shape memory alloy actuators are used to generate a smooth, seamless actuation of the chevron structure.

Morphing is used in place of conventional control surfaces for a wing which is inflated and rigidized, and thus cannot sustain a conventional hingejoint [16] [17]. Differential wing twisting of the inflated wing is used to provide roll control for maneuvering. The authors of the study considered several actuation methods, along with the cost and performance associated with each. Morphing is successfully implemented as a control solution to a wing which has desirable packaging and deployment properties.

Cesnik et. al have developed a framework for assessing the capabilities of a morphing aircraft performing a specified mission[19]. The authors describe the desired mission scenario and identify the necessary vehicle performance for success. The technology required to achieve the morphing is also considered. The evaluation is used to formulate the critical component needs for a morphing aircraft. Scoring metrics for various mission segments are aggregated to determine the relative improvement in performance.

Researchers at Purdue have been studying morphing as fundamental aircraft design element for multi-role missions[74][27] [28][69][75]. Their approach considers morphing as an independent design variable and determine the contexts in which various forms of shape change can be used advantageously. The studies consider both a single vehicle performing disparate flight tasks and a fleet of vehicles operating cooperatively. Critical need technology areas are identified by identifying applications for specific types of morphing. Actuation and structural devices needed to enable the morphing are readily identified from the analysis.

Morphing the wings of an aircraft in twist is under study for use as both a control effector and as a method to increase efficiency. A West Virginia University study is considering applications of wing twist to a swept-wing tailless aircraft, which is itself inspired by natural flight[39]. The conventional control mechanisms used on such a vehicle compromise the beneficial aerodynamics of the wing configuration. A twist mechanism has been shown to have sufficient control power while improving lift-to-drag ratio by 15% and decreasing drag by up ot 28% relative to conventional hinged surfaces. The significant

gains are achieved by adapting the quasi-static wing twist distribution according to the required flight condition.

Stanford conducted a similar study using a twist actuator to deform a flexible membrane wing for roll control[84]. Multi-objective optimality is addressed by finding the torque-rod configuration which simultaneously achieves the highest roll rate and the highest lift-to-drag ratio during a roll maneuver. A Pareto front describes the configurations which achieve various combinations of lift and roll optimality. The curve is compared to the configuration on the experimental flight test vehicle, which can achieve performance improvements through modification of the actuator.

A wind tunnel investigation has demonstrated the performance and dynamic effects achieved by quasi-static variations of the wing aspect ratio and wing span[42]. An experimental model uses telescoping wing segments to morph between retracted and extended configurations. The variable wing area allows large changes in the lift and drag magnitude, but also has large affects on the roll, pitch, and yaw dynamics. Open-loop dynamics are shown to vary considerably with symmetric wing extentions. Each of the roll, dutch roll, and spiral poles show tend toward more rapid responses as the span is increased. The authors depict a highly unstable spiral mode and are investigating differential span extensions as a means of stabilizing and controlling the divergent behavior. An additional study by the authors presents the coupled, time-varying aircraft equations of motion and explores the use of asymmetric span morphing for roll control[43].

Researchers from Georgia Tech are exploring configuration optimization for a vehicle that must perform the disparate tasks of subsonic loiter and supersonic cruise[66]. The novel aircraft configuration requires the use of response surface methodology and several stages of analysis to estimate the performance of various shapes in the design space. Aerodynamic characteristics are optimized for each mission by parameterizing the design elements and finding the set of shapes that achieves the optimal compromise between the two mission modes.

A new concept for aircraft morphing structure is proposed by researchers at Pennsylvania State University, who are studying an aircraft structure composed of compliant, cellular trusses[72]. The structure is actuated by tendons joining various points of the trusses and can achieve many types of aircraft shapes through continuous deformation. Many tendons, distributed throughout the trusses are used to generate global shape variations through aggregation of local actuation. Actuation of the wing can be achieved using relatively low forces. The weight of a proposed morphing truss wing is similar to a conventional wing, except that aeroelastic concerns may require the use of active control of the tendons.

CHAPTER 3
BIOLOGICAL INSPIRATION

3.1 Motivation

Autonomous control of air vehicles is typically performed using very benign maneuvers. Limited operating range of fixed-wing aircraft and the simple control algorithms used preclude significant variations in flight condition. Maneuvering is thus limited to small perturbations around level, cruise flight, which may involve shallow-bank turns and gradual changes in altitude. A notable exception to the maneuverability restriction is an autonomous, aerobatic helicopter in development at MIT [23], [70], [31],[32].

For fixed-wing unmanned flight, the difficulty of a broad flight envelope lies in the limitation of a static geometry in providing efficient flight over a range of airspeeds and angles of attack. Such a range is desired for an aircraft expected to operate in an urban environment. Specifically, the vehicle must maneuver safely in a complex, 3D environment where obstacles are not always known *a priori*. Rapid changes in direction require large aerodynamic forces which are generated at high slip angles and high dynamic pressures.

The motivation for studying bird physiology for insight into the design of a highly maneuverable air vehicle stems from observations of gliding birds. Rapid accelerations and flight path variations are achieved through articulation of the wing structure to promote favorable aerodynamic or stability properties. Birds in general, and laughing gulls in particular, have been observed using different wing configurations for disparate phases of flight. Windhovering, soaring, and steep descents, for instance, each require a specific trim airspeed, glide ratio, and maneuverability afforded by a different wing configuration. The present work seeks to identify the dominant wing shapes that are portable to a conventional aircraft philosophy for the purpose of expanding the achievable range of flight.

Birds are used as a source of design inspiration for urban-flight vehicles because of strong similarities in dimension and operating condition. They already achieve a remarkable range of maneuvers along complex trajectories in urban environments. The

size, weight, and airspeed of a large bird closely resemble the specifications of a small UAV. Highly dynamic geometries allow birds to continually reconfigure their aerodynamic shape in response to changing flight condition. A small UAV could mimic some of the shape-changes and exploit similar structural features as birds to expand the conventional flight envelope. The design challenge is finding the morphological operations which improve the vehicle aerodynamics, rather than those intended for physiological or flapping purposes.

3.2 Observations of Bird Flight

Gliding birds are able to achieve a wide range of maneuvers and flight paths, presumably resulting from aerodynamic effects of the wing, tail, and body shape changes. Observations of gliding flight are made to help understand the motivation for each wing shape incurred during flight. The bird species of interest is the laughing gull, *Larus atricilla*, because of the similarities in size, weight, and airspeed to small unmanned air vehicles. Perhaps most importantly, gulls spend a considerable duration of each flight in various gliding maneuvers.

Gliding birds use fore-aft wing morphing to control glide speed[88], longitudinal pitch stability[63] and lateral yaw stiffness[80]. Figure 1.1 shows three planform variations of a gliding gull, where each of the shoulder, elbow, and wrist joints are modified to change the overall wing shapes. The planforms differ markedly in wing area, span, and sweep, yet are accomplished relatively easily through skeletal joints and overlapping feathers.

Figure 3-1 shows results from Tucker establishing a relation between planform shape and gliding speed for similar glide angles[88]. A significant reduction in wing span and wing area is achieved by articulating the elbow and wrist joints such that the inboard wing is swept forward and the outboard wing is swept aft. The aft rotation of the outboard or hand wing is such that the aerodynamic center typically moves aft, increasing the pitch stiffness for operation at higher airspeed.

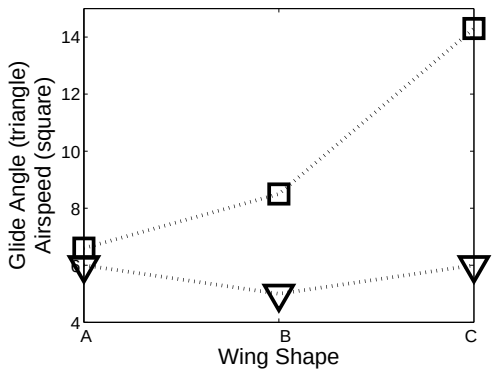

Figure 3-1. Effect of planform shape on gliding speed. See Tucker, 1970 for wing shapes A,B, and C[88]

Yaw stiffness can be achieved in bird wings with aft sweep of the outboard wings. Sachs [80] showed the magnitude of the lateral stiffness, C_{n_β}, increases with aft sweep angle and is sufficiently high such that birds do not require vertical stabilizers. Figure 3-2 shows a bird with aft wing sweep and positive yaw stability[81], which is compared by Sachs to an aircraft with similar characteristics. The aft sweep of the outboard wings has already been shown to increase pitch stability. The simultaneous increase in yaw stability allows the bird to glide at rapid speeds while maintaining a desired flight path.

Figure 3-2. Increasing yaw stiffness through outboard wing sweep

Figure 3-3 shows two gulls using different wing joint angles to deform their wings during gliding flight. The purpose of this motion has been the subject of some speculation in the literature, with some researchers arguing the benefits are predominantly aerodynamic while others cite stability improvements. In the case of the upper photograph, the bird uses outboard wings tips angled downward. The configuration has been shown to yield significant gains in L/D[22], perhaps at the expense of adverse lateral stability[87]. The lower photograph shows a bird with an 'M' wing shape when viewed from the front. The shape has been observed in use in gliding birds to vary the glide angle. A wide M-shape is used in situations requiring a shallow glide path and a correspondingly large L/D ratio. Conversely, birds in steep descents often use a narrow M-shape, presumably to reduce L/D ratio and maintain stability at the high angles of attack incurred during slow descent.

Figure 3-3. Gliding birds articulating wing joints about longitudinal axes

Figure 3-4 shows two gulls using complex morphing of the shoulder, elbow, and wrist joints about both longitudinal and vertical axes. The aerodynamics during such motion likely involve stability and performance elements from each of the individual motions. More complex flow interactions may also yield improvements in lift through leading edge vortices, as suggested by Videler[91].

Figure 3-4. Complex wing morphing shapes achieved in gliding flight

Most morphological operations are conducted symmetrically about the body, such that left and right wings generate similar aerodynamic forces. Asymmetric motions are used in certain instances of gliding flight, presumably to generate favorable moments for maneuvering, reject disturbances, or allow the bird to trim at large angles of sideslip. Figure 3-5 shows two birds using asymmetric wingspan, wing area, dihedral angle, and sweep. The upper photograph shows different articulations of the wrist joint cause the outboard wings to extend and sweep to different extents. The lower photograph shows the wrist joints of another bird at different outboard dihedral angles and extension. The configurations may be well suited for crosswind operations, considering the spanwise lift distribution and aerodynamic coupling (C_{l_β}, for instance) can be selectively varied.

Gliding birds are capable of rapid changes in flight path using aggressive maneuvers. Figure 3-6 shows two gulls near bank angles of 90° performing pull-up maneuvers to rapidly change directions in small radius turns. Both birds have deployed the tail feathers,

Figure 3-5. Gulls using asymmetric wing morphing about vertical (top) and longitudinal (bottom) axes

presumably for increased pitching moment. The left photograph shows a bird in a descending, helical path at relatively high airspeed. The orientation of the head shows that the bank angle is quite large. Aft sweep of the hand wings is likely used to maintain pitch stability at the high airspeed. The bird shown in the right photograph is performing a similar maneuver, except at a lower airspeed. Both the tail and wing feathers are deployed further than the left bird, perhaps to compensate for the reduced dynamic pressure with increased surface area. The wings are also swept forward slightly, reducing the pitch stability and possibly allowing the bird to perform an aggressive turn.

3.3 Desired Maneuvers

Several types of maneuvers are identified for a prospective urban-flight vehicle. The maneuvers are designed to allow realistic operations from deployment to recovery, with interim missions of target tracking, obstacle avoidance, maneuvering, and loitering. Each flight condition can be expressed in terms of performance metrics and modeled by an equivalent maneuver.

Figure 3-6. Rapid variations in flight path using aggressive maneuvering

3.3.1 Efficient Cruise

Cruise requirement in general favors the efficiency of the wing in terms of lift to drag, the maximum of which occurs at a specific angle of attack for a given configuration. The cruise segment requires a vehicle configuration which achieves that maximum lift to drag ratio to minimize energy expenditure from the propulsion system. Factors affecting the efficiency may include actuator requirements for active stabilization and propulsive efficiency at various airspeeds. However, airspeed and stability considerations are secondary considerations to flight efficiency. Cruise flight is anticipated for local or long-distance flights where time enroute is not an overriding concern.

3.3.2 Minimum Sink Soaring

A soaring configuration is necessary to achieve the minimum altitude-loss rate in gliding flight. Vehicles may benefit from rising air currents as a mechanism to aid in staying aloft. The minimum sink rate of an aircraft determines the minimum vertical wind needed to maintain altitude in gliding flight. Under powered conditions, smaller thrust forces can be used compared to higher sink rate conditions.

In determining the minimum sink configuration and flight condition, the airspeed and efficiency are left as variable parameters. For autonomous flight, the usefulness of such a configuration depends partly on known areas of vertical currents. Otherwise, the configuration may be used to maximize glide duration.

3.3.3 Direction Reversal

The constraints of flight in an urban environment may require direction reversal maneuvers. Such maneuvers may be necessary to maintain flight in the presence of obstacles such as alley-ways, walls, and buildings were conventional maneuvers would result in a collision. A dead-end alley between two buildings, for instance, may require a maneuver similar to an immelman-turn or split-s, depending upon the availability of space above and below the vehicle, respectively. A configuration is needed to generate large aerodynamic forces necessary to achieve the linear and angular accelerations in the maneuvers.

3.3.4 Minimum Radius Turn

A sustained, minimum radius turn configuration is useful for loitering or as an alternative to the direction reversal maneuver. The maneuver must produce a ground-track small enough to orbit continuously over a road or small target, but must also afford sufficient controllability to recover to level flight quickly and on any heading.

3.3.5 Steepest Descent

A variation on the minimum sink configuration adds additional constraints on the desired flight path to achieve a steep descent at a slow airspeed or rate of descent. The maneuver is desired for descending between tall obstacles where horizontal area is limited. Such a maneuver is useful for terminal landing, but is also important for transient maneuvers. In the latter case, it is necessary that the aircraft have sufficient control power to quickly recover to level flight.

3.3.6 Maximum Speed Dash

A final configuration is necessary to allow the vehicle to dash at maximum airspeed between waypoints. Maneuverability and energy consumption are secondary considerations to the achievable speed. A low-drag configuration is thus necessary to offset drag increase with dynamic pressure.

3.4 Morphing Degrees of Freedom

A morphing wing model is proposed based on the gross kinematics of a gull wing. The model is not intended to emulate the function of feathers or flapping, but rather seeks to identify the quasi-static wing geometry variation that contribute to the maneuverability and aerodynamic performance of the aircraft. Dimensional parameters are fully represented in the model, although not all are considered to be actively variable in flight.

The configurability of bird wings is achieved using nominally rigid bone sections connected with flexible joints. Muscles in the wing articulate the joint angles through tendons connecting contracting muscles with bones. The rotation of the joints moves the relative position of the bones and changes the gross geometry of the wing.

The bones, joints, and muscles of a bird wing can be roughly emulated using spars, hinges, and actuators in a morphing wing. Obviously the elegance of the bird movement is lost in the mechanical system, but the overall shape change is readily achieved. The biologically inspired mechanical wing uses two primary joint locations, a shoulder and an elbow, omitting the wrist articulation from bird wings.

Shoulder joint articulation is achieved on the roll and yaw axes, with respect to the body-axis conventions. The roll movement allows the wing dihedral angle to change, raising and lowering the vertical position of the outer wing. The wing on the inboard section is at a fixed incidence, although the wing surface is taken to be flexible and free to deform due to airloads.

Elbow joint articulation is similarly achieved although adds a degree of freedom in pitch to allow variations in incidence angle. The shoulder and joint articulations are both

assumed to be measured with respect to a lateral-axis fixed to the aircraft body. Thus, for a deflected inboard wing, the outboard wing is assumed to remain in a fixed orientation but translated due to the link geometry.

The respective spans of the inboard and outboard sections are considered variable in the analysis to examine different effects of relative length differences. For flight however, each link length is assumed to be fixed due to the mechanical complexity of span morphing. Additionally, there is little biological precedence, at least in gliding birds, for variable bone length.

3.5 Morphing Motions

The structure of bird wings allows a large range of motions combining rotations about the different joints. The freedom of motion is quite large, although birds typically use a subset of joint movements that yield to favorable aerodynamic characteristics. The combined joint motions are composed of simultaneous actuation of individual joints, which together produce a desirable effect. The coupled motion of the elbow and wrist joints is described by Videler [91] as the result of parallel arm bones interacting during wing extension.

Birds engage in several types of combined motions, with each having an apparent benefit in flight. Some of the dominant functions are described and related to conventional flight. The motions are, in general, easily reproduced using a mechanized aircraft wing.

3.5.1 Fore-Aft Sweep of Inboard Wings

The sweep angle of the inboard wing has the primary effect of changing the aerodynamic center position relative to the aircraft body. The center of gravity also changes due to the moving wing mass, although this change is expected to be relatively small due to light wing structures. The change in aerodynamic center position is due to both the forward rotation of the inner wing and the forward translation of the outer wing, which is connected at the mid-wing joint.

The movement of both the aerodynamic and mass centers has an important implication to the longitudinal stability of the aircraft. A conventionally configured aircraft with a stabilizing horizontal tail requires a center of gravity position ahead of the aerodynamic center for stability. The degree of stability is expressed by the static margin, which normalizes the difference in mass and aerodynamic center positions by the reference chord length.

$$static\ margin = \frac{x_{np}}{\bar{c}} - \frac{x_{ac}}{\bar{c}} \tag{3–1}$$

The fore-aft motion of the inboard wing thus affects longitudinal stability by changing the relative positions of the mass and aerodynamic centers. Assuming the mass of the fuselage is much larger than the mass of the wings, the effect will tend towards instability as the wings are swept forward and increased stability as the wings are swept aft. The inboard wing sweep can thus be used to command a desired level of performance, where a forward sweep results in increased maneuverability relative to a more stable aft sweep.

Sweep of the inboard wing also affects the angle of intersection between the wing surface and the fuselage. The effects of such a junction in interference drag are neglected due to the complexity of simulation or measurement.

3.5.2 Fore-Aft Sweep of Outboard Wings

The outboard wing is capable of a range of motion similar to that of the inboard wing. The longitudinal sweeping motion about a vertical joint axis is assumed to be coupled passively to the inboard wing using parallel linkages. Sweep of the inboard wing produces an equal and opposite sweep of the outboard wing, resulting in no net rotation for the latter relative to the fuselage. Outboard wing sweep is accomplished by actively varying the length of the trailing parallel linkage.

The sweep of the outboard wing plays a role similar to the inboard wing in affecting the positions of the mass and aerodynamic centers, although to a lesser degree. Additionally, the outboard wing sweep angle has a substantial affect on both the dynamics and

aerodynamics. Longitudinal dynamics are affected through an influence of the sweep angle on the static margin. Lateral dynamics are also affected through an increase in yaw static stability with aft outboard wing sweep. One study identifies favorable mass scaling effects that allow birds and small aircraft to fly without vertical tails, using only wingtip sweep to generate yaw stiffness and damping[80].

Aft sweep of the outboard wing is said to generate a leading-edge vortex lift [91], although this is not modeled explicitly in the current considerations.

3.5.3 Up-Down Inclination of Inboard Wings

Vertical rotation of the inboard wing about a longitudinal axis produces an effect on the lateral stability through interactions between the wing and the vertical center of gravity. This pendulum stability is a significant source of both lateral and longitudinal stability in many species of gliding animals[87]. Upward rotation of the inboard wing produces both a dihedral effect and elevates the outer wing, in both cases increasing the wing-level stability[4].

3.5.4 Up-Down Inclination of Outboard Wings

The outboard wing similarly affects the lateral stability through changes in the vertical location of the center of pressure and angular inclination. Both factors interact with sideslip to produce stabilizing roll moments. The inclination of the outboard wing also affects the control effectiveness of the twisting action. The twisting or flap deflection produces an increase or decrease in lifting force which subsequently produces a rolling moment. The roll moment decreases as the cosine of the wing inclination angle. Meanwhile, the yaw moment produced by the twist deflection increases by the sine of the wing angle.

3.5.5 Twist of Outboard Wings

The roll moment necessary for control is generated by differential twisting of the outboard wings. The actuation rate of the twist actuator is considered sufficiently fast for stabilizing tasks. The twist can also be morphed quasi-statically, both for roll and pitch trim using differential and collective twisting, respectively.

3.6 Wing Morphing Model

A mechanical model emulating the basic gull morphological operations is developed using composite materials and electro-mechanical actuators. Figure 3-7 shows an annotated view of the left wing compared to two gliding gulls using a similar form of wing morphing. It is clear that conventional aircraft metrics such as dihedral are insufficient to describe the wing articulation. Instead, the wing is treated as a serial-link robot manipulator[21], where each joint is represented by appropriate length and angle dimensions.

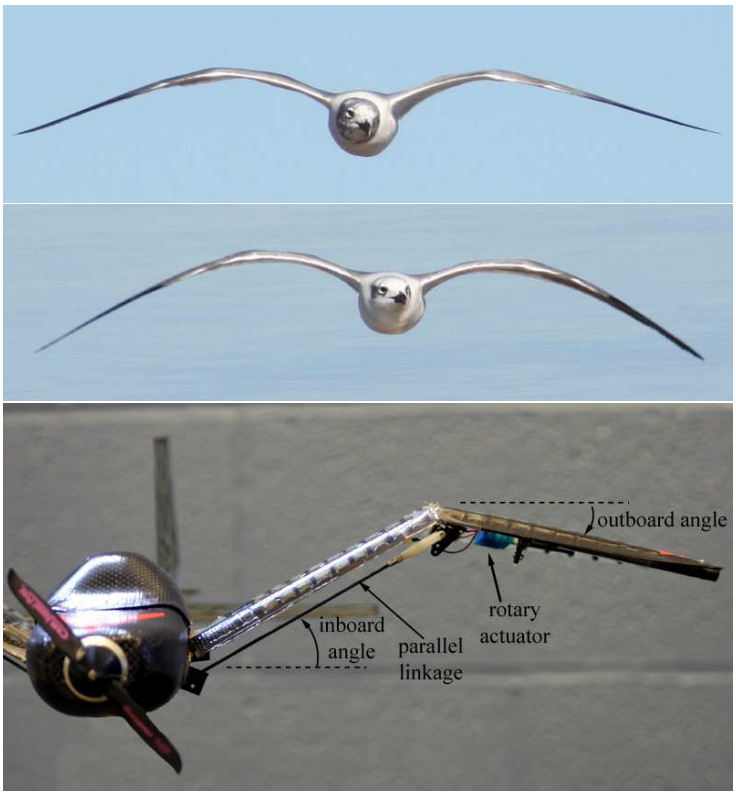

Figure 3-7. Wing articulation about longitudinal axis showing two joint angles. Gliding gulls are shown for reference.

The morphing wing is similarly equipped with joints by which to articulate the wing sections in the horizontal plane. Figure 3-8 shows the underside of a gull wing with annotations to indicate approximate positions of bones and joints. The mechanical model is of reduced complexity, having only the equivalent of a shoulder and a wrist joint.

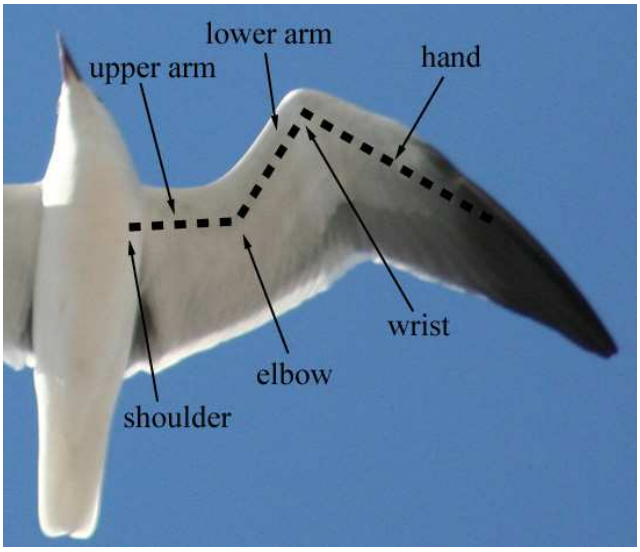

Figure 3-8. Approximate physiological diagram of a gull wing with articulations in the horizontal plane

3.6.1 Pigeon Wing Configuration

Pigeons are observed using large dihedral angles during steep glides on approach to landing. Figure 3-9 shows four consecutive frames during such a descent, where the pigeon uses a turning flight in addition to the inclined wing geometry to control the approach path. Each frame is photographed using a focal length of 300mm, making the relative size of the pigeon in the image an indication of its proximity to the camera. The arrangement of the birds in the image is artificial and does not reflect the actual flight path. However, the sequence illustrates the wing shape used to command a steep descent and also shows some maneuvering capability during the unusual joint configuration.

Tail feathers are fully extended during the steep gliding maneuver, ostensibly to increase drag and reduce lift-to-drag ratio. The wing configuration may also provide stability benefits at large trim angles of attack such that the glides can be effectively controlled for precision landings. The head orientation of the pigeon gives some indication of the angle of descent relative to the body, assuming it is looking in the direction of flight. The wing morphing shown depicts vertical articulations of the shoulder joint to achieve the dihedral angles of nearly 45° per wing side. It is difficult to discern from the photos

Figure 3-9. Composite photo of pigeon in gliding approach to landing

the amount of sweep used, but they appear to be in the neutral or even slightly forward swept configuration.

Tennekes reports in his 1996 book on the wing morphing used by pigeons to control glide speed[86]. Fully extended wings are used during low airspeed glides while forward swept inboards and highly aft swept outboard wings are used for high airspeed dives. The change in wingspan, wing area, and aspect ratio allow the bird to alter the trim glide speed by nearly a factor of three.

3.6.2 Avian Morphology Studies

Recent research on the aerodynamic and dynamic characteristics of birds have quantified the motivation behind some of the wing shape changes observed in nature. Tucker reported in 1970 on the effect of wing planform shape on the glide angle and glide speed of falcons[88][89]. Forward sweep of the shoulder or elbow joints and aft sweep of the wrist joint, as in Figure 3-8, are used in varying degrees to control the planform area and wingspan. The subsequent trim airspeed varies substantially, affording control over loitering or attack speeds.

Sachs reported findings on the role of aft wingtip sweep in providing yaw stiffness and yaw stability on the aerodynamic and inertial scales of bird flight[80]. The aft wing sweep also affects the location of the aerodynamic center and contributes to pitch stability[87].

The results partly explain the stability motivations for swept shapes adopted by birds during high speed dives.

Joint angle articulation along longitudinal axes has been shown by Davidson to increase lift to drag ratio substantially on a seagull-inspired wing model[22]. Alternate joint configurations have been shown to have the opposite effect and reduce lift to drag, allowing steep dives at moderate airspeeds[3].

Videler suggests the aerodynamics of complex avian wing shapes benefit from the deployment of individual feathers, such as the alula, in increasing the lift magnitude by promoting a leading-edge vortex[91]. Figure 3-8 shows the location of the alula feather, which is deployed forward at the wrist joint during certain wing shapes and maneuvers. The feather is said to have a profound impact in increasing maneuverability and possibly delaying stall.

The wing geometry of several bird species are presented by Liu et. al in 2006[54]. Three-dimensional scanners are used to generate models of bird wings throughout the flapping cycle. The wing geometries are presented as time-dependent Fourier series, which represent the change in the aerodynamic shape resulting from skeletal articulation. The authors use a two-jointed arm model as a simplification of bird bone structure. The arm model is characterized by three angles and achieves a sufficient range of motion to represent the flapping cycle. The wing surface is assumed to be fixed to one of two spars at the quarter-chord position and maintains proper orientation relative to the flow for all configurations. Although the research focused on flapping flight, the identified wing shapes may also be useful for gliding operations.

3.7 Aircraft Morphology

A simplified UAV wing geometry is developed to study the implications of avian-inspired shape morphology. The wing is based on an existing planform[2] which serves as the nominal configuration and also provides a baseline for performance comparison. Figure 3-10 shows four composite views of the morphing degrees of freedom and range.

The nominal configuration, a straight, elliptical wing, is shown in addition to the extreme positive and negative positions for each joint axis. The morphing is assumed symmetric about the fuselage centerline.

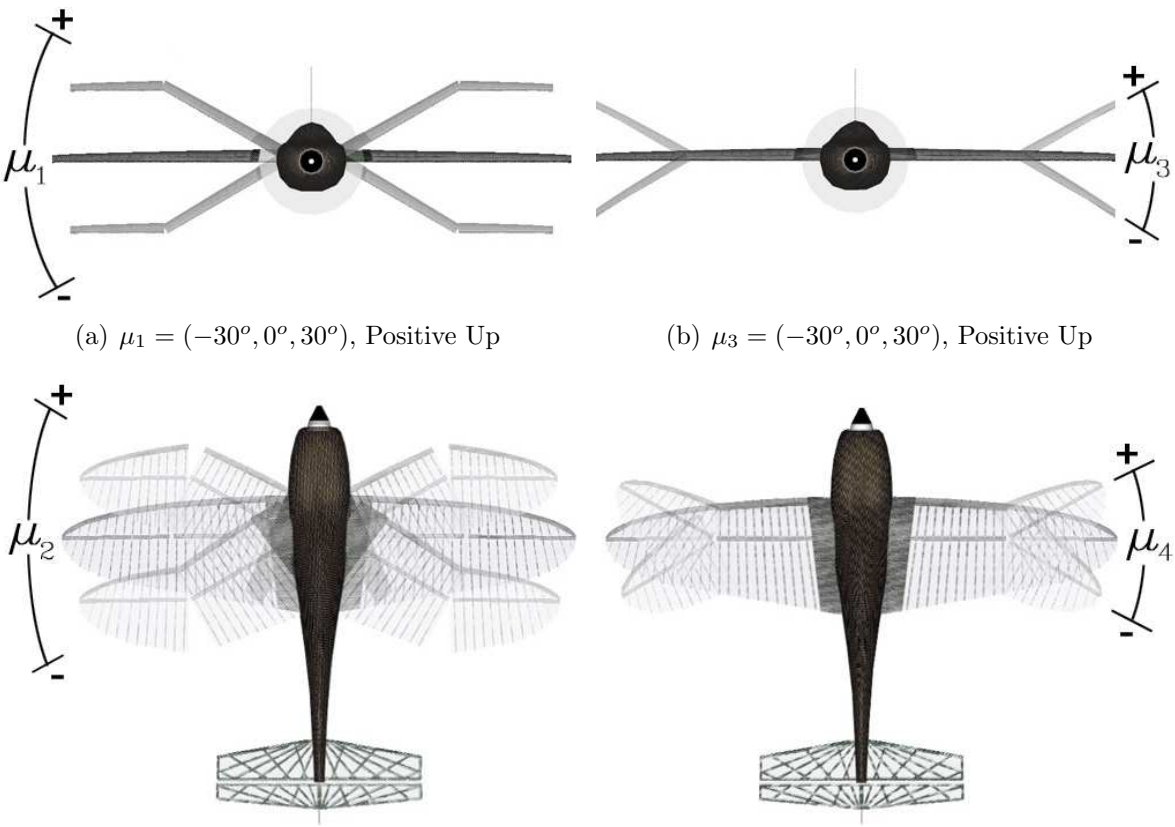

(a) $\mu_1 = (-30^o, 0^o, 30^o)$, Positive Up

(b) $\mu_3 = (-30^o, 0^o, 30^o)$, Positive Up

(c) $\mu_2 = (-30^o, 0^o, 30^o)$, Positive Forward

(d) $\mu_4 = (-30^o, 0^o, 30^o)$, Positive Forward

Figure 3-10. Morphing joint articulations for 4-degree-of-freedom wing

Wing configurations are determined by four joint axes, two at the wing root and two at the mid-span position. Inboard joint angles, μ_1 and μ_2, control the rotations about longitudinal and vertical axes, respectively. Outboard joint angles, μ_3 and μ_4, similarly control the longitudinal and vertical axis rotations, respectively. The views shown in Figure 3-10 depict variations to one joint axis for each subfigure. Inboard joints produce rotations of the inboard wing section and translations of the outboard wing section. The orientation of the outboard sections is controlled strictly by the outboard joints.

A mechanical model uses spars, hinges, and composite skins in place of the bones, joints, and feathers of a bird. The mechanization allows sufficient range of motion and structural stiffness to study the effectiveness of biologically inspired wing shapes. The model is reduced in complexity relative to a bird wing with a shoulder, elbow, and wrist joint, each having multiple degrees of freedom. Two joint locations, each with two degrees of freedom, are used per wing side. The variable area function of feathers is replaced by extensible or sliding skins[36].

For simulation, the aircraft is modeled with a similar range of motion but without the mechanical detail. A vortex-lattice computational aerodynamics package[25] is used to simulate the flight characteristics of various aircraft configurations. Simulations are performed for each combination of joint angles within the operating range. Angular resolution for each joint is 5°, giving 13 unique positions over the $\pm 30^o$ range and 28,561 combinations of joint angles. Output data from the simulations are saved to a 4-dimensional matrix for post-processing. Airspeed, angle of attack, and sideslip are fixed for each simulation at 15 m/s, 6° and, 0°, respectively. Each run is trimmed for zero pitching moment using the elevator control surface.

CHAPTER 4
DYNAMICS

4.1 Aircraft Equations of Motion

The motion of a rigid body through space is determined by the forces and moments acting on the body and by the inertial properties of the body. A body undergoing linear acceleration and angular rotation is subject to specific forces and moments in order to sustain the motion. Equations 4–1-4–3 [64][33] describe the three orthogonal forces in terms of the mass, velocity, and acceleration. The force contributions include several factors, among them body mass, m, times the linear accelerations, $\dot{u}$, $\dot{v}$, and $\dot{w}$. Cross-axis terms also contribute to the forces, where angular velocities are multiplied by the orthogonal linear velocities. A gravitational component is also included in the force equations, which accounts for the changing body attitude in a fixed gravitational field.

$$X = m(\dot{u} + qw - rv) + mg\sin\theta \tag{4–1}$$

$$Y = m(\dot{v} + ru - pw) - mg\cos\theta\sin\phi \tag{4–2}$$

$$Z = m(\dot{w} + pv - qu) - mg\cos\theta\cos\phi \tag{4–3}$$

The moments sustained by a rigid body depend upon inertial properties, angular velocities, and angular accelerations. Equations 4–4 - 4–6 show the formulation for three orthogonal moments. Each moment depends on the corresponding moment of inertia multiplied by the angular acceleration, a cross-axis angular acceleration multiplied by the product of inertia, and coupled terms relating angular velocities and inertial properties. The given moments equations are independent of the body orientation and are valid for aircraft of fixed, laterally symmetric configuration. For aircraft with rapidly time-varying and asymmetric geometries[35][36], the moment equations require inclusion of all the inertial terms, many of which are zero for conventional aircraft.

$$L = I_x\dot{p} - I_{xz}\dot{r} + qr(I_z - I_y) - I_{xz}pq \tag{4–4}$$

$$M = I_y\dot{q} + rqI_x - I_z + I_{xz}(p^2 - r^2) \tag{4–5}$$

$$N = -I_{xz}\dot{p} + I_z\dot{r} + pq(I_y - I_x) + I_{xz}qr \tag{4–6}$$

While the general equations express forces and moments in terms of body motion, the dynamics of an aircraft represent the forces and moments required to achieve a desired body motion. Furthermore, since the force and moments acting on an aircraft are composed of contributions from the various aerodynamic appendages, an alternate representation is used to account for the effect of vehicle motion on the forces and moments. The aircraft equations of motion are written in terms of the aircraft states and controls, aggregating individual force and moment contributions to determine the resulting dynamics.

Aircraft motion can be described by twelve states, which represent position, orientation, angular velocity, and linear velocity along each of three axes. The standard aircraft states are described by Table 4.1.

Table 4-1. Standard aircraft states describing vehicle motion

Axis	Position	Orientation	Linear velocity	Angular velocity
Roll	x	ϕ	u	p
Pitch	y	θ	v	q
Yaw	z	ψ	w	r

Linearized aircraft dynamics are written in a form where the effect of each state or control on each force or moment can be readily identified. Stability derivatives are coefficients describing a linear relation between a state, such as roll rate, and a force or moment, such as roll moment. Subscript notation is used for stability derivatives, such as C_{l_p}, to describe the linearized influence of roll rate on roll moment. Control derivatives are similarly expressed, relating control surface deflection to forces and moments such that $C_{l_{\delta_a}}$ describes the contribution of aileron deflection to roll moment. The individual

contribution of states and controls to forces and moments are dimensionalized by the vehicle geometric parameters, compared to inertial properties, then linearly summed to determine state accelerations.

The magnitude and direction of the stability and control derivatives are determined primarily by the vehicle geometry. Factors such as wing size and shape, tail geometry, airfoil, weight distribution, and fuselage shape directly affect the coefficients. For a variable-geometry morphing aircraft, the assumption of derivative linearity may hold for a fixed configuration, but the coefficient value is expected to change with aircraft shape. Thus, the standard derivative representation is insufficient to express the change incurred with morphing. A proper description includes functional dependence of each coefficient on the morphing parameters, $\vec{\mu}$, which represent the change in airframe shape. The nondimensional roll convergence derivative would thus be expressed as $C_{l_p}(\vec{\mu})$. The actual functional dependence may differ for each coefficient and is computed individually during modeling and simulation.

Dimensional derivatives likewise include dependence on the morphing configuration, such as,

$$L_p(\vec{\mu}) = \frac{C_{l_p}(\vec{\mu})QS(\vec{\mu})b(\vec{\mu})^2}{2I_xV} \tag{4–7}$$

where Q is the dynamic pressure, S is the reference wing area, b is the reference wingspan, and V is the airspeed. The reference dimensions, S and b, both vary with respect to morphing due to the changing wing geometery.

The linearized state-space equations of motion including the effects of quasi-static morphing are shown in Equations 4–8 and 4–9. Lateral and longitudinal dynamics are assumed uncoupled and are shown independently. The dynamics are affected only by eight states, four longitudinal and four lateral states. The remaining four states, including positions, x, y, and z, and yaw angle, ψ, are strictly for kinematic considerations.

$$
\begin{bmatrix} \dot{u} \\ \dot{w} \\ \dot{q} \\ \dot{\theta} \end{bmatrix} = \begin{bmatrix} X_u(\vec{\mu}) & X_w(\vec{\mu}) & 0 & -g \\ Z_u(\vec{\mu}) & Z_w(\vec{\mu})u_0 & 0 & 0 \\ M_u(\vec{\mu}) + M_{\dot{w}}(\vec{\mu})Z_u(\vec{\mu}) & M_w(\vec{\mu}) + M_{\dot{w}}(\vec{\mu})Z_w(\vec{\mu}) & M_q(\vec{\mu}) + M_{\dot{w}}(\vec{\mu})u_0 & 0 \\ 0 & 0 & 1 & 0 \end{bmatrix} \begin{bmatrix} u \\ w \\ q \\ \theta \end{bmatrix} + \begin{bmatrix} X_{\delta_e}(\vec{\mu}) \\ Z_{\delta_e}(\vec{\mu}) \\ M_{\delta_e}(\vec{\mu}) + M_{\dot{w}}(\vec{\mu})Z_{\delta_e}(\vec{\mu}) \\ 0 \end{bmatrix} \begin{bmatrix} \delta_e \end{bmatrix} \tag{4–8}
$$

$$
\begin{bmatrix} \dot{\beta} \\ \dot{p} \\ \dot{r} \\ \dot{\phi} \end{bmatrix} = \begin{bmatrix} \frac{Y_\beta(\vec{\mu})}{u_0} & \frac{Y_p(\vec{\mu})}{u_0} & -(1 - \frac{Y_r(\vec{\mu})}{u_0}) & \frac{g\cos\theta_0}{u_o} \\ L_\beta(\vec{\mu}) & L_p(\vec{\mu}) & L_r(\vec{\mu}) & 0 \\ N_\beta(\vec{\mu}) & N_p(\vec{\mu}) & N_r(\vec{\mu}) & 0 \\ 0 & 1 & 0 & 0 \end{bmatrix} \begin{bmatrix} \beta \\ p \\ r \\ \phi \end{bmatrix} + \begin{bmatrix} 0 & \frac{Y_{\delta_r}(\vec{\mu})}{u_0} \\ L_{\delta_a}(\vec{\mu}) & L_{\delta_r}(\vec{\mu}) \\ N_{\delta_a}(\vec{\mu}) & N_{\delta_r}(\vec{\mu}) \\ 0 & 0 \end{bmatrix} \begin{bmatrix} \delta_a \\ \delta_r \end{bmatrix} \tag{4–9}
$$

4.2 Parametric Variations of EOM

The aircraft geometry is considered to be in the nominal configuration when all four morphing joint angles (μ_1, μ_2, μ_3, and μ_4) are 0° neutral. The nominal aircraft is a straight taper with no dihedral or sweep in either the inboard or outboard wing sections. The root joint articulates about longitudinal and vertical joint axes as morphing parameters, μ_1 and μ_2 are changed, respectively. Under such actuation, the inboard wing panel changes orientation, while the outboard wing panel changes only position. The outboard wing panel orientation is decoupled from root joint morphing and is affected only by morphing parameters, μ_3 and μ_4, which cause rotations about longitudinal and vertical joint axes, respectively. The available configurations combine dihedral/anhedral

and fore/aft sweep of the inboard and outboard wing sections. The wing shapes resulting from morphing roughly represent observed natural configurations.

The morphing configuration space spans the hypervolume created by all combinations of morphing parameters, $\mu_{1,2,3,4}$ over the range of -30° to +30°. A relatively coarse angular resolution of 5° limits the number of configurations to $13^4 = 28,561$. Each of these possible configurations yields a unique value for each of the stability and control derivatives.
The equations of motion for a morphing aircraft depend on the configuration and vary according to changes in the stability and control derivatives. In addition to the dynamics, the variable shape also changes the aerodynamic performance and maneuverability of the flight vehicle.

Change in the dynamic characteristics during morphing can be quantified at the derivative coefficient level or can be abstracted to modal characteristics or performance metrics as functions of one or more aircraft parameters. Such metrics are necessary to exploit the morphing capability to perform a desired mission, since they can be used to generate cost functions describing the task-effectiveness of a particular configuration.

Although the vehicle achieves significant variation in wing shape during morphing, the relative geometry between the wing and tail remains similar for all configurations. The wing is used as the primary source for lift and remains distinct from the tail surface, which is used to oppose the pitching moment from the wing. Furthermore, the shape-change is assumed to be symmetric about a vertical plane on the fuselage centerline. The left and right wings morph collectively for all operations, apart from the differential twist action on the wing tips for roll control.

Shape change occurs at a rate much slower than the vehicle dynamic rates. Time-varying inertial terms and unsteady aerodynamics associated with the shape change are not included in the dynamic formulation due to the slow rate of morphing. These assumptions are reasonable and allow the structure of the equations of motion to be constant for

all configurations with changes occurring only in the value of the coefficients. The dynamic properties may still change substantially as a result of the variable coefficients.

The large number of possible configurations results in excessively large tables and matrices required to store the variations in each parameter. Since independent variations are available in all four joint angles, the required matrix is four-dimensional and is difficult to visualize or process. The configuration space can be simplified by fitting a line, curve, plane, hyperplane, or hypersurface through one or more dimensions. Since each configuration data is based on aerodynamic configuration modeling, it is unlikely that a simplistic fit will accurately represent the parameter variations over the entire space. However, the fit can be used to identify the local variations in parameter values with respect to a particular configuration.

Reducing the dimensionality of the 4D configuration space may afford access to many of the desired wing shapes while reducing the complexity of commanding morphing. For two dimensional configuration subspaces, the surface representing parameter variations can be quite complex and subject to significant coupling between the two morphing joint directions. A surface regression fit would require a very large number of parameters in order to achieve small errors. However, since the rate at which morphing is allowed is limited due to quasi-static assumptions, modeling of the entire configuration space is perhaps unnecessary. Local knowledge of the parameter variations may be sufficient to morph the aircraft into a shape appropriate for the mission task. Gradient descent methods are used to morph toward shapes with improved performance. Such morphing based on local knowledge is not guaranteed to converge to the globally optimal configuration.

Local, singular-actuation trends are modeled for the full 4D configuration by isolating morphing functions. A 4th-order polynomial is used to represent the parametric variations due to actuation of a single morphing joint. For the nominal configuration, the effect of μ_1 changes is modeled by constraining μ_2, μ_3, and μ_4 to neutral (0°) and tabulating the 13 parameter values for $-30^o <= \mu_1 <= 30^o$ in 5° increments. The polynomial is of the form,

$$C(\mu_1) = a_1 + a_2\mu_1 + a_3\mu_1^2 + a_4\mu_1^3 + a_5\mu_1^4 \tag{4–10}$$

where coefficients $a_{1,2,3,4,5}$ are determined by regression and $C(\mu_1)$ is the modeled parameter, which may be a stability derivative or a performance metric.

The process is repeated for μ_2, μ_3, and μ_4 such that four 4th-order polynomials describe the parametric variation in all directions through the configuration space and intersect at the chosen configuration. Linear independence of $\vec{\mu}$ components is required to achieve good results using the polynomial representation. For configuration spaces which are linearly coupled, combined morphing operations are not accurately represented at the extremes of the space, but are reasonably well defined for local variations in all morphing directions. In some cases, subspaces of the actuator space can be found where the morphing is linearly independent and this approach achieves small error over the permitted space.

4.3 Flight Metrics and Cost Functions

Morphing technology allows an air vehicle to adapt its design during flight, but that adaptation should be to satisfy some mission objective. As mission tasks change throughout a flight, the vehicle achieves a high level of performance in each role. Retasking during a flight may involve disparate objectives and require a substantial change in vehicle geometry. In order to effectively change the aircraft shape, both the capabilities of the aircraft and the requirements of the mission must be clearly understood.

Quantitative performance metrics are used to evaluate the capability of an aircraft to achieve a desired level of performance, maneuverability, agility, or efficiency. These metrics establish the effectiveness of a particular morphing shape at achieving the current mission objectives and can thus be used to motivate a change in shape, if a more appropriate configuration is available. As the aircraft is retasked, the metrics by which the aircraft is

evaluated also change. The metrics are used to generate cost functions which relate the mission requirements to vehicle capability within the configuration space.

A common measure of aerodynamic performance is the ratio of lift to drag. Lift to drag ratio, L/D, is the fundamental component of determining energy efficiency, endurance, range, glide angle, soaring capability, and descent profile. The desired L/D for a given task may be a maximum, minimum, or a power ratio of lift and drag, such as L^3/D^2.

For a fixed configuration, lift and drag vary with angle of attack and airspeed. Optimizing a morphing aircraft for L/D requires a change in configuration in addition to variation in flight condition. The optimal flight condition for one configuration may be different from another, suggesting that morphing capability may be used to find efficient configurations across a range of angles of attack and airspeeds.

The flight conditions for which the aircraft configuration is optimized are segments of a desired UAV mission. The most common condition is maximum lift to drag, which achieves both the longest range cruise[7] and the highest glide ratio[9]. Configuring a powered UAV for range allows the vehicle to travel the maximum distance for a given quantity of fuel. In the unpowered case, maximizing lift to drag allows the vehicle to glide the maximum horizontal distance for a given initial altitude.

Inviscid aerodynamic modeling is used to generate data for morphing configurations, neglecting sources of drag such as skin friction and interference drag. Modeling results are supplemented by a simple drag model based on a minimum, zero-lift drag with a quadratic approximation of lift-induced drag. The drag coefficient is given by,

$$C_D = C_{D_o} + \frac{1}{\pi ARe} C_L^2 \tag{4–11}$$

where C_{D_o} is the minimum, zero-lift drag, AR is the wing aspect ratio, and e is the wing efficiency factor.

C_{D_o} is crudely estimated for each configuration using the projected frontal area to determine pressure drag. The wing efficiency factor is then computed by solving for the quadratic curve that simultaneously satisfies C_{D_o} and the lift and drag output of the modeling. The drag model is used to estimate aircraft performance during cruise, loiter, descent, and maneuvering flight phases. Figure 4-1 shows variations of drag with lift for an inviscid, symmetrical wing. The location of the maximum lift to drag occurs where a line originating at the origin is tangent to the quadratic drag polar. The lift to drag ratio is plotted to show show the wing efficiency changes with lift coefficient. The minimum L/D occurs symmetrically about the C_L axis, at a negative angle of attack.

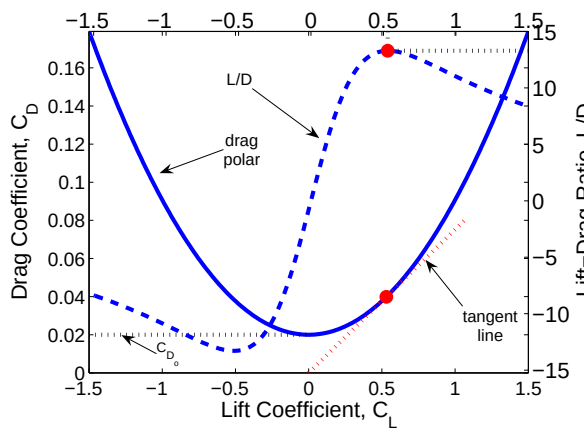

Figure 4-1. Drag polar and lift to drag ratio showing graphically location of max L/D

4.3.1 Cruise

The requirements of cruise flight are primarily related to minimizing energy expenditure, unless time enroute is additionally restricted. Propulsive and actuator energy demands are required to be low during cruise flight. Maneuvering is generally not required during cruise, so actuator usage is not expected to be high, provided the aircraft system is open-loop stable. Thrust requirements are related to the aerodynamic efficiency of the aircraft as measured by lift to drag ratio (L/D).

Equation 4–12 from Anderson [7] shows the inverse relationship between L/D and thrust-required to weight ratio (T_r/W). T_r decreases as L/D increases for fixed W.

Assuming the magnitude of thrust is related to energy consumption, the minimum energy condition occurs at the maximum L/D for the aircraft.

$$\frac{L}{D} = \left(\frac{T_r}{W}\right)^{-1} \tag{4–12}$$

Equation 4–13[7] shows the factors that affect L/D for an aircraft in level flight, where the lift is equal to the weight. The equation includes terms from the drag polar and the wing loading, both of which are expected to change with different morphed configurations.

$$\frac{L}{D} = \left(\frac{\rho_\infty {V_\infty}^2 C_{D,0}}{2(W/S)} + \frac{2K}{\rho_\infty {V_\infty}^2}\frac{W}{S}\right)^{-1} \tag{4–13}$$

4.3.2 Maneuvering Metrics

Maneuvering and agility metrics describe the ability of an aircraft to achieve desired angular velocities and angular rates[10], respectively. A change in course requires an initial acceleration about one or more axis, followed by a sustained angular velocity, and concluded by accelerating to a terminal flight condition. The desired accelerations and velocities are large when the maneuver is subject to space and time considerations. A target engagement, for instance, may require rapid rolling and pitching to acquire the target in the sensor field of view, followed by precise flight path tracking to maintain a desired position relative to the target. The aerodynamic requirements for such maneuvers are different than those for a benign flight segment such as cruise or loiter. The corresponding geometry that achieves the maximum agility and maneuverability is also expected to differ from the optimal efficiency configuration.

Several metrics for aircraft maneuverability exist and have been used extensively to quantify fighter aircraft performance [61] [78]. The basic measure of agility in the current study is the magnitude of angular acceleration about the three body-axes, $\dot{p}$, $\dot{q}$, and $\dot{r}$.

Similarly, the measure for maneuverability is the magnitude of sustained angular velocity about the three body-axes, p, q, and r.

The physical limitations which constrain both agility and maneuverability for manned aircraft include structural load limits, stall boundaries, pilot or occupant G-tolerance, control surface deflection and rate limits, and available thrust. Linearized morphing models lack the fidelity to reflect each of these factors, so the limitations will be primarily assessed from control surface limits, angle of attack limits, and sideslip angle limits. The structural and occupant factors are not expected to be concerns for MAVs, considering the high structural strength and pilotless flight, respectively.

4.3.2.1 Agility

Roll acceleration agility is determined from a steady, level flight trim condition where p, r, and β are initially zero.

The roll acceleration dynamics from the lateral equations of motion (Equation 4–8) are,

$$\dot{p} = L_\beta \beta + L_p p + L_r r + L_{\delta_a} \delta_a + L_{\delta_r} \delta_r \tag{4–14}$$

In level flight, the sideslip roll coupling, roll damping, yaw-roll coupling terms are zero. Assuming rudder primarily affects yaw moment, the roll acceleration is,

$$\dot{p} = L_{\delta_a} \delta_a \tag{4–15}$$

Maximum roll acceleration occurs when the ailerons or wing twist deflect at the travel limits, $\delta_{a,max}$.

$$\dot{p}_{max} = L_{\delta_a} \delta_{a,max} \tag{4–16}$$

For uniform deflection limits for all configurations, the roll agility is determined strictly by the aileron or wing twist roll moment control effectiveness. The magnitude of $C_{l_{\delta_a}}$ changes significantly due to articulation of the outboard wing with respect to the flow direction. The dimensional derivative, L_{δ_a}, changes further due to variations in the reference wing area and reference span due to morphing.

Yaw agility is derived with similar trim assumptions, namely that all states perturbations are zero. Maximum yaw acceleration occurs when the rudder is deflected at the travel limits, $\delta_{r,max}$.

$$\dot{r}_{max} = N_{\delta_r}\delta_{r,max} \tag{4–17}$$

Pitch agility is computed about a linearized flight condition, where angle of attack, velocity, and pitch rate perturbations are zero. The maximum pitch acceleration is determined simply by the elevator pitching moment effectiveness with the elevator at the deflection limits, $\delta_{e,max}$.

$$\dot{q}_{max} = M_{\delta_e}\delta_{e,max} \tag{4–18}$$

4.3.2.2 Maneuverability

The agility obviously changes with flight condition, reaching zero acceleration when the aircraft reaches the maximum maneuvering rate. Maneuvering limits determine the capacity to achieve angular velocity along a single axis while maintaining a trim value along orthogonal axis. Maximum rate is thus determined by cross-axis coupling terms in addition to rate damping and control effectiveness terms.

The maximum roll maneuverability is derived by first considering the roll acceleration dynamics.

$$\dot{p} = L_\beta \beta + L_p p + L_r r + L_{\delta_a} \delta_a + L_{\delta_r} \delta_r \tag{4–19}$$

For a simple case that ignores yaw coupling, roll maneuverability is computed for $\beta = r = \dot{p} = 0$. Pitch coupling is already ignored due to separation of lateral and longitudinal dynamics. Without coupling, unaccelerated roll dynamics are used to compute the single-axis maximum roll rate, given by,

$$0 = L_p p + L_{\delta_a} \delta_a \tag{4–20}$$

$$p_{max} = \frac{-L_{\delta_a} \delta_{a,max}}{L_p} \tag{4–21}$$

Without coupling, the maximum roll rate is simply the maximum aileron or twist deflection scaled by the ratio of aileron effectiveness to roll damping.

Single-axis pitch and yaw rate limits are similarly computed. In all cases, rate limits are simple expressions relating the control power to the rate damping. The stabilized roll, pitch, or yaw rate is achieved when the moment generated by aileron, elevator, or rudder deflection is equally opposed by the damping moment opposing aircraft rotation.

$$q_{max} = \frac{-M_{\delta_e} \delta_e}{M_q} \tag{4–22}$$

$$r_{max} = \frac{-N_{\delta_r} \delta_r}{N_r} \tag{4–23}$$

Realistically, coupling exists between the aircraft axes and sustained angular rates are affected by both primary and secondary effects. An aileron deflection primarily affects roll moment, although it may also cause yaw moment coupling for some configurations. The yaw moment consequently causes a non-zero yaw rate, which is a secondary and undesirable effect for a roll-only command. Thus, the actual rate performance must account for cross-axis coupling and use all applicable control surfaces to achieve maximum

rate in only the desired axis. The roll rate command may require rudder deflection to oppose the aileron-generated yaw moment. This additional deflection has an effect on the roll moment which will cause a change in sustained performance relative to the single-axis case.

The roll rate maneuverability with coupled dynamics is readily derived using the expressions for roll and yaw acceleration.

$$\dot{p} = L_\beta \beta + L_p p + L_r r + L_{\delta_a} \delta_a + L_{\delta_r} \delta_r \tag{4–24}$$

$$\dot{r} = N_\beta \beta + N_p p + N_r r + N_{\delta_a} \delta_a + N_{\delta_r} \delta_r \tag{4–25}$$

For the desired maneuver, the aircraft achieves maximum, unaccelerated roll rate with no coupling to the other states such that,

$$p = p_{max} \tag{4–26}$$

$$r = 0 \tag{4–27}$$

$$\beta = 0 \tag{4–28}$$

$$\dot{p} = 0 \tag{4–29}$$

$$\dot{r} = 0 \tag{4–30}$$

Substituting the state values into the yaw acceleration expression and solving for roll rate, p, yields,

$$p = \frac{-N_{\delta_a} \delta_a - N_{\delta_r} \delta_r}{N_p} \tag{4–31}$$

Substituting this expression into the roll acceleration equation yields an expression that combines the roll and yaw dynamics and compares the relative magnitude of control power required to maintain the maneuver conditions.

$$L_p\left(\frac{-N_{\delta_a}\delta_a - N_{\delta_r}\delta_r}{N_p}\right) + L_{\delta_a}\delta_a + L_{\delta_r}\delta_r = 0 \tag{4–32}$$

$$\frac{L_p}{N_p}\left(-N_{\delta_a}\delta_a - N_{\delta_r}\delta_r\right) = -L_{\delta_a}\delta_a - L_{\delta_r}\delta_r = 0 \tag{4–33}$$

$$\frac{L_p}{N_p}\left(-N_{\delta_a}\frac{\delta_a}{\delta_r} - N_{\delta_r}\right) = -L_{\delta_a}\frac{\delta_a}{\delta_r} - L_{\delta_r} \tag{4–34}$$

$$-\frac{L_p}{N_p}N_{\delta_a}\frac{\delta_a}{\delta_r} - \frac{L_p}{N_p}N_{\delta_r} - L_{\delta_a}\frac{\delta_a}{\delta_r} - L_{\delta_r} \tag{4–35}$$

$$\frac{\delta_a}{\delta_r}\left(-\frac{L_p}{N_p}N_{\delta_a} + L_{\delta_a}\right) = -L_{\delta_r} + \frac{L_p}{N_p}N_{\delta_r} \tag{4–36}$$

$$\frac{\delta_a}{\delta_r} = \frac{L_{\delta_r} - \frac{L_p}{N_p}N_{\delta_r}}{\frac{L_p}{N_p}N_{\delta_a} - L_{\delta_a}} \tag{4–37}$$

The expression for $\frac{\delta_a}{\delta_r}$ gives the ratio between aileron deflection and rudder deflection required to maintain a roll rate without yaw rate coupling. A ratio greater than 1 requires larger aileron deflection than rudder deflection. A positive value indicates aileron and rudder in the same direction, while a negative value indicates opposing control directions. Maximum roll performance is computed at the deflection limit of one of the control surfaces. The performance for each configuration depends on the deflection ratio and the deflection limits for each surface.

In the case of yaw rate maneuverability, the rudder-aileron control ratio is similarly computed, with the final result a function of control effectiveness and damping along both roll and yaw axes.

$$\frac{\delta_r}{\delta_a} = \frac{L_{\delta_a} - \frac{L_r}{N_r}N_{\delta_a}}{\frac{L_r}{N_r}N_{\delta_r} - L_{\delta_r}} \tag{4–38}$$

Pitch rate maneuverability with respect to coupling in the longitudinal states cannot be solved algebraically. The final value theorem [65] and some bounding assumptions on the states are needed in order to determine the maximum pitch rate. The expression

includes velocity and angle of attack perturbations, which are expected to depart from the trim values during pitch maneuvering.

$$q = \frac{-M_v V - M_\alpha \alpha - M_{\delta_e} \delta_e}{M_q} \tag{4–39}$$

4.3.2.3 Aggregate maneuverability and agility metrics

Maneuverability and agility metrics are computed for individual morphing configurations along each of the three aircraft body axes. Aggregate metrics for both maneuverability and agility can be computed by combining performance along individual axes.

The maneuverability cost function is given by,

$$J_m(\vec{\mu}) = W_p|p_{max}(\vec{\mu})| + W_q|q_{max}(\vec{\mu})| + W_r|r_{max}(\vec{\mu})| \tag{4–40}$$

where axis weights W_p, W_q, and W_r are arbitrary scale factors that are used to bias maneuverability function value, J_m, to emphasize performance along a particular axis.

The agility cost function is given by,

$$J_a(\vec{\mu}) = W_p|\dot{p}_{max}(\vec{\mu})| + W_q|\dot{q}_{max}(\vec{\mu})| + W_r|\dot{r}_{max}(\vec{\mu})| \tag{4–41}$$

The configuration which achieves the highest level of performance for a mission designated by a set of axis weights yields the maximum value for J_m and J_a.

Typical aircraft maneuvering requires significantly higher roll rates than either pitch rates or yaw rates. Roll maneuvering is necessary for changing bank angle to initiate turns, reject gust disturbances, and perform axial rolls. Pitch maneuvering is required during climb and dive transitions as well as during loop segments. Both pitch and yaw maneuvers occur in conjunction with roll during coordinated turns. A standard set of axis weights is used to reflect the emphasis on roll maneuverability, with secondary

considerations for pitch maneuvering, and tertiary account for yaw maneuvering. The standard axis weight values are,

$$W_p = 3 \tag{4–42}$$

$$W_q = 2 \tag{4–43}$$

$$W_r = 1 \tag{4–44}$$

Morphing configurations which maximize J_m and J_a are determined using the given axis weights and stable dynamics criteria. The criteria stipulates that all dynamic modes must be stable with small unstable allowances for divergent spiral and phugoid modes.

Figure 4-2 shows the most maneuverable configuration under the simulated conditions. The wing assumes an unusual shape near the boundaries of the configuration space, with limit dihedral and aft sweep on the inboard wing combined with limit anhedral and large forward sweep on the outboard wing.

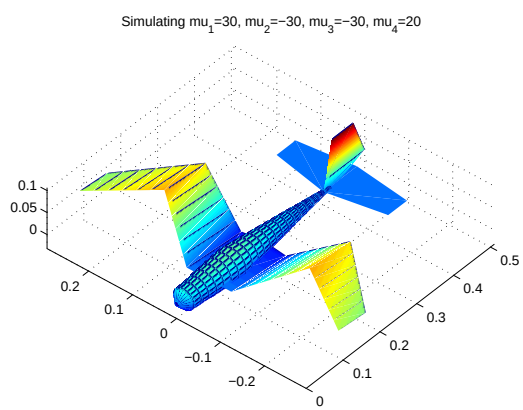

Figure 4-2. Maximum maneuverability configuration using stable dynamics criteria ($\mu_1 = 30^o$, $\mu_2 = -30^o$, $\mu_3 = -30^o$, and $\mu_4 = 20^o$)

The configuration achieves a roll rate of 13.9 rad/s, a pitch rate of 0.05 rad/s, and yaw rate of 13.1 rad/s. The low pitch rate magnitude is a result of the low elevator control effectiveness in the simulation model in addition to the large pitch moment of inertia. The pitch maneuverability may also improve when perturbed velocity and angle

of attack are included in the metric formulation. The large yaw rate is achieved by the forward swept wingtips, which reduce the sideslip and yaw rate damping.

Figure 4-3 shows the most agile configuration, which assumes a much more nominal shape than the maneuverable shape. The wing shape uses moderate anhedral on the inboard wing and slight forward sweep for both inboard and outboard wings. It is interesting to note the disparity between the two shapes that results from the addition of damping terms in the maneuverability cost.

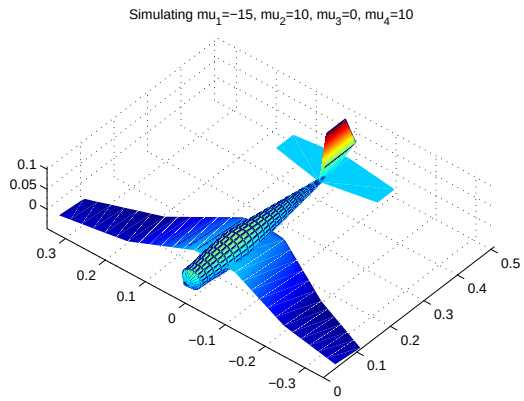

Figure 4-3. Maximum agility configuration using stable dynamics criteria ($\mu_1 = -15^o$, $\mu_2 = 10^o$, $\mu_3 = 0^o$, and $\mu_4 = 10^o$)

The agility of the configuration is quite substantial, considering the large roll rate acceleration of 211.2 rad/s^2. Acceleration along the other axis are much smaller, with 70.1 rad/s^2 and 20.8 rad/s^2 for the pitch and yaw axes, respectively.

While the shapes do not appear directly inspired by nature, certain aspects of the wing shape reflect observations made of bird flight. The forward swept wingtips of the maneuvering configuration are common to seagulls performing rapid changes in glide path and bank angle. The anhedral of the agile configuration are similar to down-turned wings seen on several species of birds while in accelerating flight.

The morphing configuration space is hyper-dimensional and thus cannot easily be visualized. Metrics or parameters that depend on each of the four morphing joint angles may incur highly complex changes through the configuration space. These changes are

represented using slices of the 4-dimensional morphing space hypervolume. Figure 4-4 shows six views of the configuration space. Plots on the top row are fixed at $\mu_4 = 15^o$ and show variations in the maneuverability metric due to changes in μ_1, μ_2, and μ_3. The color of each square in the plots represents the magnitude of the metric, while its location indicates the morphing angles. Slices are shown at the space extremes ($\mu_1 = 30^o$, $\mu_2 = 30^o$, and $\mu_3 = -30^o$). A fourth slice is shown at values of $\mu_1 = (-15^o, 0^o, 15^o)$. The four plots show that maneuverable configurations are concentrated at negative values of μ_3 with positive values of μ_2. An additional concentration occurs at positive values of μ_1 with negative values of μ_2.

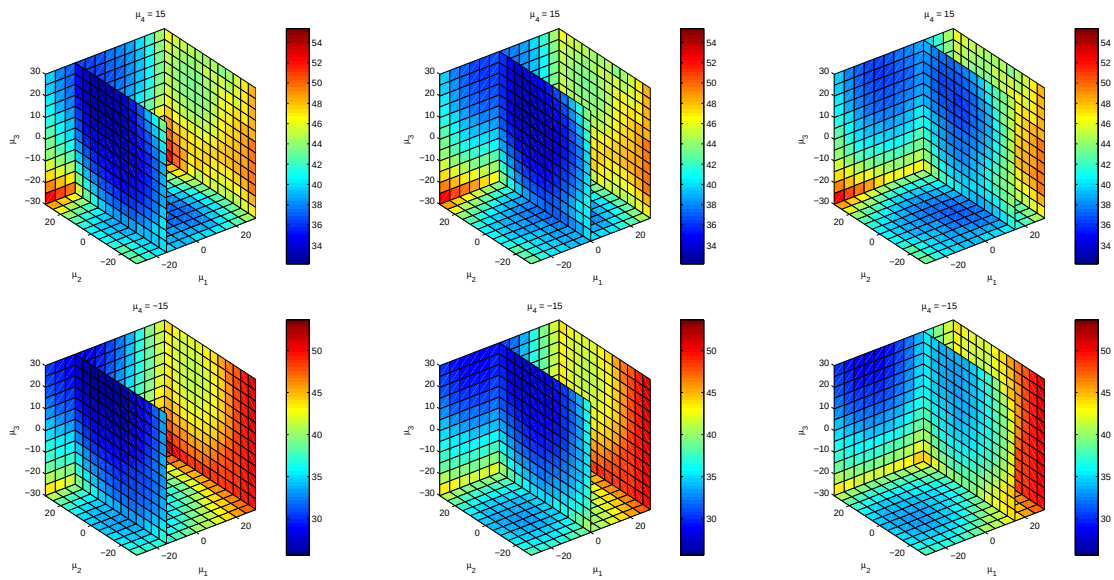

Figure 4-4. Maneuverability index shown as slices of 4-dimensional hypervolume at $\mu_4 = 15^o$ (top) and $\mu_4 = -15^o$ (bottom)

The bottom row of plots in Figure 4-4 show maneuverability metric data for $\mu_4 = -15^o$. The distribution of maneuverability conditions has changed markedly, with most occuring at large positive values of μ_1 with negative values of either μ_2 or μ_3. The distribution of maneuverable shapes is wider than the case for $\mu_4 = 15^o$, although the disparity in the colorbar index show the most desirable conditions exist with positive morphing of μ_4.

Figure 4-5 represents the maneuverability index for each morphing configuration as a histogram. Although actuator contextualization is lost, the distribution of values shows insight into the relative scarcity of highly maneuverable configurations. The average metric value is 37.3 rad/s, yet the highest value is 57.1 rad/s along a positive skew.

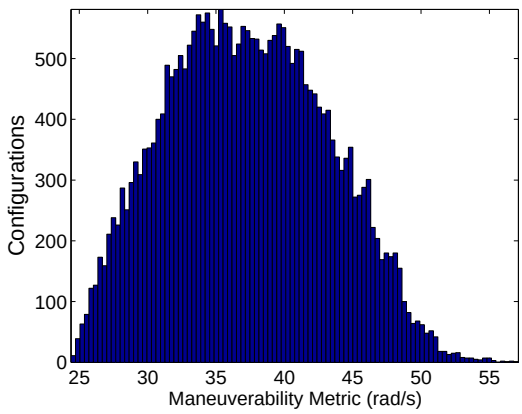

Figure 4-5. Histogram of maneuverability metric for all morphing configurations ($\mu_{1,2,3,4} = [-30, 30]$)

Figure 4-6 shows the agility metric for configurations with $\mu_4 = 15^o$ (top row) and $\mu_4 = -15^o$ (bottom row). For both cases, the agile configurations exist at positive values of μ_1 and near nominal values of μ_2 and μ_3. The top right plot indicates that the maximum agility shown occurs at a moderate value of μ_1, rather than at the extreme. Relatively non-agile shapes exist along several corner extremes of the space.

Figure 4-7 shows the histogram for the agility metric associated with all configurations. The distribution shows negative skew, with an average agility metric of 599.3 rad/s^2. Variations in metric magnitude are large through the configuration space, ranging from a minimum of 298.2 rad/s^2 to a maximum of 807.9 rad/s^2.

4.4 Coupling Morphing Parameters

Changing aircraft shape between missions usually requires a trajectory through the configuration space which invokes multiple joint actuations. Individual joint actuation has limited usefulness in mission adaptation, whereas variations to combined actuation

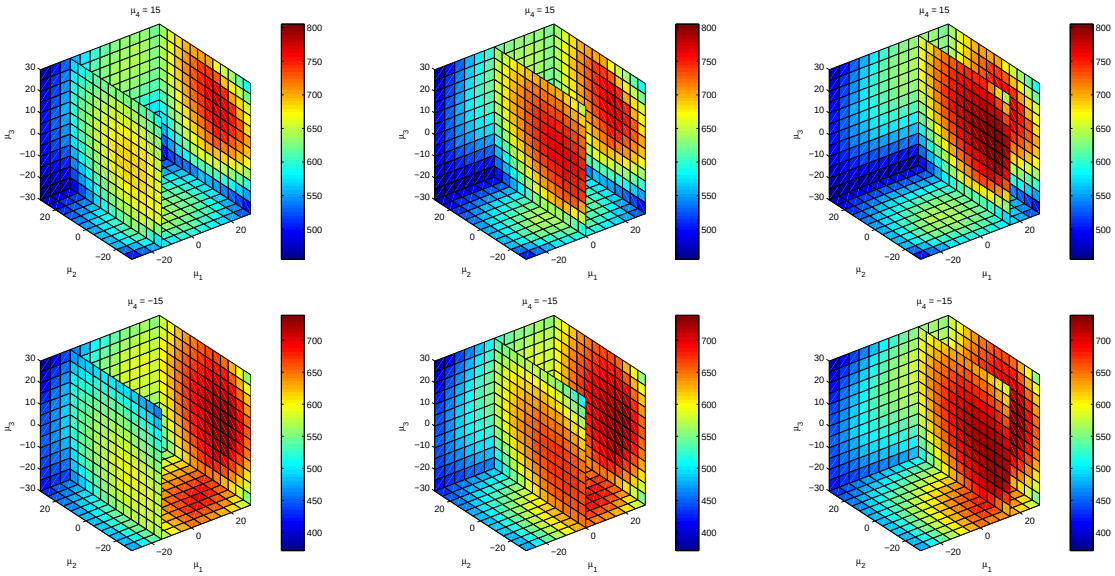

Figure 4-6. Agility index shown as slices of 4-dimensional hypervolume at $\mu_4 = 15^o$ (top) and $\mu_4 = -15^o$ (bottom)

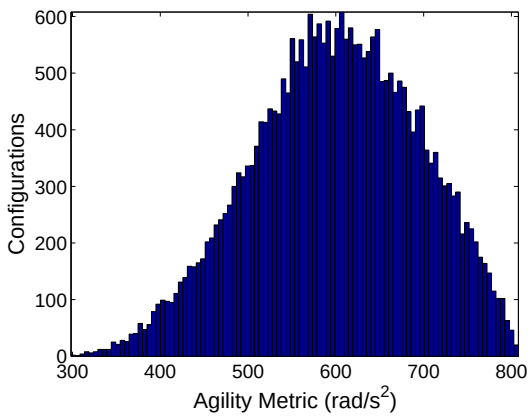

Figure 4-7. Histogram of agility metric for all morphing configurations ($\mu_{1,2,3,4} = [-30, 30]$)

can accomplish simultaneous objectives, such as varying aerodynamic performance while preserving handling qualities.

Biologists have reported observing birds morph wing shape with significant coupling between joint articulation [91]. Although a bird wing is highly configurable, often only a subset of the possible shapes are used in flight. The skeletal structure in the wing promotes coupling through mechanical interaction between the elbow and wrist joint[87]. Two parallel bones between the elbow and wrist allow simultaneous extension of the

joints[91]. The dynamics of the resulting shapes are always controllable[54], yet allow the bird to perform a diverse set of flight tasks.

Similarly, a biologically inspired aircraft may not require the entire configuration space and may benefit from coupling major morphing motions. Combining morphing operations simplifies the shape command by reducing dimensionality and also removes portions of the configuration space offering limited usefulness.

Desired combinations are identified from 4-dimensional performance or maneuvering metrics by applying principle component analysis (PCA) to a set of desired configurations. For individual metrics, such as lift to drag ratio, the shapes which achieve minimum and maximum values are sampled to generate point clouds in the morphing space. Both minimum and maximum L/D conditions are desired for descent and cruise flight, respectively. Many configurations are sampled in the upper and lower percentages, such as 20%, of the metric range. Combined morphing operations are found by performing PCA on the configuration points to find the dominant, orthogonal axes through the space which affect L/D. Reducing the dimension to 2 generates a transformation matrix which relates morphing operations on the new axes, $\mu_{A,B}$, to the original axes of $\mu_{1,2,3,4}$. Morphing commands to $\mu_{A,B}$ directly affect the L/D performance and can be commanded directly by the controller or adaptation system. Transformation to $\mu_{1,2,3,4}$ becomes a lower-level operation that is performed automatically by the actuation system.

Figure 4-8 shows a comparison between the lift to drag performance metric for the original space and for a reduced-order space with dimension of two. Sampling the configurations having L/D metrics in the upper and lower 20% at 8.3% density (1 of 12 shapes) yields 953 sets of actuator positions. All configurations were subject to sampling, regardless of dynamic characteristics. The distribution of the reduced-dimension set shows a maximum value close to the actual maximum L/D of 15.1. The minimum L/D value, however, is 0.61 higher than the actual minimum of 10.5.

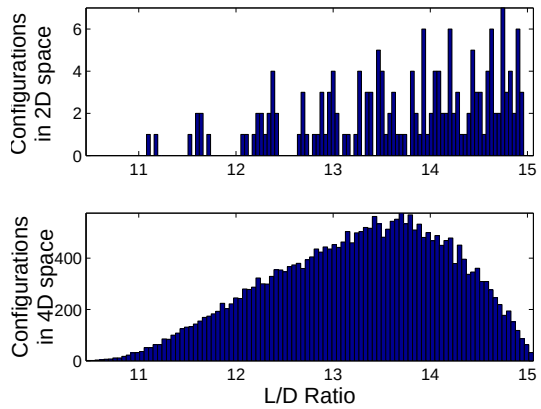

Figure 4-8. Comparison of L/D metric histograms for reduced-dimension space (top) and original configuration space (bottom)

The L/D values for points in the transformed 2D space can be visualized using a response surface. The space consists of orthogonal axes, μ_A and μ_B, which represent combined morphing operations. Figure 4-9 shows the variations in L/D with respect to changes in μ_A and μ_B. Primary axis, μ_A, has a dominant effect on the lift to drag ratio, while the secondary axis, μ_B has a somewhat smaller effect. The response surface is still somwhat complicated and shows significant coupling between the axes and trend reversal along individual axes. For negative values of μ_A, for instance, increasing μ_B decreases the L/D ratio to the minimum value. Conversely, at positive values of μ_A, increasing μ_B increases L/D to the maximum value.

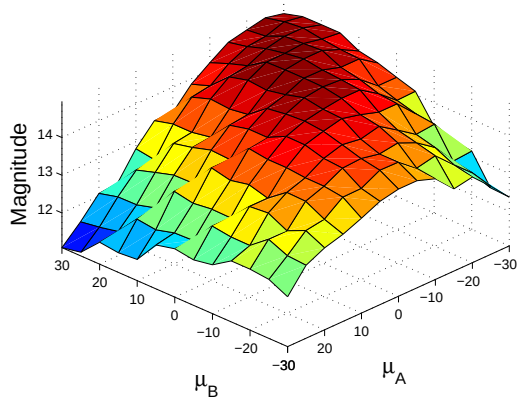

Figure 4-9. Response surface of L/D metric in reduced-dimension space

The general form of the transformation from the 2D combined morphing space to the 4D joint-angle space is,

$$\begin{bmatrix} \mu_1 \\ \mu_2 \\ \mu_3 \\ \mu_4 \end{bmatrix} = T_{\mu_{A,B}}^{\mu_{1,2,3,4}} \begin{bmatrix} \mu_A \\ \mu_B \end{bmatrix} \tag{4–45}$$

The transformation matrix has the form,

$$T_{\mu_{A,B}}^{\mu_{1,2,3,4}} = \begin{bmatrix} \mu_{A,1} & \mu_{B,1} \\ \mu_{A,2} & \mu_{B,2} \\ \mu_{A,3} & \mu_{B,3} \\ \mu_{A,4} & \mu_{B,4} \end{bmatrix} = \begin{bmatrix} 0.57 & -0.41 \\ 0.70 & 0.27 \\ 0.40 & -0.24 \\ 0.17 & 0.84 \end{bmatrix} \tag{4–46}$$

The numerical values of the transformation matrix show the magnitude and convention of the joint angle coupling. For instance, commands to μ_B result predominantly in changes to joint μ_4, with roughly half the deflection in μ_1, but in the opposite direction. Smaller commands are issued to μ_2 and μ_3 in the same and opposite directions, respectively, to μ_4.

Reducing the dimensionality of the configuration space based on a single metric offers limited benefit compared to a transformation which accounts for multiple mission metrics. Point clouds are generated using desired values for maneuverability, agility, L/D, power required, and other metrics. The points are sampled from minimum metric values, in the case of power required and turn radius, from maximum values, in the case of maneuverability and agility, or from both extremum values in the case of L/D or airspeed. Applying PCA to the heterogeneous metric point cloud finds the transformation which allows the vehicle to transform between various mission-related shapes.

A linear transformation is a relatively simplistic method of reducing the dimensionality of a complex point cloud distribution in the 4-dimensional morphing space. The result may be inadequate to achieve desired performance in one or more metric. Furthermore, the shapes transformed space are not guaranteed to comply with dynamic criteria used to generate the original points.

4.5 Stability Criteria

Several levels of stability criteria are implemented to achieve the desired dynamics in the optimized morphing configuration. The criteria are based on the operating condition and the operator, each of which can change over the course of the mission. Mission tasks requiring a human operator may seek only wing configurations which achieve excellent handling qualities. Other tasks using an autopilot for routine or long-term operations may allow any stable configuration. For agile maneuvering, the criteria may allow even open-loop unstable dynamics, provided that sufficient sensing and actuation capability exist to stabilize the system.

4.5.1 Handling Qualities Criteria (HQC)

The stability criteria used for remotely piloted tasks must ensure the dynamics are appropriate for the human operator. The modes must, in general, be stable and lie within a range of natural frequencies, damping ratios, and/or time constants. Requiring good handling qualities allows the operator to perform maneuvers manually, without having to rely on stability augmentation or autopilot. For mission tasks such as take-off or landing, the pilot must maneuver the aircraft along a precise flight path. Manual operations may also be required for testing new instrumentation or control systems. In each case, the vehicle must respond predictably to the control inputs and maintain a reasonable level of pilot workload during the task.

Table 4-2 shows the criteria used to assess handling qualities from the modal characteristics. The criteria corresponds to Class 1 aircraft operating in Category A, which is applied to light aircraft engaged in precision maneuvers[64]. The numerical values for the

upper or lower modal parameter limits have been determined by qualitatitive pilot evaluation over years of flight testing[20]. The use of manned-flight criteria for an unmanned aircraft may result in conservative performance, considering that the remote pilot is not subject to the oscillations and loading of the vehicle. However, it will ensure a minimum level of pilotability in areas where handling criteria for unmanned flight vehicles are not available.

Mode	Time to double	Time constant	Natural Frequency	Damping Ratio
Spiral Divergence	$T_{2,S} > 12$ seconds	—	—	—
Roll Convergence	—	$\tau_R < 1.0$ second	—	—
Dutch Roll Mode*	—	—	$\omega_{n,DR}$ >1.0 rad/s	$\zeta_{DR} > 0.19$*
Short Period Mode	—	—	$0.35 < \zeta_{SP} < 2.0$	—
Phugoid Mode	$T_{2,PH} > 55$ seconds	—	—	$\zeta_{PH} > 0.04$

Table 4-2. Handling qualities criteria for morphing configuration.
*Dutch roll damping ratio must also satisfy constraint $\zeta_{DR}\omega_{n,DR} > 0.35$ rad/s

4.5.2 Stable Dynamics Criteria (SDC)

Most of the UAV mission will use an autopilot to perform relatively benign maneuvers. The presence of a controller relaxes the handling qualities requirement placed on human-operated flight tasks. The stability criteria for morphing configurations can be changed to requiring stable poles for all modes. The control gains can be used to obtain desirable closed-loop dynamics. Requiring stable dynamics prevents excessive actuation usage resulting from stabilizing an open-loop unstable plant.

Table 4-3 shows the allowable range of eigenvalues for the stable dynamics criteria. Modes that are classically unstable or marginally stable such as the spiral divergence and the phugoid mode are allowed to have slightly positive real values. The remaining modes are allowed to lie anywhere in the left-half plane. The criteria also allows the modes to deviate from classical form, in that oscillatory modes such as dutch roll and short period may consist of two negative real poles.

Mode	Criteria
Spiral Divergence	$\Re(\lambda_S) < 0.5$
Roll Convergence	$\Re(\lambda_R) < 0.0$
Dutch Roll Mode	$\Re(\lambda_{DR}) < 0.0$
Short Period Mode	$\Re(\lambda_{SP}) < 0.0$
Phugoid Mode	$\Re(\lambda_{PH}) < 0.5$

Table 4-3. Stable dynamics criteria for morphing configurations

4.5.3 Unrestricted Dynamics Criteria (UDC)

The final criteria allows unrestricted variation in the dynamics in the morphing configuration space. Highly unstable dynamics such as forward-swept wings are permitted to exploit the aerodynamic performance afforded by such configurations. The criteria makes a number of assumptions about the flight control system that may be unrealistic for an implementable system. The size of the control surfaces are assumed to be large enough to trim and perturb the aircraft for all configurations. Actuator rate and motion are also assumed to have sufficient bandwidth and operating range for stabilization and control. Finally, it is assumed that the controller can adequately sense the aircraft state and feedback appropriate commands to the control effectors. In practice, the final criteria may need modification to allow only a limited range of unstable dynamics. For simulation purposes, the criteria remains unconstrained.

CHAPTER 5
MANEUVERING CONTROL

5.1 Overview

A morphing aircraft controller must achieve stabilization and command tracking for all shape configurations and all mission tasks. The highly variable vehicle dynamics necessitate a change in the controller with changes to the wing shape. The controller must achieve desired closed-loop performance in the presence of large changes to the control surface effectiveness and open-loop stability characteristics. The desired controller performance relates to the mission-task, which mandates rapid responses for accelerating flight phases and benign, conservative responses for cruise and loitering phases. Such variations in the performance change as a result of dynamic variations, which must be properly represented in the control design.

Mission flight commands generate navigation and guidance trajectories which should be followed for satisfactory task completion. The commands, such as turn, dive, and pursue, represent outer-loop commands which invoke the maneuvering actions of the aircraft. The outer control loop accounts for the aircraft dynamics to determine the allowable accelerations, which may be different than the commanded accelerations. Disparities between allowable and commanded trajectories motivate shape changes which seek to reduce flight path errors and improve mission performance[48]. As the dynamics change, the maneuvering controller compensates to achieve stabilization and tracking of the inner-loop rate and angular states.

At the most basic level, the purpose of the inner-loop maneuvering controller is to stabilize and track commands to the angular rates, p, q, and r, and the angles of attack and sideslip, α and β. Tracking control objectives for each of these states is determined by the relative aggressiveness of the mission task. Time- and space-critical flight tasks require rapid response and allow large actuator usage, whereas other flight tasks emphasize energy conservation and slower accelerations.

Attitude, force, velocity, and position control are considered as part of the outer-loop control, which produces commands driving the inner-loop tracking. Each of these functions relies directly on the inner-loop control of angular rates and flight angles. The design of the outer-loop controllers are motivated by mission tasks but are independent of the configuration. Such a decoupling will produce large tracking errors for configurations not suited for certain mission tasks. These errors are used to drive shape adaptation which seeks to find a new configuration to improve performance.

Each morphing configuration is assumed to be represented by a slowly time-varying linear model. Corresponding control designs are linear and do not include time-dependent aerodynamic or inertial terms. For fixed configurations, the dynamics are represented by linearized, small-perturbation theory.

As the aircraft varies morphing configuration, the dynamics are known to vary substantially from the nominal aerodynamics. Given the large configuration space and the corresponding complex wing shapes, the dynamics and performance vary over a wide range and can be adapted to achieve high-performance in a variety of mission scenarios.

Adaptation or scheduling of the control gains is required to achieve the desired controllability and stability for all intermediate and extreme configurations. The change in the controller gains is directly motivated from the change in the open-loop dynamics, which in turn change due to aircraft shape. However, even a coarsely discretized configuration space results in an excessively large number of possible shapes. Computing a controller for each of the thousands of configurations is impractical in time and memory constraints.

One approach is to exploit the smooth variations in the dynamic parameters to reduce the number of required controllers. Design points are chosen within the configuration space to provide a simplified representation of the parametric variations due to morphing. Controllers are developed for these design points and interpolated in the enclosed spaces using a linear parameter varying (LPV) or quasi-LPV approach. The latter method allows

straightforward interpolation of the controller gains for configurations lying between design points. Although shown effective in studies[83], the methodology lacks the theoretically satisfying proof of stability or robustness existing at the design points. The simplistic gain interpolation can be replaced by a properly designed LPV system, which accounts for closed-loop performance stability guarantees for all possible configurations.

The choice of design point density relates to the allowable parametric variations in the baseline control design. A control synthesized to be robust to 10% uncertainty in the parameters requires a new design point whenever the change in the parameter values exceeds 10%. In a large configuration space that defines a complicated change of wing shape, the aerodynamic parameters vary over large ranges. Small tolerance to uncertainty necessitates extremely dense design point grids that approach the density of the original space. Such a large number of design points trivializes the computational benefits of interpolation and fails to provide a satisfactory solution to the control challenge.

The 13^4 wing configurations achievable by the morphing aircraft each require an appropriate compensator for closed-loop stability and controllability. Designing controllers for each configuration is computationally unreasonable and requires significant memory for storage. An alternative approach of linearly interpolating controllers over subspaces of the configuration space is computationally tractable only for a coarse distribution of design points. Such a coarse distribution results in significant errors in modeling the complex parameter response surface resulting from morphing. The scheme linearly interpolates controller gains, even for cases where the dynamics are not well represented by piecewise linearity. The errors lead to intermediate configurations using highly off-design controllers.

The desired approach to controlling a highly configurable morphing aircraft is by allowing the controller to adapt to changes in the vehicle dynamics. Since the morphing is assumed to be quasi-static, the system does not violate the constant/slowly time varying assumption necessary for convergence and stability of adaptive controllers. Robust and optimal control techniques are used to synthesize nominal and design point controllers,

which provide a coarse grid of closed-loop systems with known behavior. At intermediate points, an adaptive component is added to the baseline interpolated controller to allow the system to adapt to unmodeled dynamics. The technique can also be used without interpolation by simply allowing the controller gains to slowly adapt with the dynamic variations.

The control augmentation uses the form of Model Reference Adaptive Control (MRAC), which also requires definition of an additional system to provide the desired or reference system response[50]. This reference system changes as a function of mission task to represent varying control objectives. The baseline controller gains are adapted until the system output closely matches the reference model response.

The MRAC controller structure uses a feedback gain matrix to relate sensor output to control surface input and a feedforward matrix to relate reference commands to control input. Both gain matrices are adapted in response to error between the actual and desired system response. The feedback component is identical to a regulating/tracking control task. LQR and robust synthesis are used to identify the initial feedback gains, which provide the desired level of performance and robustness at the design points. The feedforward component is initialized to relate reference commands to logical control surfaces, such as using ailerons primarily for roll commands and rudder for sideslip and yaw commands.

5.2 Single Degree-of-Freedom Morphing Systems

A single degree-of-freedom morphing system uses coupled joint articulation to limit reconfiguration to a subset of the configuration space. A single allowable actuator trajectory is defined through several desirable points in the space. Each point may correspond to a particular mission or metric optimization. The trajectory is in the form of a 4-dimensional spline to include all desired configurations and guarantee dynamic and performance requirements along intermediate shapes. While the trajectory is allowed to take complex shape, it is mostly monotonically varying through the space. Commanding

morphing operation is greatly simplified, while the geometric wing variation remains quite complex.

While the wing shapes of the single-degree-of-freedom system are complex, the actuator trajectory is defined at a relatively small number of configurations. A straight line in the actuator space passing through the nominal configuration encompasses 13 points. The 4D spline trajectory defines less than 20 points, which are easily stored in memory and recalled during morphing.

Dynamic models for the small number of allowable configurations are used to design individual controllers. The control design uses either MRAC-based gain scheduling and H_∞ robust control. In the latter case, interpolation of the controller gain matrix for changes in a parameterized dynamic model have been shown in simulation to yield reasonable closed-loop results[83]. H_∞ controllers have also been used in switching schemes[44], where the dynamic model varies over a large range and one controller is used to control a subset of the dynamic variations.

An effective switching-controller approach[44] switches between adjacent configurations by using a set of phantom controller. Both adjacent controllers are continually reinitialized using the states and actuator positions of the current dynamics and controller. When the morphing is commanded, the adjacent controller assumes control of the modified dynamics while preserving continuity of the actuator command. The rate of morphing is assumed to be slow enough that no transient effects are caused by the shape reconfiguration.

5.2.1 Robust Control Design

Robust controllers for each configuration are designed with a synthesis model which uses frequency-dependent weighting functions to penalize tracking errors and actuator usage. Figures 5-1 and 5-2 show the synthesis models for the lateral and longitudinal controllers, respectively. The dynamic model and the weights are functions of the wing shape

and mission, respectively. For each configuration in the reduced space, the components of the synthesis model are assumed to be static.

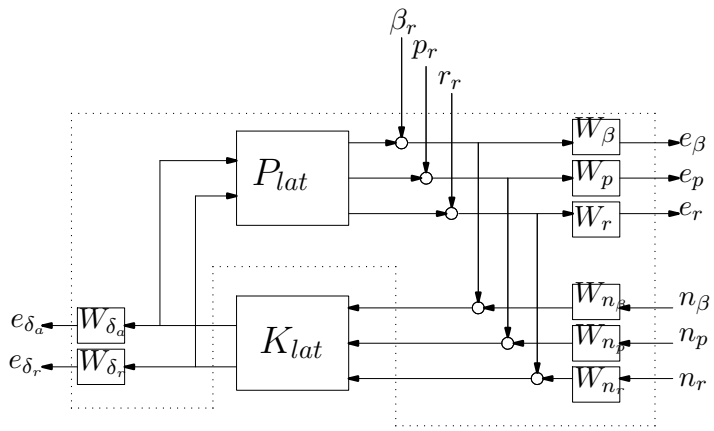

Figure 5-1. Lateral H_∞ controller synthesis model

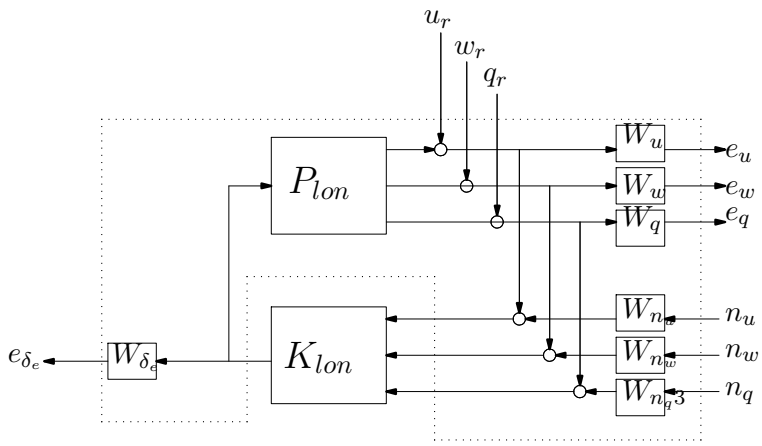

Figure 5-2. Longitudinal H_∞ controller synthesis model

Performance synthesis weights are penalties on the tracking or regulating errors of each state output. The weight magnitude at a particular frequency is inversely related to the allowable error. This error penalty generally varies with frequency such that low frequencies near steady-state are tracked with very small errors. At high frequencies, beyond the point at which the vehicle can physically respond, the penalty is reduced so that large errors are allowed. The transition from high to low penalty occurs at different frequencies for the various missions. Cruise flight involves benign maneuvers mostly near

steady-state trim. Thus, the frequency threshold for the performance weight is low, since tracking acquisition is not critical during trim perturbations. For aggressive flight with rapid maneuvering, the tracking penalty continues to higher frequencies, forcing small tracking errors.

Actuator synthesis weights are penalties on the actuator usage. The magnitude of the actuator weight is related to the allowable motion. The weight is typically small at low frequency and large at high frequency, allowing large, slow motions and only small, rapid motions. The weights are often used to define an actuator model in the controller. For a multi-mission aircraft, the weights are also used to promote conservative actuator use for benign mission tasks and allow full authority control during critical flight regimes.

The variation of the actuator weights between mission segments can allow higher frequency usage for maneuvering tasks compared to cruise segments. Alternatively, the magnitude of the actuator deflection can be varied, with only small movements allowed for cruise while actuation at the deflection limits is allowed for maneuvering. Both the rate at which the control surfaces are actuated and the deflection angle affect energy consumption. Thus, the restrictive actuation during benign flight is intended to promote energy conservation at the expense of transient tracking performance.

Inputs to the lateral synthesis model are reference commands to sideslip, roll rate, and yaw rate. The sideslip command is typically zero, promoting a regulating rather than tracking function. Roll rate is commanded by the roll angle error during turns and roll maneuvers. Yaw rate is commanded during turns in conjunction to the roll rate and roll angle command to achieve coordinated flight. Aileron and rudder control surface actuations generated by the controller also input to the synthesis model directly to the plant. Noise is added in general to the plant outputs, although is not used in the simulations.

Inputs to the longitudinal synthesis model are reference commands to angle of attack and pitch rate. The angle of attack is commanded to maintain the required lift force for

steady or maneuvering flight. Pitch rate is commanded from pitch angle error during looping flight. Elevator is the sole control input to the longitudinal synthesis model.

The outputs from both the lateral and longitudinal synthesis models include sensor outputs to the controller, and scaled performance and actuator errors. Performance errors are tracking or regulating errors scaled by the synthesis weights, while actuator errors are control inputs scaled by the actuation weights.

The H_∞ design computes controller gains that minimize the performance and actuator errors from the synthesis model. Robustness of the resulting controller is expressed in terms of the minimum parametric perturbation that can result in instability. The desired value for this measure of perturbation, γ, is less than 1 for normalized weights. For certain dynamic systems, penalties, and actuator constraints, this desired value is unrealistic and the controller achieves a γ of greater than 1. Reports in the literature indicate that such a controller is still both effective and robust over small uncertainty[29]. Controller robustness despite high γ is due to conservatism due to unrealistic constructs such as complex uncertainty and infinitely fast signals[97].

5.2.2 Simulation Results

5.2.2.1 Overview

The simulations are based on the computational models generated for the variable gull-wing aircraft. The range of morphing is assumed to be identical to the modeling section, namely inboard vertical angle $\mu_1 = \pm 30^o$ and outboard vertical angle $\mu_3 = \pm 30^o$. Both sweep joints remain in the neutral position, $\mu_2 = \mu_4 = 0^o$. The model is assumed to be single-degree of freedom since the morphing occurs only between the identified configurations, although two wing joints articulate simultaneously.

Simulated responses are generated for each mission phase, where the aircraft model is assumed to be morphed at the optimum configuration specified by Equation 5–1. Simple inner-loop control responses are used to show the different closed-loop objectives for each mission. The worthiness of a given controller is determined by the ability to track roll

rate, pitch rate, or sideslip commands. Any of the outer-loop control efforts are ultimately dependent on one or more of these inner-loop controller. Thus, the controller performance shown here, although simplistic, is indicative of the general applicability of the morphing and control design to a desired flight regime.

$$\min_{\vec{\mu}} J = W_{lat}\|P_{lat}(\vec{\mu}) - P_{lat,desired}\| + W_{lon}\|P_{lon}(\vec{\mu}) - P_{lon,desired}\| \tag{5–1}$$

Where W_{lat} and W_{lon} are design weights, $P_{lat,desired}$ is a reference system exhibiting the desired lateral response, $P_{lon,desired}$ is a reference system exhibiting the desired longitudinal response, and $P_{lat}(\vec{\mu})$ and $P_{lon}(\vec{\mu})$ are the lateral and longitudinal dynamics, respectively.

5.2.2.2 Cruise flight

The optimal morphing angles predicted by Equation 5–1 for the cruise condition with weights $W_{lat} = 0.0$ and $W_{lon} = 1.0$ are inboard angle $\mu_1 = -10^o$ and outboard angle $\mu_3 = 5^o$.

The ultimate requirement of cruise flight is simply to maintain a straight-and-level attitude at a desired airspeed, altitude, and heading. The airspeed chosen will balance between energy efficiency (endurance), range, and time-enroute. Cruise altitude is also related to efficiency, but for small unmanned vehicles, the desired altitude is most likely influenced by ground-obstacle clearance and observability. Finally, heading is chosen primarily to be toward the area of interest, but may be varied during the flight to circumnavigate obstacles.

Level airspeed and angle of attack, α, can be considered as the parameters that most directly affect L/D and energy efficiency, and thus the objective of the cruise controller will be to pitch to achieve and maintain a desired airspeed and α. The performance of the controller in tracking a pitch rate doublet is shown in Figure 5-3-left. The transient response of the controller is somewhat slow, although the pitch rate converges to the desired value with little steady-state error. The slow response is necessitated by the low

actuator rate condition. High actuator usage unecessarily expends energy, since cruise flight does not require particularly fast response. The lower plot of Figure 5-3-left shows the elevator position for the both the desired model and the actual morphing plant. These do not need to correspond, since they are attempting to control different plant models. The solid line shows the actual elevator deflection required to achieve the pitch rate shown in the upper plot. The actuator moves slowly and smoothly, yet is able to stabilize and track pitch rate satisfactorily.

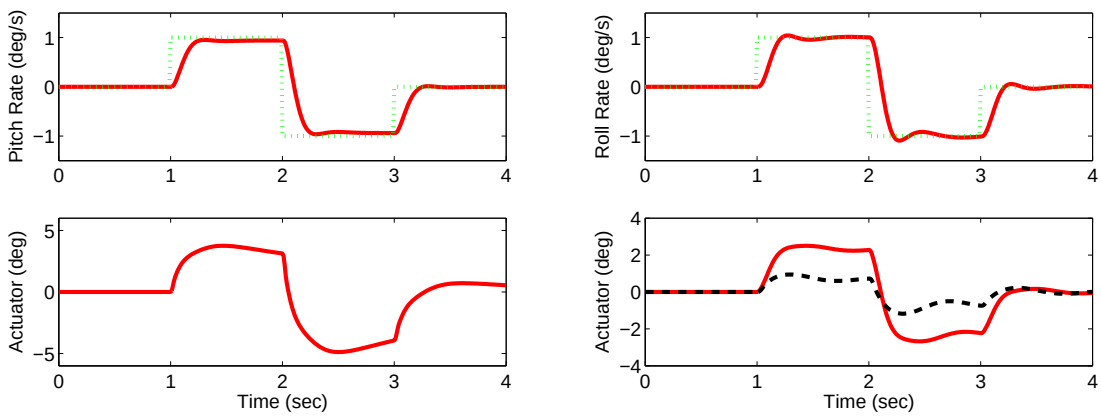

Figure 5-3. Pitch rate pulse (left) and roll rate pulse (right) command simulation for cruise flight. Linetypes: — actual responses and elevator/aileron, - - - rudder, ... command

Figure 5-3-right shows the roll rate response and associated aileron and rudder deflections during a roll rate doublet. As with the pitch response, the roll rate achieves the desired value within *0.25 s* and maintains little error for the duration of the pulse. The control surface deflections are shown in the lower plot. Both aileron and rudder are used to track the roll rate command. The rudder input results from adverse yaw coupling from the ailerons and the penalty on incidental yaw in the controller formulation. Thus, the rudder actuates to reduce the yaw rate and sideslip fluctuations during the roll doublet. The rudder also has proverse roll effects, which assists the ailerons in achieving the commanded roll rate.

5.2.2.3 Maneuvering flight

The optimal morphing angles predicted by Equation 5–1 for the maneuver flight with weights $W_{lat} = 1.0$ and $W_{lon} = 0.5$ are inboard angle $\mu_1 = 5^o$ and outboard angle $\mu_3 = -10^o$.

The requirements of maneuvering flight are dissimilar to the cruise flight objectives in that the aircraft is assumed to be constantly accelerating in pitch, roll, or heading. Maneuvers may require large, rapid control deflections to achieve high rise times and good tracking performance. A maneuvering mode may be appropriate for tasks such as following a target of interest, avoiding an unexpected obstacle, or maneuvering in a densely populated environment.

The maneuvering target model has been specified to emphasize fast dynamics and large force response. The control synthesis weights on the plant outputs and actuators are determined to exploit the high rates and achieve fast maneuvers. The actuation weight penalties have been modified relative to the cruise controller to allow movement at higher frequencies. Additionally, the performance weights are adjusted so that a penalty is assessed on tracking errors, even at high frequencies.

The results of the maneuvering simulation are shown in Figure 5-4. The response to a pitch rate doublet is shown on the left and the response to a roll rate doublet is shown on the right. In both cases, the morphed model achieves a rise time of roughly *0.15 s*. The required actuation for such performance is notably faster than the cruise actuation. Rapid elevator deflection is required at each step, including a small direction reversal at the peak.

The aileron actuation required to achieve the roll performance is also quite rapid, although without the reversal necessary in the elevator actuation. Only a small amount of rudder deflection is necessary to complete the maneuver. The differences between the levels of control actuation in the cruise and maneuvering models is related to the different B-matrices for each condition. The maneuvering model incurs less coupling from aileron actuation to yaw rate and sideforce, and thus requires less corrective rudder.

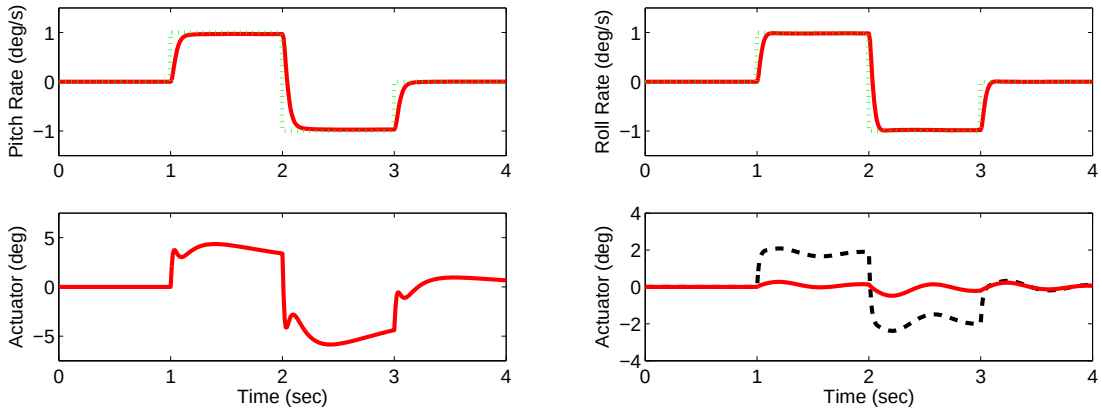

Figure 5-4. Pitch rate pulse (left) and roll rate pulse (right) command simulation for maneuvering flight. Linetypes: — actual responses and elevator/aileron, - - - rudder, ... command

5.2.2.4 Steep descent flight

The optimal morphing angles predicted by Equation 5–1 for the steep descent flight with weights $W_{lat} = 1.0$ and $W_{lon} = 1.0$ are inboard angle $\mu_1 = -25^o$ and outboard angle $\mu_3 = 25^o$.

Flight conditions at high angles of attack cannot be effectively simulated using vortex-lattice method codes or linear models. As a result, the control results presented here are for simple maneuvers at morphing conditions that have been shown in flight tests to be suitable for steep descents. The objectives are simply to track pitch and roll commands fast enough to be useful in maneuvering during a steep dive and recovering to level flight.

Figure 5-5 shows the simulated response of the dive-aircraft to pitch and roll rate doublets. The responses show relatively fast rise times achieved by reasonable levels of elevator, aileron, and rudder actuation. The pitch rate response, shown on the left, exhibits little steady state error. The roll rate rise time is slightly faster than the pitch rate rise time. Both aileron and rudder are used to achieve the roll tracking, especially in the transient phase of the response. The use of rudder is an indication of the increased levels of rudder to roll moment coupling and sideslip to roll moment coupling, both of which will improve the roll rate response of the rudder.

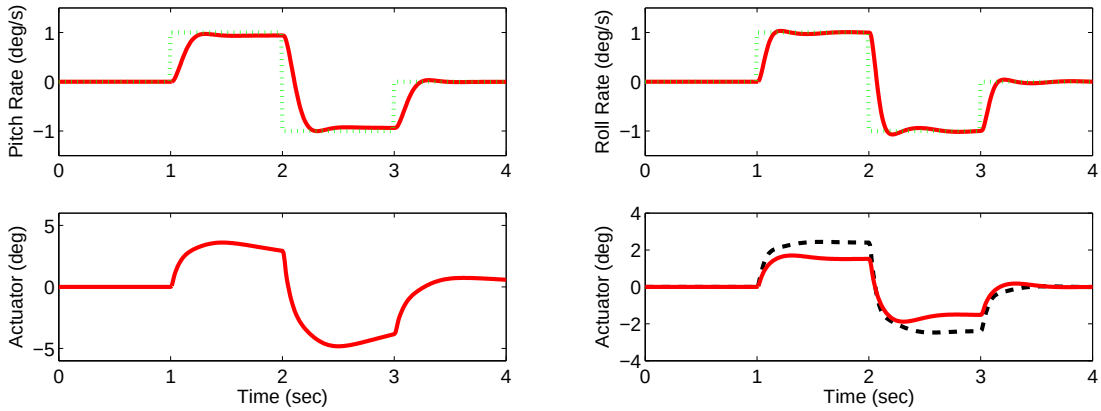

Figure 5-5. Pitch rate pulse (left) and roll rate pulse (right) command simulation for steep-descent flight. Linetypes: — actual responses and elevator/aileron, - - - rudder, ... command

5.2.2.5 Sensor-pointing flight

The optimal morphing angles predicted by Equation 5–1 for the sensor-pointing flight with weights $W_{lat} = 1.0$ and $W_{lon} = 0.1$ are inboard angle $\mu_1 = 25^o$ and outboard angle $\mu_3 = -20^o$.

The final phase of the mission consists of a sensor-pointing task, where the vehicle must decouple the velocity and attitude in order to favorably direct the field of view of a sensor while maintaining a favorable flight path. The example used here of sideslip commands assumes that a target of interest has moved laterally in the field of view. The aircraft will command a sideslip in return the target to the center of the sensor footprint.

A generic unit-step doublet is used to evaluate the sideslip tracking. Figure 5-6 shows the sideslip, roll rate, and yaw rate responses to the sideslip command. The aircraft is constrained to maintain low roll rates while tracking sideslip. The morphing optimization emphasized small sideslip to roll coupling, although some opposite aileron deflection is necessary to counteract the small amount of coupling remaining in the model.

The desired sideslip is achieved in just over 0.3 seconds. The steady-state error in sideslip is very small, indicating good tracking. Some roll rate oscillation is evident in the transient phase of the maneuver, although it is not excessive. Large rudder deflections

are necessary to achieve the desired sideslip. The magnitude of the rudder deflections are perhaps overpredicted due to the small B-matrix values estimated by the aerodynamic code.

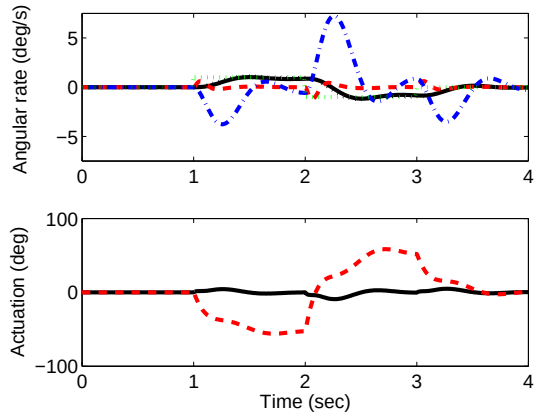

Figure 5-6. Sideslip pulse command simulation for sensor-pointing flight. Linetypes: — sideslip and aileron, - - - roll rate and rudder, -.-. yaw rate, ... command

5.3 Multiple Degree-of-Freedom System

Morphing systems with multiple degrees-of-freedom are more flexible in adapting to disparate mission scenarios. The improved configurability of the wing spans a larger subset of the configuration space at the expense of an increased number of possible shapes. The approach is more versatile in adapting to shapes that are far apart in the space and cannot be easily contained in a single actuator trajectory. However, the increased dimensionality precludes an approach relying on dynamic model and controller storage for each shape, as used in the single degree-of-freedom case.

A linear parameter varying approach can be used to solve the multiple degree of freedom morphing control problem while preserving reasonable memory storage requirements. The approach assumes that the dynamics vary linearly with the morphing parameters. The parameters may be the actuator joint angles for a 4D case or the transformed morphing commands for reduced-dimension cases. A two-dimensional case will be used in developing the control approach, although it may be extended to higher dimensions with some increased complexity and memory capacity.

Controllers are computed at a few points where the dynamics are known and interpolated elsewhere. For dynamics that do not vary linearly, this form of interpolation will introduce modeling errors and may degrade the performance of the controller. However, for small allowances of parametric variation, the approach has been successfully demonstrated, despite having no guarantee of robustness[83].

5.3.1 Optimal-Baseline Adaptive Control

The general architecture used for control of morphing vehicles is model reference adaptive control. The framework allows sufficient flexibility to achieve a high level of performance in the presence of uncertain, shape-dependent dynamics, and varying mission objectives. Optimal control techniques can be used with the MRAC design to achieve known closed-loop characteristics at select design points. For off-design points, the controller adapts to reduce tracking errors and is shown to have Lyapunov stability[94].

Figure 5-7 shows a block diagram of the MRAC architecture for a lateral controller[94]. The input to the system is a vector of external commands, r, for each of the lateral states. A reference model, P_m, represents a set of desirable dynamics which produce favorable state output, x_m, when subject to the external command, r. The state response from the vehicle dynamics, P, is given by vector x, which is used in feedback to the adaptive controller to produce a vector of actuator inputs, u. The difference between the desired and actual responses is given by error, e, and is used to drive the adaptation law. The controller parameters, $\hat{K}$, are adapted in order to change the closed-loop dynamics and reduce the model-following error.

The MRAC structure is extended to encompass a plant model with dynamics that vary with morphing actuator positions, $\vec{\mu}$. The reference model dynamics also change with mission task, M_i, allowing the desired response to match disparate mission objectives. The adaptation function of the controller is preserved, except that a nominal controller, K_o is designed and known for several points in the actuator space, $\vec{\mu}$.

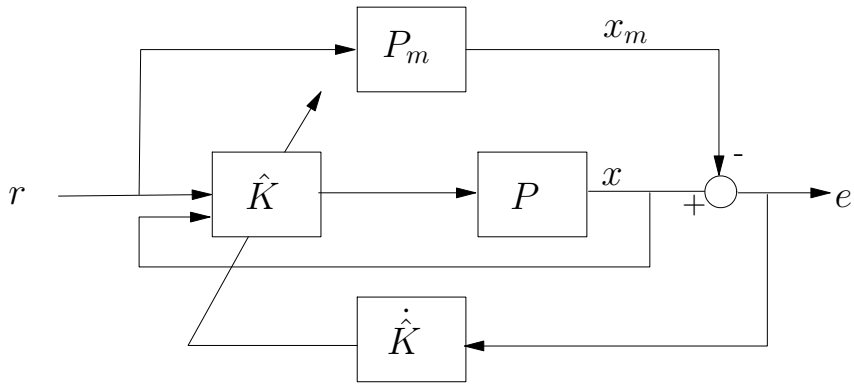

Figure 5-7. Model reference adaptive control (MRAC) architecture for lateral dynamics

MRAC can readily accommodate systems with arbitrary uncertainty in the parameters of the plant model. For the simple case where the plant structure and parameters are known and the reference model is given, the control task reduces to gain scheduling. In such a case, the desired controller can be directly computed by algebraic matrix manipulation.

Systems with known dynamics for all configurations are considered as a separate and somewhat trivial case of the morphing control problem. In general, the aircraft is considered free to change shape and achieve dynamics that are not exactly known to the controller during operation. The general form of the MRAC problem for lateral control requires computing a desired reference model, estimating the dynamics of the aircraft, and adapting the control to reduce disparities between the reference and actual responses.

The dynamics of a general morphing system are represented by,

$$\dot{x}(t) = A(\vec{\mu})x(t) + B(\vec{\mu})u(t) \tag{5–2}$$

Both lateral and longitudinal open-loop dynamics are given in this form in Equations 4–8 and 4–9. The state vector, x, can represent the lateral, longitudinal, or combined states. Control input vector, u, is the output of a controller for the closed-loop system. System matrices, A and B, are dependent on the geometry of the morphing wing.

Equation 5–4 shows the form of the lateral reference model. The structure is similar to the lateral vehicle dynamics in the A-matrix. The B-matrix represents acceleration sensitivities with respect to a series of external commands, r, rather than actuator inputs. The desired states β_m, p_m, and r_m are direct analogs of actual states. The numeric value for each of the reference model terms is computed using modal or derivative shaping procedures.

$$\dot{x}_m = A_m x_m + B_m r \tag{5–3}$$

$$\begin{bmatrix} \dot{\beta}_m \\ \dot{p}_m \\ \dot{r}_m \end{bmatrix} = \begin{bmatrix} \frac{Y_{\beta_m}}{u_0} & \frac{Y_{p_m}}{u_0} & -(1-\frac{Y_{r_m}}{u_0}) & 0 \\ L_{\beta_m} & L_{p_m} & L_{r_m} & 0 \\ N_{\beta_m} & N_{p_m} & N_{r_m} & 0 \\ 0 & 1 & 0 & 0 \end{bmatrix} \begin{bmatrix} \beta_m \\ p_m \\ r_m \end{bmatrix} + \begin{bmatrix} Y_{\beta_r} & Y_{p_r} & Y_{r_r} \\ L_{\beta_r} & L_{p_r} & L_{r_r} \\ N_{\beta_r} & N_{p_r} & N_{r_r} \end{bmatrix} \begin{bmatrix} \beta_r \\ p_r \\ r_r \end{bmatrix} \tag{5–4}$$

The output of the adaptive controller depends on both the external command, r, and on the system states, x. Control input to the plant, u, with gain matrices for both the feedforward and feedback components is given by,

$$u = \hat{K}_x^T x + \hat{K}_r^T r \tag{5–5}$$

Where $\hat{K}_x$ is the adaptive feedback gain and $\hat{K}_r$ is the adaptive feedforward gain.

The control law is included in the open-loop dynamics to yield the closed-loop system given by,

$$\dot{x} = (A + B\hat{K}_x^T)x + B\hat{K}_r^T r \tag{5–6}$$

The convergence of the system output to the desired response depends on the existence of gains, $\hat{K}_x$ and $\hat{K}_r$, to satisfy the model matching condition,

$$A_m = A + B\hat{K}_x^T \tag{5–7}$$

$$B_m = B\hat{K}_r^T \tag{5–8}$$

If A, B, A_m, and B_m are known, $\hat{K}_x$ and $\hat{K}_r$ can be determined algebraically by solving a system of linear equations. Such a method provides a simple gain scheduling approach that can be used to rapidly compute a controller.

For uncertain dynamics, controller adaptation is necessary to achieve the desired performance. The closed-loop system response is compared with the reference model to generate a tracking error, given by,

$$e = x - x_m \tag{5–9}$$

Tracking errors in the response drive adaptation of gain matrices, $\hat{K}_x$ and $\hat{K}_r$. Adaptation laws are designed to guarantee Lyapunov stability in the response and guarantee that all the signals and inputs are bounded. The standard form for the adaptation laws includes step-size and directional parameters, which are used to regulate and tune adaptation behavior. The adaptation laws are given by Wise and Lavretsky[94] as,

$$\dot{\hat{K}}_x^T = -\Gamma_x x e^T P B \tag{5–10}$$

$$\dot{\hat{K}}_r^T = -\Gamma_r r e^T P B \tag{5–11}$$

Where Q, Γ_x and Γ_r are symmetric, positive definite matrices. P is computed by solving the algebraic Lyapunov equation[94]

$$PA_m + A_m^T P = -Q \tag{5–12}$$

The feedback gain matrix, K_x, is initialized as an optimal LQR controller[47] for a design point in the configuration space. K_x is a solution to the LQR cost function[34] and achieves desired performance at the design point, although it does not guarantee robustness to parametric uncertainty.

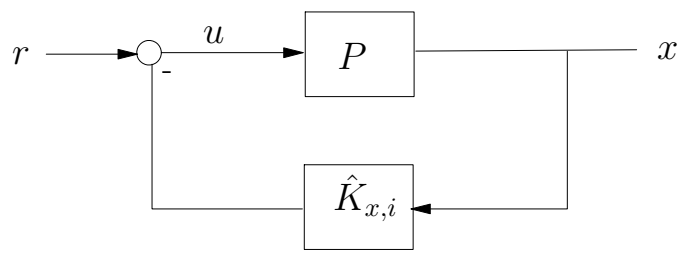

Figure 5-8. Linear quadratic regulator (LQR) controller used for initialization of gain matrix, $\hat{K}_x$.

Equation 5–13 gives the LQR cost functional, which is minimized by finding the optimal control input, u.

$$J = \int_{t_o}^{t_f} \left[x'(t)Qx(t) + u'(t)Ru(t)\right] dt + x't_f Q_f x(t_f) \tag{5–13}$$

Where Q and R are penalty matrices affecting the state error and control actuation power, respectively.

The controller assumes full state feedback and is of the form,

$$u(\cdot) = -Kx(\cdot) \tag{5–14}$$

Where K is the controller gain matrix.

The quadratic regulator problem is easily extended to tracking systems by augmenting the dynamics to include a tracking error state. The tracking LQR system includes a feedforward component from the external command and a feedback component from the state tracking error. The structure is similar to MRAC and is readily used to generate initial gain values for design point configurations.

Gains K_x and K_r are subsequently adapted as the aircraft is reconfigured and the dynamics diverge from the design point model. The gains are reinitialized as the wing configuration returns to a design point. The interpolated gains can also be used as a backup controller in a switching sense. The interpolated controller operates as a phantom system, computing the input and state errors without affecting the actuators. If the state errors are less than the adapted gains for a specified time threshold, the system can switch to the interpolated gains to prevent adaptation divergence and poor performance.

5.3.2 Reference Model Design

The MRAC architecture is based on adapting the closed-loop dynamics to match a desired response. The design method readily accommodates a multi-role mission scenario, since the reference model can be changed for each flight task. Designing an appropriate model response is critical to achieving the desired level of mission performance. Reference model design considers two broad flight conditions of an accelerating phase demanding rapid response and small errors and a benign, non-critical phase tolerant of a slower response and larger errors.

The lateral reference model is designed to achieve pure responses in the roll and dutch roll modes. The two are uncoupled in the design to promote precise control over roll rate, yaw rate, and sideslip. Modal approximations[64] are used to formulate the desired reference dynamic model. The approximations simplify the design process and allow for direct solution of the model in terms of the transient requirements of the mission.

Roll dynamics are approximated by a first-order function relating roll rate and aileron deflection to roll acceleration through roll damping and aileron effectiveness, respectively. The damping term resists roll rate and causes the mode to converge for most conventional aircraft geometries. Roll response dynamics are characterized by a time-constant of the exponential response. A small time-constant indicates large damping and rapid convergence, while a large time-constant indicates the opposite. The first-order roll approximation[64] is given by,

$$\dot{p} = L_p p + L_{\delta_a} \delta_a \tag{5–15}$$

The desired roll damping term, $L_{p,m}$, is related to the mission-specified roll time-constant, $\tau_{r,m}$, and roll mode eigenvalue, $\lambda_{r,m}$, by,

$$L_{p,m} = -\frac{1}{\tau_{r,m}} = \lambda_{r,m} \tag{5–16}$$

The magnitude of the roll time constant lies between the respective requirements for the fastest, most time-critical missions and the slowest, least-time-critical missions.

$$\tau_{fast} \leq \tau_{r,m} \leq \tau_{slow} \tag{5–17}$$

Dutch roll dynamics are more complex than the simple first-order roll response. The dynamics are often oscillatory and heavily coupled between the lateral states. An approximation to dutch roll given by Nelson[64] removes the roll rate component and describes the motion as a coupled response in sideslip, β, and yaw rate, r. The dutch roll dynamics of the reference model are given by,

$$\begin{bmatrix} \dot{\beta}_m \\ \dot{r}_m \end{bmatrix} = \begin{bmatrix} \frac{Y_{\beta,m}}{u_0} & -\left(1 - \frac{Y_{r,m}}{u_0}\right) \\ N_{\beta,m} & N_{r,m} \end{bmatrix} \begin{bmatrix} \beta \\ r \end{bmatrix} + \begin{bmatrix} Y_{\beta_r} & Y_{r_r} \\ N_{\beta_r} & N_{r_r} \end{bmatrix} \begin{bmatrix} \beta_r \\ r_r \end{bmatrix} \tag{5–18}$$

The second-order response can be designed to achieve a desired natural frequency and damping ratio, each depending upon the time-rate and tracking requirements of the mission task. Time-critical missions use a high-frequency, highly damped dutch roll model while benign missions use a lower-frequency model.

The desired natural frequency, $\omega_{n,m}$ and damping ratio, ζ_m, can be readily related to the stability derivatives of the reference model using the relations from Nelson [64],

$$\omega_{n,m} = \sqrt{\frac{Y_{\beta,m}N_{r,m} - N_{\beta,m}Y_{r,m} + u_0 N_{\beta,m}}{u_0}} \tag{5–19}$$

$$\zeta_m = \frac{-1}{2\omega_{n,m}} \left(\frac{Y_{\beta,m} + u_0 N_{r,m}}{u_0} \right) \tag{5–20}$$

The reference model stability derivatives are grouped and scaled relative to the parameters from a nominal model to achieve the desired modal characteristics. Damping derivatives, $Y_{\beta,m}$ and $N_{r,m}$, are grouped and collectively scaled in the computation of the damping ratio. To achieve the desired natural frequency, N_β is varied while the remaining derivatives are held fixed. Y_r remains at the nominal value due to a small relative magnitude.

The expressions relating $Y_{\beta,m}$ and $N_{r,m}$ to nominal parameter values $Y_{\beta,0}$ and $N_{r,0}$ are given by,

$$Y_{\beta,m} = Z_{\omega_{n,m}} Y_{\beta,0} \tag{5–21}$$

$$N_{r,m} = Z_{\omega_{n,m}} N_{r,0} \tag{5–22}$$

Where scale factor $Z_{\omega_{n,m}}$ is given by,

$$Z_{\omega_{n,m}} = \frac{\omega_{n,m}^2 u_0 - Y_{\beta,0} N_{r,0}}{-N_{\beta,0} Y_{r_0} + u_0 N_{\beta,0}} \tag{5–23}$$

Similarly, the expression relating $N_{\beta,m}$ to the nominal derivative, $N_{\beta,0}$, is given by,

$$N_{\beta,m} = Z_{\zeta_m} N_{\beta,0} \tag{5–24}$$

Where the scale factor Z_{ζ_m} is given by,

$$Z_{\zeta_m} = \frac{-\zeta_m 2\omega_{n,m} u_0}{Y_{\beta,0} + u_0 N_{r,0}} \tag{5–25}$$

The scaled stability derivatives are used to compute the desired set of lateral dynamics, where the roll and dutch roll modes are distinct. Since the derivatives are computed using simple algebraic scaling, the modal frequency and damping ratio are direct results of the desired values previously set.

The simplistic desired model does not account for coupling between the modes that is likely to exist in realistic dynamics. This discrepancy can lead to poor adaptation performance, as the system attempts adaptation to an unachievable model. Including some coupling between the modes in the reference model may improve adaptation performance while mostly preserving the desired, uncoupled response.

An extreme logical extension of the reference model design process is individual stability and control derivative shaping, as studied in [1]. Each term is shaped individually to the mission requirements and aggregated in the equations of motion to yield the desired dynamics. This process yields favorable results for simple response, although does not guarantee modal characteristics. Shaping the derivatives directly may cause undesirable oscillatory or unstable responses to occur in the reference model. Conversely, designing the modes directly may command unrealistic stability derivatives. A successful solution may be some combination of both techniques, as in the case of adding light coupling to the designed reference model.

5.3.3 Design Point Gridding

Design points provide anchors of dynamic truth within a sea of parametric uncertainty. They are select locations in the configuration space with known dynamics. The controllers designed at these points will be interpolated for intermediate morphing shapes. The locations and density of the design points affect the accuracy of the linear dynamics assumption, the performance of the resulting closed-loop system, and the memory storage

requirement. Relatively few points must be selected from within the large configuration space to make the interpolation problem tractable.

The locations of the points are chosen such that modeling errors are minimized. A simplistic rectangular grid, for instance, may result in many design points in an area of sparse parametric change or few design points in an area of rapid variation. In the former case, the system uses excessive memory while the latter case causes unacceptable modeling errors and control results.

The use of design points and interpolation is useful even if adaptive control is used. The interpolated controller can provide the baseline compensator which is subsequently adapted to reduce errors. The system can also revert to the interpolated controller if the adaptive system begins to diverge and produce larger errors than the baseline case.

The design point gridding operation can be performed on spaces of arbitrary shape and dimension, including the full, 4D actuator space, a 2D transformed subspace, or a 1D spline trajectory. For illustration, the process is described with respect to a square, 2D grid with 13 configurations along each dimension and 169 possible shapes. The nominal configuration exists at the center of the space, although this is not necessarily true in general.

The gridding procedure identifies points that are parametrically dissimilar as candidate design points. The configuration space is initially seeded with design points at the nominal configuration, the boundary intersections, and the boundary mid-points. These points are included in the design space regardless of parameteric similarity to ensure that boundary conditions are properly modeled.

Starting at the nominal configuration, an outward concentric search is performed to determine the extent of the parametric variation. Configurations immediately adjacent to the nominal configuration are evaluated relatively using,

$$\delta_p = \left| \frac{P_{adj} - P_{nom}}{P_{nom}} \right| \tag{5–26}$$

Where P_{nom} is generally a matrix of parameters from the nominal configuration. The parameters can be stability derivatives or can be a set of performance metrics, in which case P_{nom} is a vector. P_{adj} is a vector or matrix of similar parameters from the neighboring configuration under evaluation, and δ_p is a matrix of relative differences in the parameters.

The parameters by which the space is segmented can be either performance metrics, modal characteristics, stability derivatives, or any other means by which configurations are differentiated. A single parameter results in a segmented space that is easy to visualize and is effectively populated with design points. For multiple, simultaneous parameters, where P_{nom} and P_{adj} are matrices, the variation trends and resulting design spacing are less obvious.

The design point threshold, T_{dp}, limits the allowable parametric variation. The threshold is related to the degree of robustness of the control design. For instance, $T_{dp} = 0.1$ for a controller that is robust to 10% uncertainty in the parameters. If the δ_p for points adjacent to the nominal configuration exceed T_{dp}, then the point is selected as a design point. An upper limit, $T_{dp,max}$ on the threshold can be used to prevents the points from being excessively dissimilar.

The design point criteria is,

$$\delta_p > T_{dp} \tag{5–27}$$

$$\delta_p < T_{dp,max} \tag{5–28}$$

If both conditions cannot be satisfied, then the grid is refined to reduce the parametric variation.

As the configuration search continues concentrically beyond the first layer of shapes around the nominal configuration, the parametric variation metric is changed slightly to,

$$\delta_p = \left| \frac{P_{adj} - P_{nea}}{P_{nea}} \right| \tag{5–29}$$

Where P_{nea} is a matrix of parameters for the nearest design point.

The Euclidean distance between the current point and each of the design points, whether seeded or assigned, is computed throughout the search. The variation metric and threshold then apply to the current and nearest design point, building the grid outward from the center of the space.

As the search reaches the boundaries, the configuration is gridded such that all points are parametrically dissimilar from the nearest design point by a magnitude less than or equal to the chosen threshold. The method guarantees a maximum amount of uncertainty in the interpolated points, which is used in conjunction with known robustness properties of the controllers to infer stability results.

The configuration space is segmented by Delaunay triangles[60], whose vertices are at the design points and whose interiors are spatially most similar to the corresponding vertices. Figures 5-9 and 5-10 show the identified design points for single and multiple parameter cases. Design points are connected to form the Delaunay triangles. The design point grids are shown for several values of threshold parameter, T_{dp}, increasing from left to right. A large threshold for the single parameter case eliminates the need for any design points apart from the pre-seeded nominal and extremal points. The single parameter case shows a relatively sparse point distribution over much of the space. Clustered points indicates areas where the parameter is changing rapidly and exceeding the difference threshold. The multiple parameter case shows a much denser grid. For many parameters whose dependence on the space varies arbitrarily, the design point grid approaches the density of the original configuration space. In such a case, the interpolation offers little computational advantage over a large array of stored dynamic models.

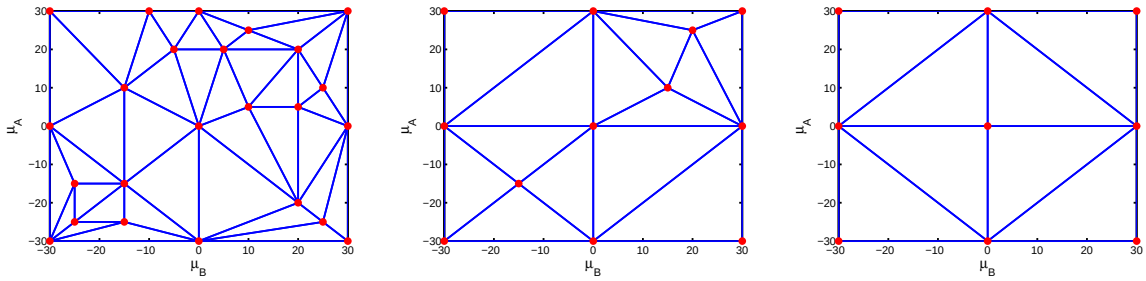

Figure 5-9. Design point grid distribution and triangular segmentation based on lift to drag value. Threshold, T_{dp} is 5% (left), 10% (center), and 25% (right)

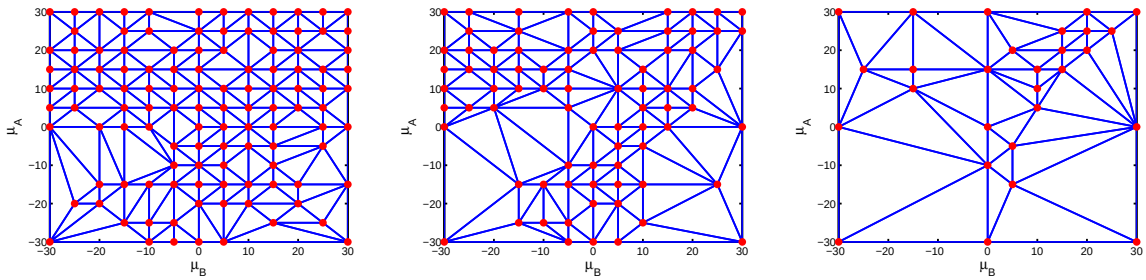

Figure 5-10. Design point grid distribution and triangular segmentation based on lateral stability derivatives. Threshold, T_{dp} is 25% (left), 50% (center), and 200% (right)

The triangle distribution is used to generate an interpolation schedule between the arbitrarily located design points. Vertices of each triangle are co-planar or co-hyperplanar for higher dimensions. Values of points lying in the interior are easily determined by finding the intersection point between a line normal to the configuration space plane and the plane occupied by the three vertices.

Figures 5-11 and 5-12 show surface plots of the triangularly interpolated parameter response compared to the original parameter response surface. The modeling errors, δ_p, are zero at the design point and bounded by $T_{dp,max}$ elsewhere.

The faceting of the surface is a result of the triangular interpolation between the design points. Improper point spacing generates facets that fail to properly represent the parameter variations. Surfaces for the large single-parameter segmentation show deviations from the original data in the region of negative μ_A and positive μ_B. Geometric artifacts, such as false peaks and valleys, stem from the inability to recreate a complex surface

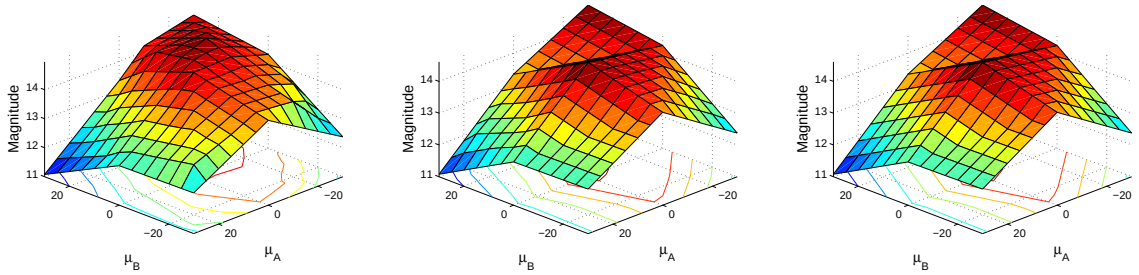

Figure 5-11. Interpolated values for lift to drag based on single parameter segmentation. Threshold, T_{dp} is 5% (left), 10% (center), and 25% (right)

from sparse point spacing. The errors are thus much larger for large values of threshold, T_{dp}. The balance between acceptable errors and computational tractability is ultimately determined with the design of this threshold.

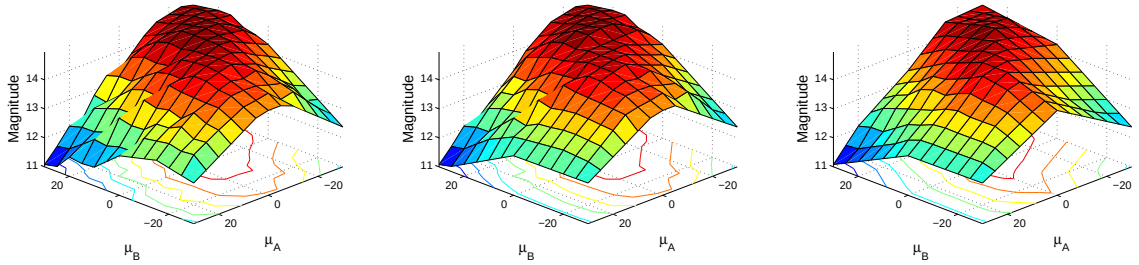

Figure 5-12. Interpolated values for lift to drag based on multiple, simultaneous parameter segmentation. Threshold, T_{dp} is 25% (left), 50% (center), and 200% (right)

Narrow threshold of the multiple parameter segmentation achieves accurate surface reproduction. The number of required design points may be prohibitively large, especially with limited error tolerance. The simultaneous variation of nearly 30 parameters, each having a unique dependence on the morphing, creates a significant challenge in segmenting the configuration space based on interpolated errors. Selective use of parameters may offer improvements in storage and computation requirements by emphasizing the terms which have the largest affect on the stability and performance.

5.3.4 Simulation Results

Simulations of the maneuvering controller are performed with various commanded trajectories and reference models. Each system is morphed from the optimal cruise

configuration to the optimal maneuvering shape along a predetermined path through the 4-dimensional actuator space. Feedback control gains are initialized for each simulation using LQR synthesis and subsequently adapted, along with the feedforward control gains.

Figure 5-13 shows the permissible trajectories through the 4-dimensional configuration space for three morphing operations. The trajectories permit morphing between configurations optimized for cruise, maneuverability, and agility. μ_1, μ_2, and μ_3 are represented spatially with projections shown on the space boundaries for clarity. μ_4 is represented in colorspace as hue and is indicated by a colored marker at each intermediate trajectory. Dynamic criteria is applied in the computation of the actuator paths and yields intermediate configurations with satisfactory stability characteristics.

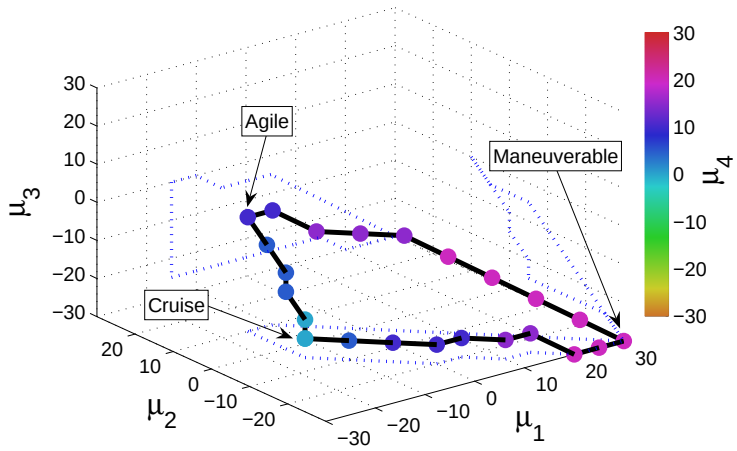

Figure 5-13. Permissible 4D actuator trajectory between three disparate configurations

Figure5-14 shows a set of simulation results for a morphing system tracking the response of a fixed reference system. Histories for states β, p, and r are shown in the left plots for the morphing aircraft (top) and the reference model (bottom). A low-frequency, small-amplitude roll rate sinusoid is used as a reference input, which causes some coupling to the remaining lateral states due to off-diagonal terms in the reference model control-effectiveness matrix.

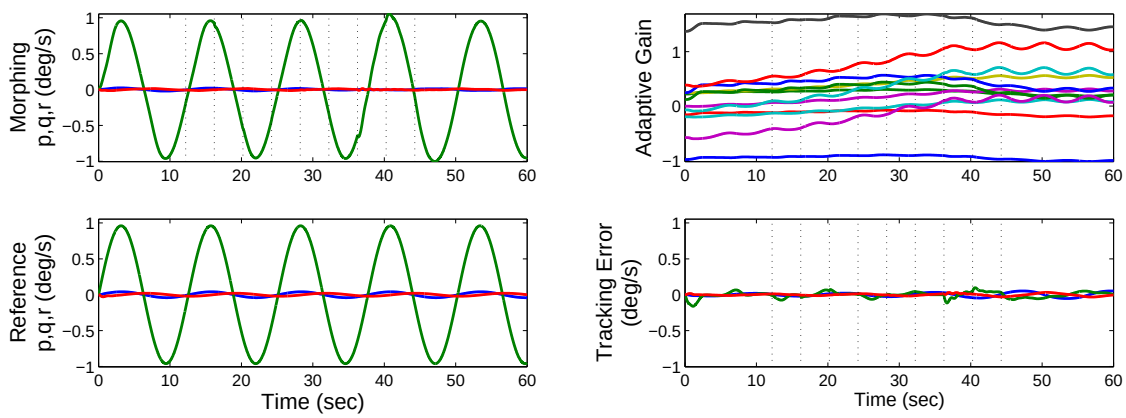

Figure 5-14. Control results during cruise to maneuvering reconfiguration with a sinusoidal trajectory command. A) Angular rate response of morphing and reference model systems. B) Gain adaptation and tracking errors

The morphing aircraft has an initial response that generates small error relative to the reference response. Gains adapt slightly until the first morphing increment is commanded at $t = 13.2 seconds$. The morphing is commanded discontinuously, where the dynamics are switched in a discrete step between time intervals. The relatively large 5° angular resolution of the morphing joints contributes to a large change in the dynamics and contributes to tracking errors as the dynamics switch.

Discrete morphing events are indicated by vertical dotted lines and occur every 4 seconds until the aircraft has morphed into the maneuverable configuration. Shape change contributes to variations in the closed loop system and causes tracking errors. The errors drive gain adaptation using the gradient descent method, which subsequently improves tracking performance. Gains continue adapting until the aircraft reaches the final shape.

Figure 5-15 shows simulation results for a similar morphing trajectory and constant reference system subject to a variable-frequency roll rate command. Gain adaptation occurs rapidly following morphing operations, but applies selectively to certain gains. The morphing model achieves good tracking performance throughout the shape-change, although incurs some cyclical error in the final configuration. The error contributes to oscillatory gain adaptation. Such undesirable behavior may be reduced with the application of deadband modification to the adaptation laws[94].

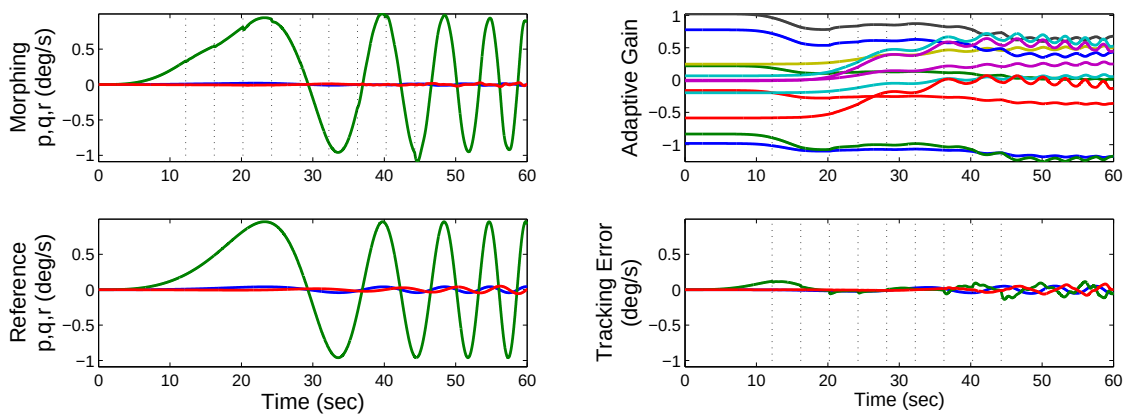

Figure 5-15. Control results during cruise to maneuvering reconfiguration with a variable-frequency trajectory command. A) Angular rate response of morphing and reference model systems. B) Gain adaptation and tracking errors

The adaptive morphing controller can tolerate large initial errors in the baseline controller and large variations in the dynamics. Figure 5-16 shows time histories for state, error, and gain trajectories for a model with a poor initial controller design. Initial response incurs large errors are rapid adaptation in the controller gains. The first morphing operation at $t = 13.2s$ involves a large discontinuity with joint actuations exceeding 5°. The gains adapt further to stabilize the new dynamics and reduce the large transient error. The controller achieves reasonable tracking performance for subsequent morphing and fixed configurations.

Although the controller successfully stabilizes a model with severe initial errors, this strategy is not recommended for use in a flight test vehicle. Poor baseline controllers and rapid dynamic variations both cause tracking errors that require several seconds of adaptation to subside. The criticality of this adaptation time depends greatly on the vehicle and flight condition. Adaptation times greater than several seconds may lead to loss of control or unintended interaction with surrounding obstacles.

The success of a morphing aircraft in tracking a fixed reference system demonstrates the versatility of the control system. The constant reference, however, may violate disparate mission constraints and reduce the effectiveness and function of morphing. A

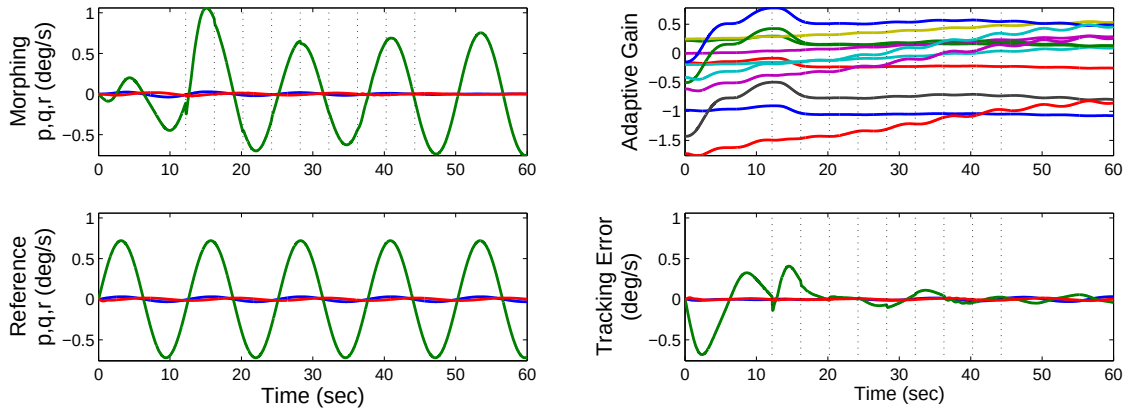

Figure 5-16. Control results during cruise to maneuvering reconfiguration with a sinusoidal trajectory command and poor initial control design. A) Angular rate response of morphing and reference model systems. B) Gain adaptation and tracking errors

more realistic approach uses a mission-dependent reference model in order to emphasize either conservatism or performance.

Figure 5-17 shows the responses of an aircraft morphing from a cruise configuration to a maneuvering configuration. The reference model initially uses a long time constant in both the roll and dutch roll modes. At $t = 30s$, the reference model switches discretely to shorter time constants in both modes and slightly higher damping in the dutch roll mode. The change in the reference model occurs in near the midpoint of the morphing operation between discrete shape changes. A vertical dashed line indicates the reference model change, which is accompanied by tracking errors and rapid gain adaptation. The controller summarily adapts to the higher-performance model and achieves good tracking results. Controller gains continue to adapt with each subsequent morphing and achieve relatively constant values for the maneuvering configuration.

The transient behavior observed during the reference model switching is partially a result of discontinuities in the aileron and rudder deflections. A rate filter on the aircraft controls and an improved switching technique would prevent large errors from inciting rapid control and state responses. Despite the error, the system recovers quickly and stabilizes the aircraft.

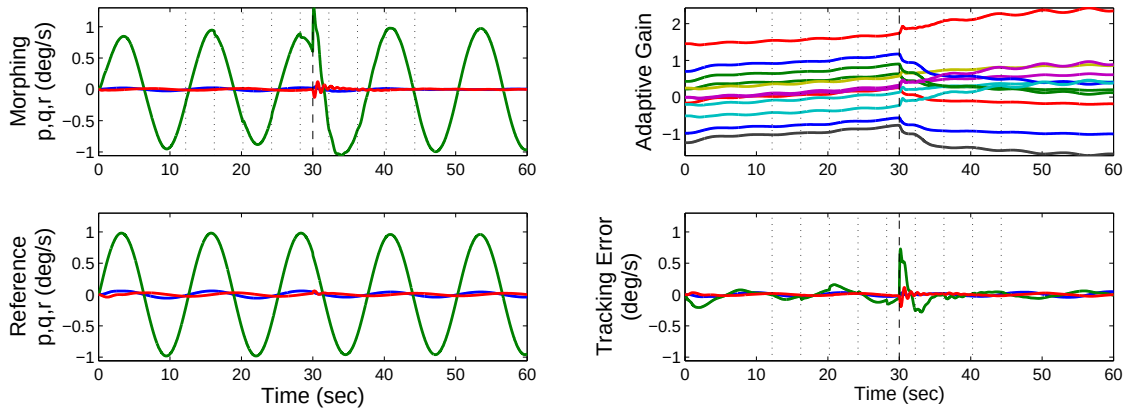

Figure 5-17. Control results during cruise to maneuvering reconfiguration with a sinusoidal trajectory command. A) Angular rate response of morphing and variable reference model systems. B) Gain adaptation and tracking errors

The multiple-reference model, morphing system is subject to a chirp command, which is a sinusoid whose frequency increases with time. The chirp simulates benign motions of the cruise condition initially and develops into rapid motions for maneuvering flight. Figure 5-18 shows simulated control results for the system. Roll rate command is slowly increased, which allows the morphing aircraft to easily achieve tracking even in the presence of controller errors. The gentle command violates the persistence of excitation condtion[50][94] and fails to adapt the controller gains. Morphing changes generate tracking errors due to the switch dynamics and invoke gain adaptation. The adaptation rate increases somewhat with the increasing frequency of the commanded roll.

Tracking errors occur during the reference model switching, causing the gains to adapt rapidly in response. Adaptation continues as the aircraft completes the morphing operation and tracks the chirp command in the maneuvering configuration. Closed-loop performance is good throughout the simulation, apart from the error excursion during the reference model switch and cyclical errors in the high-frequency rate tracking.

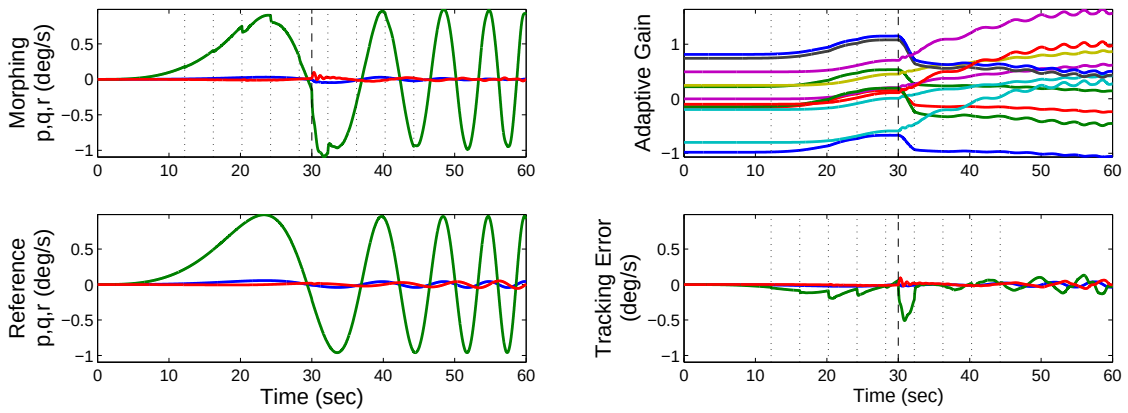

Figure 5-18. Control results during cruise to maneuvering reconfiguration with a variable-frequency trajectory command. A) Angular rate response of morphing and variable reference model systems. B) Gain adaptation and tracking errors

CHAPTER 6
OPTIMAL CONTROL

The morphing aircraft adaptation and control problem can be solved partly or entirely using optimal control techniques. Optimal control finds the desired state trajectories and control inputs to minimize a performance index when subject to boundary and path constraints. The framework is well suited for computing optimal solutions for systems with variable dynamics, control objectives, and multiple phases. The formulation allows as inputs the states, vehicle shape, and control surface deflections.

In computing the optimal inputs, the technique can be used to determine the state trajectories required for a desired maneuver[41][49], the optimal shape variation throughout one or more missions, or the required inner-loop compensation for the changing vehicle dynamics. Solving the optimal control problem becomes progressively more complicated as the number of inputs and states increases.

This chapter considers several variations of the problem, where the optimal control is used either in conjunction with the developments from previous chapters or in place of them. For instance, the section on rate trajectory generation strictly commands the inner-loop rates to perform part of a mission-task maneuver. The inner-loop stabilization and tracking is achieved by an independent controller while the vehicle shape is adapted by an independent adaptation law.

Adaptation can be included in the problem such that the trajectory and morphing shape are solved simultaneously. In such a case, the trajectories are modified according to the performance capabilities of the permissible shape. Maneuvering controllers are used independently to stabilize the shape-changing vehicle and track trajectory commands.

Complete consideration of the problem commands states, morphing, and control surfaces simultaneously. The unified framework for path planning, shape adaptation, and inner-loop control can achieve the optimal solution for a particular set of cost functions, although at considerable computational expense. The performance of the unified controller

can be compared to that of individual control components to examine possible benefits and complications.

Optimality is not guaranteed, since a direct numerical method is used with no costate information. Convergence is also not guaranteed with the unified scheme. The optimal control methodology may be most useful in a mission-planning context, while separate systems may be implemented using the optimal solution as guidance. Isolating the system control and adaptation with multiple time-scales may provide the most dependable performance.

Solutions to optimal control problems are evaluated relative to a performance index, which is a cost functional relating state and input trajectories to the performance metric. The performance index is minimized for the optimum set of trajectories. The performance index is also subject to the boundary and path constraints of the problem, such that only physically realizable trajectories are admissible as possible solutions.

Performance and maneuvering metrics by which morphing aircraft are adapted are readily used in the optimal control performance indices. Additional spatial and temporal metrics are established from mission environments. The combined cost functional relates aircraft capability and mission requirements and is used to find solutions for objectives such as,

- Minimum power/energy consumption
- Minimum time enroute
- Maximum maneuverability
- Minimum area maneuvering
- Minimum path deviation

The general form for the performance index[73] is,

$$J = \Phi(x(t_0), t_0, x(t_f), t_f) + \int_{t_0}^{t_f} \mathcal{L}\left[x(t), u(t), t\right] dt \tag{6–1}$$

where t_0 is the initial time, t_f is the final time, x is the state vector, u is the control vector, Φ is the constraints vector, and $\mathcal{L}$ is the Laplacian of the system parameters.

The system dynamics are first-order and quasi-static with parametric dependence on morphing configuration.

$$\dot{x} = f(x, u, \vec{\mu}, t) \tag{6–2}$$

The rate of morphing is limited to isolate the adaptation time-scales from the aircraft and controller dynamics. Rate limits on the morphing actuation are established using a design threshold, $T_{\dot{\vec{\mu}}}$. The allowable value of this threshold is determined by iterative simulation. Adaptability constraints are necessary to preserve the quasi-static assumptions used in formulating the dynamics and control strategies.

$$\left|\dot{\vec{\mu}}\right| \leq T_{\dot{\vec{\mu}}} \tag{6–3}$$

The initial and terminal constraints must satisfy,

$$\phi(x(t_0), t_0, x(t_f), t_f) = 0 \tag{6–4}$$

The trajectories are subject to path constraints

$$g(x(t), u(t), \vec{\mu}(t), t) \leq 0 \tag{6–5}$$

6.1 Rate Trajectory Generation

A straightforward application of optimal control to morphing is generating the inner-loop rate commands required to follow a desired flight path. Neither the vehicle shape nor the actuated surfaces are directly controlled. Rather, the state trajectories are

idealized and force the aircraft to morph in order to sustain tracking. Changing aircraft shape subsequently changes the dynamics, which requires adaptation in the controller to maintain stability and control. Each of the processes invoke disparate control systems, which operate independently. The optimality exists only in the state trajectory, which is subject to mission-specific temporal and spatial constraints.

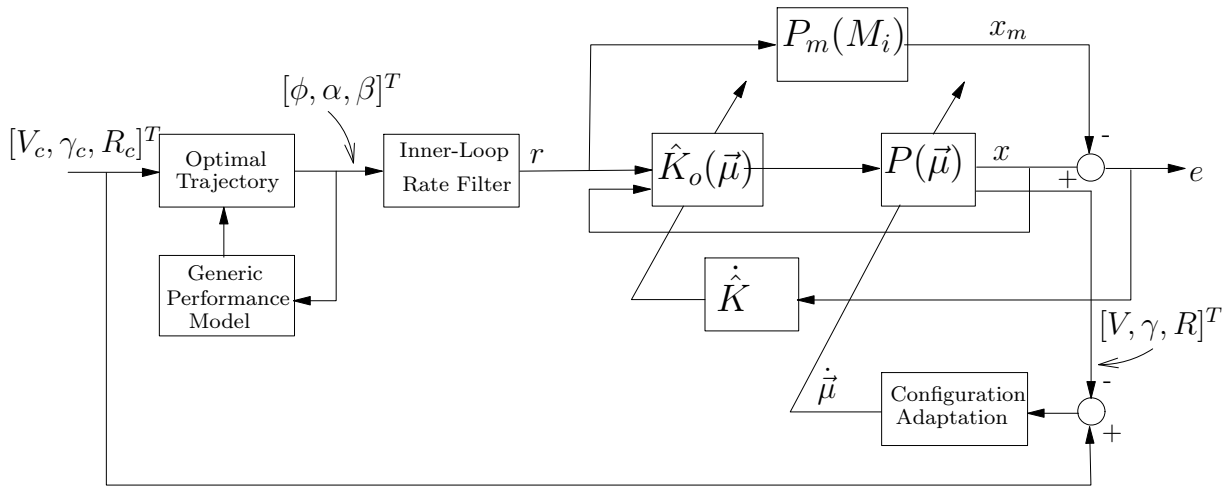

Figure 6-1. Optimal rate trajectory framework with independent flight control and shape adaptation processes

A fictitious dynamic model is used in the formulation of the optimal trajectory. The model achieves maximum performance in all performance and maneuvering metrics. Although knowingly unrealistic for a single configuration, the model permits an aggressive trajectory that is achievable for an aircraft that changes shape appropriately. Tracking errors resulting from configurations unable to follow the trajectory drive adaptation and allow subsequent improvements in tracking performance.

The optimal control solves for trajectories of angle of attack, sideslip, and roll angle to produce accelerations necessary to follow the desired flight path. Vertical and lateral forces are used to determine the flight path based on a 3 degree-of-freedom model[78] given in Equations 6–6, 6–7, and 6–8.

$$\dot{V} = [X(\cos\alpha\cos\beta) + Y(\sin\beta) + Z(\sin\alpha\cos\beta) - g\sin\gamma] \tag{6–6}$$

$$\begin{aligned}\dot{\gamma} =& (1/V)[X(\cos\alpha\sin\beta\sin\phi + \sin\alpha\cos\phi) \\ & - Y(\cos\beta\sin\phi) + Z(\sin\alpha\sin\beta\sin\phi - \cos\alpha\cos\phi) - g\cos\gamma]\end{aligned} \tag{6–7}$$

$$\begin{aligned}\dot{\psi} =& (1/V\cos\gamma) + [-X(\cos\alpha\sin\beta\cos\phi - \sin\alpha\sin\phi) \\ & + Y(\cos\beta\cos\phi) - Z(\sin\alpha\sin\beta\cos\phi + \cos\alpha\sin\phi)]\end{aligned} \tag{6–8}$$

Accelerations X, Y, and Z are generated from the fictitious performance model through variations of angle of attack and angle of sideslip. The stability coefficients used to relate flight angles and forces are the maximum performance values among all configurations.

The commanded trajectories for roll angle, angle of attack, and sideslip are used to generate inner-loop commands to roll rate, pitch rate, and yaw rate. A rate filter acts as on outer-loop and uses linear gains to command each of the rates from angular tracking errors. Saturation is implemented in the filter to limit the magnitude of the command.

A baseline controller tracks inner-loop rate commands with reference to a mission-specific dynamic model. The baseline controller is scheduled on morphing configuration, which is externally adapted. The controller gains adapt to reduce errors between the reference model response and the current model response.

Control deflection limits bounds the vehicle response rates and will introduce flight path errors when the morphing configuration is unsuitable for the desired mission. Tracking errors in airspeed, flight path angle and turn radius drive the external adaptation mechanism, which seeks configurations that achieve higher mission performance.

6.2 Trajectory and Adaptation

An extended implementation of optimal control theory includes the nonlinear dynamic variation due to morphing in the problem formulation. The controller solves for both the trajectory and the wing shape. The distinct advantage over the earlier method is that the

effects of morphing are used explicitly in determining the desired trajectory. Thus, the versatility of the shape change is exploited along the flight path to achieve a high level of performance. Maneuvers, whether aggressive or benign, are commanded simultaneously with the appropriate configuration.

The vehicle dynamics can include morphing throughout all or a subset of the configuration space. Dimensionality reduction techniques can be applied to reduce the problem complexity. With appropriate design, the subspace permits a high level of performance with considerably lower computational cost than the full space.

Morphing configuration is considered as an input and is optimized by the controller with respect to the performance index and constraints. Including effects such as lift, drag, and energy consumption in the cost allows the controller to achieve find efficient shape and flight path solutions. Adding elements such as temporal and spatial costs yields solutions that are both efficient in time and energy. In seeking the lowest cost, the controller will automatically seek maneuverable configurations for the transient flight phases and efficient configurations for steady phases.

Although the optimal solution is determined using a direct, numerical method, an indirect method is used to gain insight into the problem structure. Specifically, the first order optimality conditions are formulated to show the dependence of the problem on the morphing configuration. A 1-dimensional configuration space is used for simplicity, where the vehicle dynamic parameters vary along separate 4th-order functions with respect to the singular morphing actuation.

The functional-dependence of the parameters on morphing are used explicitly in the optimility conditions. The desired state and input trajectories and associated performance index relate heavily to the choice of morphing shape. Since the shape is controlled by the optimal system, it can be reconfigured along the trajectory such that the solution achieves a minimal cost.

Figure 6-2 shows the architecture of an optimal controller for rate trajectory and shape adaptation. The external morphing command block is replaced with an expanded optimal system that adapts the wing shape directly. The inner-loop rate filter operates as before, operating on the flight angle output of the optimal controller and generating limited rate commands to the aircraft. The rate commands are used in the adaptive, model-reference design to generate the desired system response. The controller gains subsequently adapt to reduce errors in the tracking performance of the reconfigured aircraft.

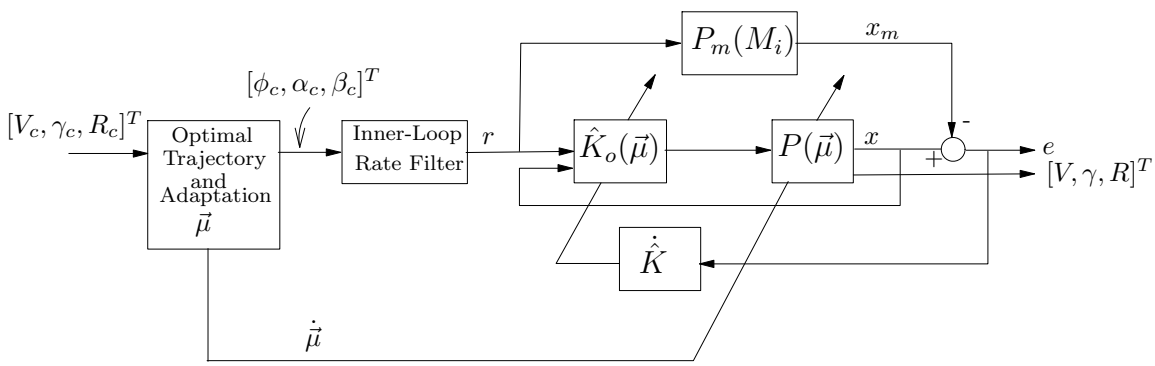

Figure 6-2. Optimal rate trajectory and shape adaptation framework with independent flight control

6.3 Trajectory, Adaptation, and Control

A complete implementation of optimal control for a morphing aircraft replaces both the control and adaptation functions. The system yields the desired flight path, morphing configuration, and control surface deflection throughout the mission. The addition of stabilizing tasks requires the controller to operate at a rate equivalent to the vehicle dynamics. An increase in the controller rate significantly increases the computational burden relative to the sporadic control allowed by the quasi-static morphing. The unified optimal control architecture is presented for completeness, although with critical limitations in practicality acknowledged by the author.

Flight dynamics linearized for each configuration are included in the problem formulation. Variations in the lateral and longitudinal parameters are modeled over the allowable

configuration space, which may be the original actuator space or a subspace. Estimated functional dependencies are given for low-dimensionality spaces while smoothed look-up tables are given for higher-order space.

The state and input orders increase markedly due to the inclusion of angular rates, linear velocities, and control surface deflections. The stability and control derivatives each are affected by the morphing. Additional parameters are needed to establish the dependencies of these derivatives on morphing.

The complete problem structure becomes somewhat cascaded due to the disparate time scales affecting the states and inputs. Bang-bang behavior may be observed in the lower-level controls, such as the elevator, when the system is subject to extreme actuator commands. A rate filter may alleviate actuator excitability, although this may undermine the optimality of the solution.

CHAPTER 7
MISSION RECONFIGURATION

7.1 Mission Tasks

An urban mission may consist of disparate maneuvering tasks with each having unique dynamic and aerodynamic requirements. Each task requires the vehicle to optimize one or more metrics in order to achieve a high level of performance. The maximization of each metric occurs at a particular geometric configuration and flight condition.

The mission tasks selected for simulation reflect the shift in UAV use towards a multi-role reconnaissance vehicle which is capable of efficient loitering, target pursuit, and maneuvering in a complex urban environment. The most basic requirement is that the vehicle must be easily operable by a remote pilot for deployment and recovery. Once aloft, the vehicle must cruise efficiently to an area of interest or loiter efficiently awaiting commands. An aggressive maneuvering mode is also required to avoid obstacles or pursue elusive targets. Other requirements include relatively inefficient modes that enable steep descents or large sideslip trim angles for sensor pointing.

7.1.1 Deployment and Recovery

The beginning and end of every UAV mission requires vehicle deployment and recovery, respectively. The ground station may be situated in an environment with a small clearing surrounded by trees, buildings, poles, or other obstacles generally hazardous to UAVs. The deployment of small UAVs is mostly performed without a runway by hand-launching or catapult-launching. Either method initiates the flight in an often-precarious situation of low airspeed and unusual attitude. The aircraft must be quickly stabilized into a climb to clear surrounding obstacles and accelerate to normal flying speed. Even operations in unobstructed areas require care in piloting during the first few moments after launch.

The complexity of the launch environment often mandates that the vehicle is manually piloted by a remote operator for the deployment and initial maneuvers. Such remote piloting requires that the aircraft respond predictably to control inputs and achieve a

high level of performance to enable maneuvers at low airspeeds. The handling qualities requirement can be represented by a range of allowable time constants, damping ratios, or natural frequencies for each of the dynamic modes. The performance requirement can be represented by an aerodynamic metric such as lift-to-drag ratio. A suitable deployment configuration is then one that achieves the highest lift to drag ratio while possessing acceptable dynamic characteristics.

Figure 7-1 shows the simulated configuration for piloted takeoff and landing. The shape has a relatively high lift-to-drag ratio of 14.6 in addition to good handling qualities for both lateral and longitudinal modes. The wing has increasing aft sweep toward the tip, with -5° on the inboard section and -10° on the outboard section. It uses an inverted gull-wing shape with -5° anhedral on the inboard section and 10° dihedral on the outboard section.

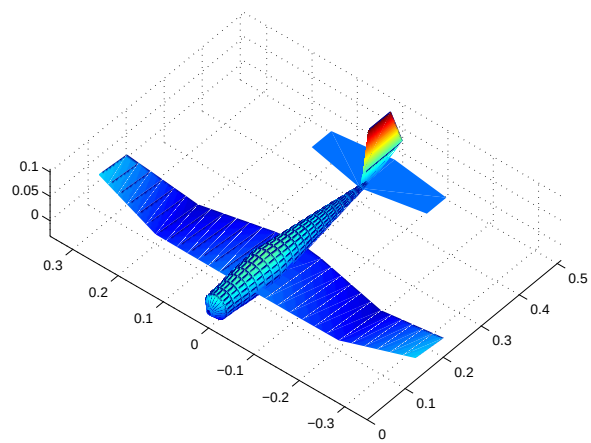

HQC: $\mu_1 = -5^o$, $\mu_2 = -5^o$, $\mu_3 = 10^o$, $\mu_4 = -10^o$

Figure 7-1. Manually piloted deployment and recovery configuration

7.1.2 Long Range Cruise

A non-critical phase of most missions is a cruise segment where the vehicle travels from one area of interest to another. The metric by which cruise flight is assessed is typically energy efficiency per unit distance traveled, assuming that this task does not include reconnaissance or time-critical objectives. The most efficient cruise for an aircraft is achieved at the maximum lift to drag ratio, which is given by Equation 7–1 [7]. Equation

7–2 shows the Breguet Range formula, which gives an estimate for the range based on aircraft aerodynamic, propulsion, and structural characteristics [40].

$$\frac{L}{D} = \left(\frac{\rho_\infty {V_\infty}^2 C_{D,0}}{2(W/S)} + \frac{2K}{\rho_\infty {V_\infty}^2} \frac{W}{S} \right)^{-1} \tag{7–1}$$

Where L is lifting force or coefficient, D is the drag force or coefficient, V is the velocity, $C_{D,0}$ is the zero-lift drag coefficient, W is the weight, S is the wing area, $\rho_\infty$is the dynamic pressure, and K is the drag-polar coefficient.

$$Range = V_\infty \frac{L}{D} I_{sp} \ln \left(\frac{W_{initial}}{W_{final}} \right) \tag{7–2}$$

Where I_{sp} is the specific impulse, $W_{initial}$ is the initial weight and, W_{final} is the final weight. For battery-powered aircraft with no deployable payload or ordinance, the initial and final weights are expected to be identical, since no fuel is exhausted by the propulsion system.

Figure 7-2(b) shows the configuration that achieves the maximum lift-to-drag ratio using the stable dynamics criteria. The wing uses spanwise-increasing anhedral and slight aft sweep to produce an open-downward crescent shape. The configuration closely resembles that of birds such as albatrosses, pelicans, or seagulls gliding for extended periods or close to the water surface. Figure 7-2(a) shows a seagull gliding for an extended length in ground effect. It is also similar to the NASA Langley Hyper-Elliptical Cambered Span wing, which was reported to achieve a 15% greater lift-to-drag ratio than a similarly scaled conventional wing[22].

The configuration which achieves the most distance-efficient cruise also serves an important function for gliding operations. Both maximum range and shallowest angle of glide are achieved by maximizing the lift to drag ratio. The metric by which glide performance is gauged is typically glide ratio, which compares the horizontal distance traveled to the altitude loss during a portion of the glide. The glide ratio is equal to

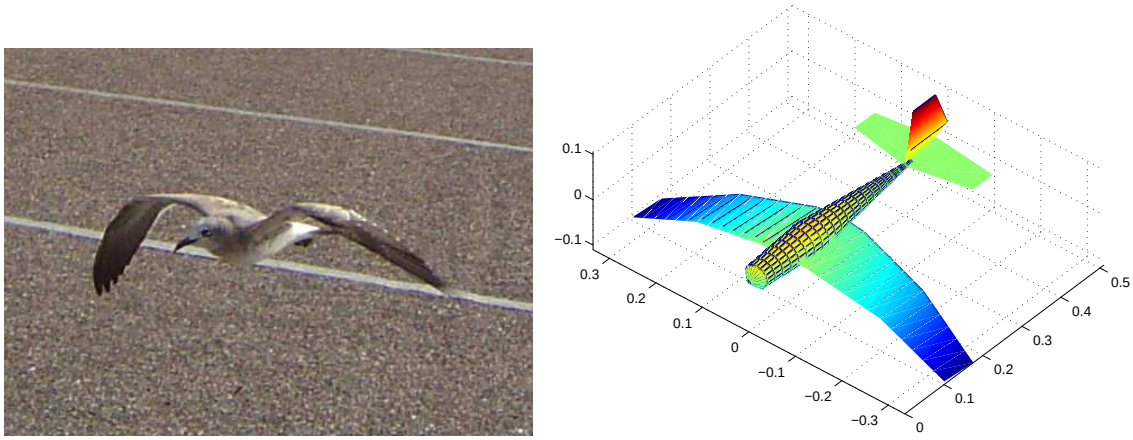

(a) Seagull gliding in vicinity of ground (b) SDC: $\mu_1 = -15^o$,$\mu_2 = -5^o$,$\mu_3 = -25^o$,$\mu_4 = 0^o$

Figure 7-2. High lift seagull wing shape (left), Maximum lift to drag configuration (right)

the lift to drag ratio during unaccelerated gliding flight, so an aerodynamically efficient configuration allows the vehicle to glide for a long distance.

Gliding flight is not normally invoked during either manned or unmanned operations, although it may become useful for exploiting atmospheric currents to improve the range and endurance of a UAV[6]. Researchers are currently evaluating the performance of an autonomous glider which seeks rising currents of air on which to stay aloft. Extended flight durations may be possible by alternating between powered and gliding modes. Glides are frequently used by larger birds to fly without flapping. Both thermal and deflected winds are exploited by birds of prey and sea-borne birds as sources of energy for extended periods of gliding flight[91]. The range configuration and others can be used for different phases of gliding flight for a UAV.

7.1.3 Endurance Loiter

A variation on the range cruise is the endurance loiter, which maximizes energy efficiency relative to time rather than distance traveled. The flight condition is appropriate for persistence operations, where the vehicle must maximize time aloft or minimize energy consumption during the mission segment.

Equation 7–3 [40] shows an estimate for power required in level flight as a function of aerodynamic characteristics and airframe geometry. The configuration which achieves the minimum power required is also the highest endurance and most energy-efficient.

$$P_{req} = \frac{1}{2}\rho V^3 S C_{D_0} + \frac{W^2}{\frac{1}{2}\rho V S}\left(\frac{1}{\pi e AR}\right) \tag{7–3}$$

The endurance flight task is generally employed when the vehicle is not required to traverse large distances or perform specific maneuvers. It may be used when loitering over an area while awaiting commands or providing persistent surveillance of a region of interest. It can also be used if the aircraft operates as a communications repeater, which requires that the aircraft stay within a confined region for long periods of time.

Figure 7-3(a) shows the configuration for endurance cruise and minimum unpowered rate of descent. The shape is very similar to the nominal configuration apart from 10° dihedral on the wingtips. The non-uniform dihedral is similar to competition sailplane wings, which are also optimized for minimum power required in gliding flight with handling qualities constraints[52]. The configuration requires 2.503 *watts* to maintain flight.

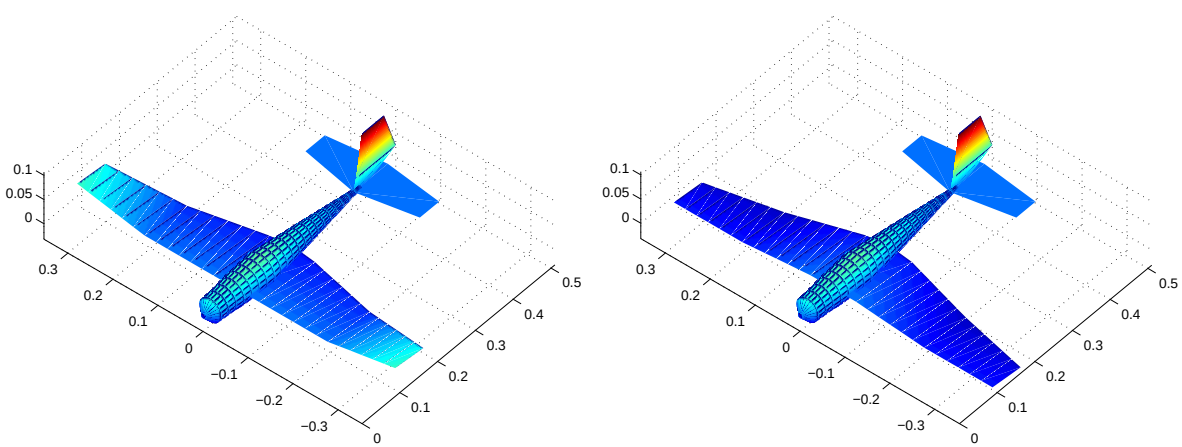

(a) HQC: $\mu_1 = 0^o$, $\mu_2 = 0^o$, $\mu_3 = 10^o$, $\mu_4 = 0^o$ (b) SDC: $\mu_1 = -5^o$, $\mu_2 = 0^o$, $\mu_3 = 0^o$, $\mu_4 = 0^o$

Figure 7-3. Maximum endurance and minimum rate of descent configuration

Using both the stable and unstable dynamics criteria, the endurance configuration changes slightly to anhedral on the inboard wing and nominal joint angles elsewhere, as shown in Figure 7-3(b). The relaxed criteria require 2.497 *watts* for level flight, marginally less power than the shape generated based on handling qualities. The improvement is not significant and comes at the expense of pilotability. For an automatically controlled aircraft, however, this issue is not an important consideration.

The minimum-power-required configuration is also the best shape for maximizing glide duration. An unpowered aircraft achieves equilibrium by using the loss of potential energy to oppose the power required to maintain flight[9]. Minimizing the power required thus minimizes the loss of potential energy and minimizes the rate of descent.

The lowest rate of descent configuration allows an unpowered aircraft to stay airborne for the longest time. The condition is useful for exploiting atmospheric currents as energy sources or increasing the decision time for contingencies in the event of powerplant failure. The configuration are most frequently seen in birds using thermals to loiter over an area in gliding flight.

7.1.4 Direction Reversal

Successful operation in a crowded environment depends on the ability of a flight vehicle to change direction in a confined area. The minimum radius turn performance is an appropriate metric for gauging the ability of a vehicle to avoid obstacles or reverse course. Equation 7–4 shows the radius of turn is reduced for low airspeeds, large lifting forces, and steep angles of bank. Equation 7–5 shows that wing loading, W/S, and drag must be low to achieve a small radius turn. Thrust force, T, must be also be maximized to compensate for the increased drag as the aircraft banks to perform a turn. Thrust is constant for all simulations to focus on the role of morphing in effecting the flight performance.

$$R = \frac{mV^2}{L \sin\phi} = \frac{V^2}{g \tan\phi} \tag{7–4}$$

$$R_{min} = \frac{4K(W/S)}{g\rho_\infty (T/W)\sqrt{1 - 4KC_{D,0}(T/W)^2}} \tag{7–5}$$

The configuration which achieves the minimum radius turn when subject to the handling qualities criteria is identical to the HQC maximum endurance wing shape shown in Figure 7-3(a). The weight and thrust forces are assumed constant for all configurations. The large wing planform area achieves a low wing loading while the dihedral wingtips preserve desirable lateral dynamic response. The stable dynamics configuration is simply the nominal wing shape with all joint angles zero. Maximum wing area is achieved without morphing, producing the largest lift magnitude. Minimum turn radii are assessed at the simulated airspeed and thus the configurations are considered based on the simplified drag estimates and the available wing area.

7.1.5 Steep Descent

Flight maneuvers performed in the vicinity of obstacles can require aerodynamic characteristics very different from flight in open environments. Steep descent maneuvers favor relatively inefficient configurations to stabilize the aircraft in a steep descent angle or high rate of descent. The lowest-lift-to-drag and the maximum-power-required configurations achieve the steepest descent and fastest rate of descent maneuvers, respectively.

The steepest angle of descent flight mode is required when large changes in elevation are commanded in areas with limited horizontal space. A descent from building-top level to street level presents such a scenario, where the vehicle must lose considerable altitude within the hard limits of the horizontal distance between buildings. A steep spiraling flight path can be used to descend quickly without requiring a large flying area.

Figure 7-4(a) shows one possible configuration for a steep descent mode. The vehicle uses a gull-wing shape with large dihedral on the inboard and large anhedral on

the outboard. Wing sweep decreases outward, with the maximum aft sweep on the inboard section and moderate aft sweep on the outboard section. Such a configuration is similar to observed seagull wing shapes used to regulate glide ratio, where increasing dihedral/anhedral angles decreases glide ratio[68]. Handling qualities criteria is used in the selection of the wing shape.

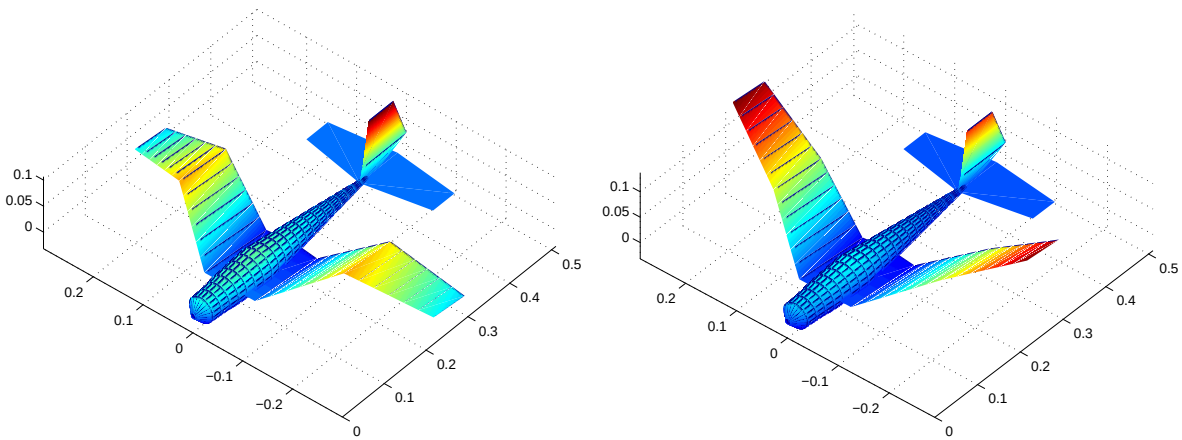

(a) HQC: $\mu_1 = 30^o$, $\mu_2 = -30^o$, $\mu_3 = -15^o$, $\mu_4 = -30^o$

(b) SDC: $\mu_1 = 30^o$, $\mu_2 = -30^o$, $\mu_3 = 30^o$, $\mu_4 = -20^o$

Figure 7-4. Steep descent angle configuration

The aerodynamically inefficient steep descent mode is favored over a simple dive due to airspeed considerations. A configuration optimized for cruise will significantly gain airspeed during a dive, as opposed to the slow descent of high-drag geometry. The slow descent of the current configuration also facilitates recovery to level flight at the termination of the dive.

An alternate form of diving is the maximum rate of descent mode, which achieves a change of elevation in minimum time. The maneuver is appropriate for time-critical descents where horizontal flight space is afforded. The best configuration for rate of descent occurs at the maximum power required condition, which is opposite to the requirement for soaring flight. The large power requirement for trimmed flight is provided by the loss of potential energy during the descent. When the potential energy loss is maximized for a fixed airspeed, the rate of descent is also maximized.

The minimum lift-to-drag wing shape is also the maximum power-required configuration. Figure 7-4(a) thus shows the geometry that is optimal for both descent angle and descent rate. This result is expected given the constraint on fixed airspeed.

The configuration that achieves the steepest descent angle and maximum rate of descent using the stable dynamics criteria is shown in Figure 7-4(b). The wing uses the maximum dihedral angle for both inboard and outboard wings along with maximum aft sweep for the inboard and moderate aft sweep for the outboard wing. The wing shape is similar to the form used by homing pigeons, as in Figure 3-9 during the steep descent phase preceding landing. The configuration generated using the unstable dynamics criteria is similar to the stable shape, except that the outboard wing uses the maximum aft sweep.

7.1.6 Sensor Pointing

A UAV engaged in reconnaissance of a moving object or general area may find difficulty in maintaining the target in the sensor field of view. Vision sensors are typically fixed to the aircraft body, which must fly through the air in a particular attitude to maintain appropriate angle of attack and sideslip. A surveillance mission targeting the face of a building would require that the aircraft fly parallel to the building side where only one part of the sensor field of view is providing useful information. Flying the aircraft toward the building can offer a better perspective, but only allows surveillance for brief periods between circling maneuvers to fly away from and re-acquire the target area in the image.

An alternative approach to the mission is to provide sensor pointing capability by partially decoupling between attitude and velocity. The vehicle would then operate at large sideslip angles in order to fly parallel to the building side while directing the sensor footprint towards the area of interest. The technique would also allow the aircraft to track a moving road vehicle while flying to the side of the roadway.

Trimmed flight at large sideslip requires relatively weak stability derivatives and strong control derivatives. Stiffness and coupled derivatives such as C_{n_β} and C_{l_β}, respectively, should be low such that the vehicle is not subject to large yawing and rolling

moments. Equation 7–6 shows a simple cost function to find the configuration which minimizes the combined, squared stiffness and coupled derivatives.

$$\min_{\mu_1,\mu_2,\mu_3,\mu_4} J = C_{n_\beta}^2 + C_{l_\beta}^2 \tag{7–6}$$

The minimization is also subject to additional constraints with respect to dynamic characteristics and handling qualities. For example, although the directional stiffness will be reduced, C_{n_r} can remain stable, preventing divergence from a stabilized sideslip condition.

Figure 7-5(a) shows the configuration which achieves the minimum cost, J, with good handling qualities. The shape is non-conventional by both biological and aviation standards in that the inboard wings are swept aft while the outboard wings are swept forward. The wing also uses a gull-wing configuration with large dihedral on the inboard and moderate anhedral on the outboard. The unusual orientation of the outboard wings are expected to contribute to the large sideslip constraint. Anhedral wing tips reduce the vehicle tendency to produce a roll moment in response to sideslip[64] while the forward sweep reduces the directional stiffness, C_{n_β}[80][9]. The opposite attitude of the inboard wings are used to maintain an appropriate position of the aerodynamic center relative to the vehicle body for the desired dynamic response.

Relaxing the stability criteria to allow unstable dynamics produces a qualitatively similar shape except that the wingtips are not angled downward and are swept forward. Figure 7-5(b) shows the resulting wing configuration. The cost for the unstable criteria is $J = 0.0005$ whereas for the handling qualities criteria $J = 0.0263$. In both cases, the desired sideslip characteristics are mostly achieved. The unstable configuration produces a moderately divergent spiral mode and a highly divergent short period mode with a time to double of $T_2 = 0.5$ *seconds*. The configuration determined by the stable dynamics criteria

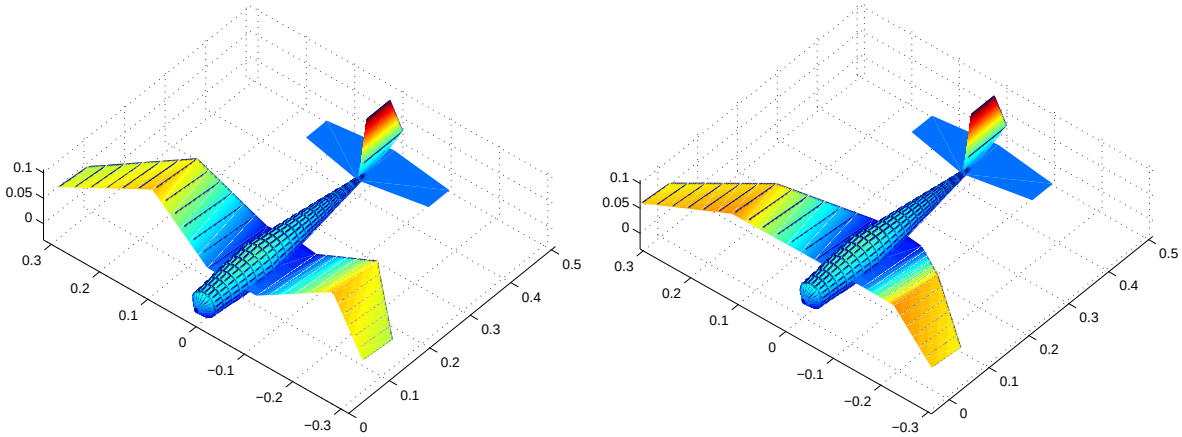

(a) HQC: $\mu_1 = 25^o$, $\mu_2 = -10^o$, $\mu_3 = -10^o$, $\mu_4 = 30^o$

(b) UDC: $\mu_1 = 30^o$, $\mu_2 = 25^o$, $\mu_3 = 0^o$, $\mu_4 = 30^o$

Figure 7-5. Maximum trimmable sideslip

is similar to the unstable shape with joint angles of $\mu_1 = 30^o$, $\mu_2 = 15^o$, $\mu_3 = -5^o$ and, $\mu_4 = 30^o$.

Interestingly, a very conventional wing configuration is found when the cost function in Equation 7–6 is maximized. Figure 7-6 shows the wing shape that achieves the highest value of $C_{l_\beta}^2 + C_{n_\beta}^2$ is similar to the swept-back design of airliners and other aircraft that seek to reduce sideslip divergence, among many other factors.

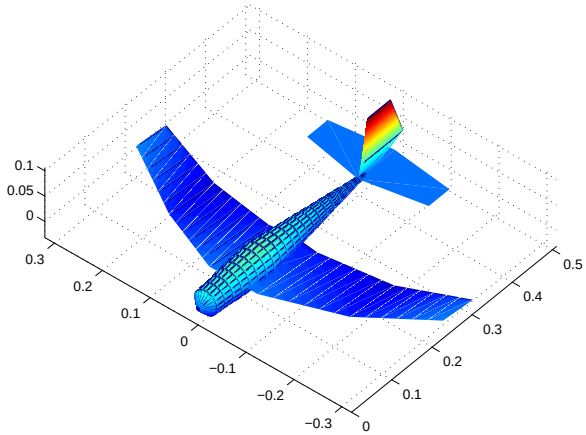

HQC: $\mu_1 = -5^o$, $\mu_2 = -25^o$, $\mu_3 = 5^o$, $\mu_4 = -30^o$

Figure 7-6. Maximized sideslip cost function configuration

Maximum trimmed sideslip angle simulations are performed for the identified aircraft by constraining the control surfaces to each move a maximum of $\pm 15^o$. Table 7-1 compares the maximum sideslip achieved by four aircraft. The movement of the aileron, elevator, and rudder control surfaces are constrained to trim to zero the rolling, pitching, and yawing moments, respectively. The sideslip is increased until the limit deflection is achieved in one of the surfaces.

Parameter	A	B	C	D
Sideslip (β_{max})	22.6^o	36.1^o	45.0^o	11.5^o
Aileron (δ_a)	15.0^o	15.0^o	5.05^o	15.0^o
Elevator (δ_e)	6.30^o	7.8^o	-7.98^o	18.4^o
Rudder (δ_r)	-11.1^o	-8.36^o	-7.57^o	-3.50^o

Table 7-1. Maximum sideslip and control deflections for several aircraft configurations. A) HQC Aircraft - Fig.7-1 B) HQC $\min_{\vec{\mu}} J$ - Fig.7-5(a) C) SDC $\min_{\vec{\mu}} J$ - Fig.7-5(b) D)HQC $\max_{\vec{\mu}} J$ - Fig.7-6

The nominal configuration used for takeoff is listed in the first aircraft column. The outboard wings have shallow dihedral and the aircraft achieves a moderate value for the cost function, J. A maximum sideslip angle of 22.6^o is achieved with maximum right aileron and 74% left rudder deflection. Similar aileron and rudder deflections stabilize the HQC-sideslip airplane in a 36.1^o sideslip. Both aircraft exhibit desirable dynamic characteristics, yet the optimized aircraft achieves significantly larger sideslip angles, affording a wider range of sensor pointing. The SDC-sideslip aircraft achieves the sideslip angle limit of 45° with conservative control surface deflections. The aircraft is able to trim at yet larger angles, although sustained flight in such attitudes may be unrealistic without unconventional propulsion or descending flight to counteract the large sideforce drag.

The jet-like wing planform in contrast achieves a maximum sideslip of 11.5^o with the aileron saturated to the right and the rudder deflected left mildly. The elevator exceeds allowable deflection for all sideslip ranges in order to stabilize the wing in pitch due to the aft neutral point position. The large elevator deflection underscores an important aspect

of morphing aircraft requiring large wing and tail control effectors in order to stabilize and control the large forces and moments generated by the wing.

7.2 Mission Profile

A simulated mission is presented to illustrate the function of a morphing vehicle in a multi-role scenario. The mission consists of each maneuvering task performed for an equal length of time. The success of each task is determined by the aerodynamic or dynamic metric governing the maneuver. Long range cruise flight performance, for instance, is gauged by the lift to drag ratio of the chosen morphing configuration. The performance of each maneuver is normalized by that of the launch configuration, which is taken as the nominal or baseline aircraft. Overall mission performance is determined by averaging the improvement percentage from each task, where the mission segment durations are assumed equal.

7.2.1 Performance Improvement

Table 7-2 shows two example missions for aircraft flown with with different stability criteria regulating the morphing configurations. Each aircraft is optimized within the configuration space to achieve best value for the each maneuver metric. The handling-qualities criteria restricts the solutions to those that achieve good handling qualities, while the stable dynamics criteria is less restrictive and allows any open-loop stable configuration.

Mission Task	Metric	Nominal Value	HQC (% Change)	SDC (% Change)
Launch	$\left(\frac{L}{D}\right)_{max}$	14.6	14.6 (0%)	14.6 (0%)
Cruise	$\left(\frac{L}{D}\right)_{max}$	14.6	14.6 (0%)	15.1 (3.21%)
Loiter	$P_{req,min}$	2.52W	2.50W (0.8%)	2.50W (1.0%)
Turn	R_{min}	17.8m	17.1m (4.0%)	16.9m (5.2%)
Descent	$\left(\frac{L}{D}\right)_{min}$	14.6	11.7 (19.6%)	11.3 (22.8%)
Sideslip	$\beta_{max,trim}$	22.6^o	36.1^o (59.7%)	45° (99.1%)
Recovery	$\left(\frac{L}{D}\right)_{max}$	14.6	14.6 (0%)	14.6 (0%)
Improvement	—	—	12.0%	18.8%

Table 7-2. Mission tasks and associated performance metrics relative to launch configuration

Most of the performance improvement for both stability criteria comes in the later mission tasks where the aircraft must achieve unconventional aerodynamic and dynamic properties. The baseline aircraft is optimized to achieve a high lift-to-drag ratio with good handling qualities, so it is expected to perform well in cruise and maneuvering tasks. The performance improvement achieved through morphing is thus relatively small for such tasks. Reconfiguration for the descent maneuver achieves large gains for both HQC and SDC missions. The lower lift to drag ratio of both biologically inspired configurations allows steeper and faster dives. Actual gains may be larger if angle of attack is allowed to vary, although the current results are presented at a constant angle. Maximum trimmable sideslip angle improves with morphing due to the unconventional wing configuration with low sideslip coupling to roll and yaw moments. The HQC sideslip vehicle achieves a 59.7% improvement in the maximum sideslip with the same control deflection limits as the nominal aircraft. The SDC vehicle achieves a greater improvement and reaches the $\beta = 45^o$ simulation limit without saturating control surface deflection.

7.2.2 Morphing Joint Trajectories

A morphing aircraft must obviously change shape in order to be useful in flight. The previous discussion considers only the optimal morphed configurations, whereas a realistic mission would require intermediate wing shapes as the vehicle morphs from one mission task to another. The transient morphing shapes are subject to the same constraints as the initial and final configurations. Namely, the dynamic characteristics must satisfy the stability criteria by which one or both of the shapes are limited. For instance, an aircraft morphing from a launch configuration to a manually piloted steep-descent mode must preserve good handling qualities at each intermediate shape. Thus, the joint trajectory through the configuration space is limited to those paths which achieve specified damping ratios, natural frequencies, and time constants.

Equation 7–7 shows the desired morphing direction in configuration space is simply a direct line from the current joint angles to the desired joint angles. The desired direction is normalized by the distance between the initial and final shapes.

$$\vec{\mu}_{desired} = \frac{\vec{\mu}_{end} - \vec{\mu}_{current}}{||\vec{\mu}_{end} - \vec{\mu}_{current}||} \tag{7–7}$$

Where $\vec{\mu}_{current} =< \mu_{1,current}, \mu_{2,current}, \mu_{3,current}, \mu_{4,current} >$ is the current joint configuration of the wing and $\vec{\mu}_{end} =< \mu_{1,end}, \mu_{2,end}, \mu_{3,end}, \mu_{4,end} >$ is the final or desired joint vector.

Each morphing joint is allowed to move by one increment at each time step independently of the remaining three joints. The angle increment is taken as the 5° minimum joint resolution used in the simulation and the resulting 4-dimensional data matrix. Increment vectors i, j, k, and l represent incremental changes to the joint angles μ_1, μ_2, μ_3, and μ_4, respectively. Each vector may take the value of $+5^o$ for increasing the joint angle, -5° for decreasing the joint angle, or 0° for no change. Thus, $3^4 = 81$ possible morphing operations exist at each time step. The number of possible morphing shapes is decreased when the aircraft is at the boundary of the configuration space where one or more joint angles is saturated at the extreme position.

The reconfiguration options are sorted according to Equation 7–8, which determines the desirability of the reconfiguration command, $< i, j, k, l >$, based on the similarity to the desired morphing direction, $\vec{\mu}_{desired}$.

$$\mu_{error} = \left|\left|\mu_{desired} - \frac{< i, j, k, l >}{||< i, j, k, l >||}\right|\right| \tag{7–8}$$

The reconfiguration command which achieves the lowest magnitude of direction error, μ_{error}, is checked against the applicable stability criteria to determine the suitability of the dynamics. If the configuration meets the criteria, the joint angles are morphed and $\vec{\mu}_{current}$ is updated until $\vec{\mu}_{end}$ is reached. Should the configuration violate the dynamic

requirements, less direct $< i, j, k, l >$ are tested until an alternate joint angle path is found. The aircraft is thus able to morph around unstable or undesirable configurations.

Figure 7-7 shows the four joint angle trajectories as the aircraft morphs between mission task shapes. Each mission task shape is identified by a vertical dashed line and a text annotation. The duration of the mission task is not represented in the plot. Instead, closed circles show the optimized morphing shapes which are constant for each maneuver. The initial configuration shown at time increment 1 corresponds to the manually piloted launch shape from Figure 7-1. The aircraft is then morphed to the anhedral cruise configuration from Figure 7-2(b) by changing all joint angles apart from μ_2, which remains constant at -5°.

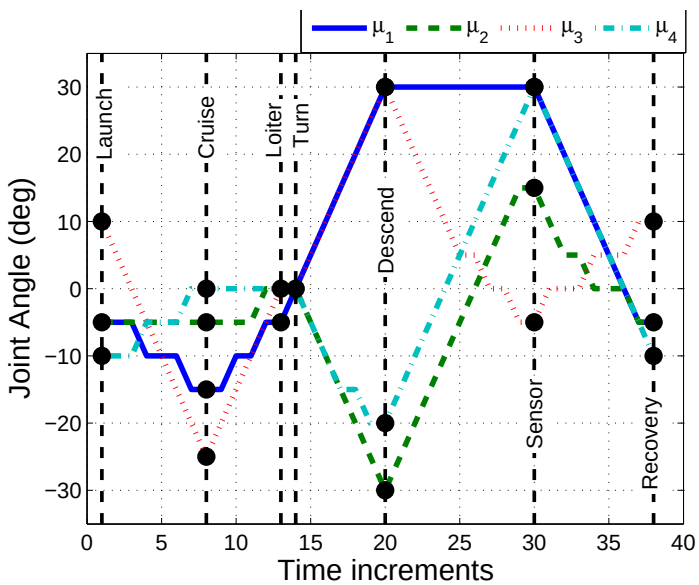

Figure 7-7. Morphing joint angle trajectories for mission tasks subject to SDC

The following two missions, endurance loiter and minimum radius turn, use joint configurations close or equal to the unmorphed shape from Figure 7-3. The next mission uses the large dihedral, aft swept wing shape (Figure 7-4(b)) to perform steep descents and scatters the joint angles to the extremities of the plot. The vehicle then transforms to the sensor-pointing configuration from Figure 7-5 by increasing μ_2 and μ_4 while reducing μ_3.

Figure 7-8 shows a similar profile for a mission using HQC to limit both mission task and intermediate configurations. The restricted configuration set causes several maneuvers to use identical wing shapes. Launch and cruise are both optimized for lift-to-drag ratio so both use the configuration from Figure 7-1. The aircraft then morphs into the shape used for both endurance loitering and minimum radius turn. Slight dihedral is used on the outboard section while the remaining angles are zero, as in Figure 7-3(a).

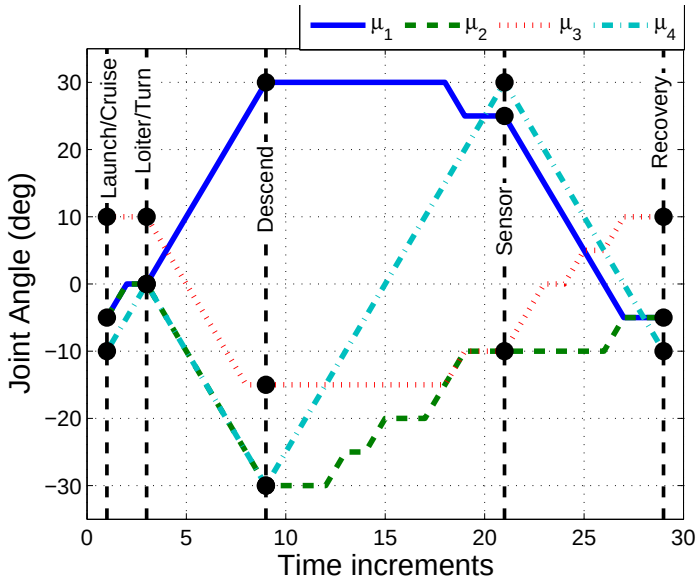

Figure 7-8. Morphing joint angle trajectories for mission tasks subject to HQC

Steep descent is performed by morphing into the seagull-inspired gull-wing shape of 7-4(a). The joint trajectories follow nearly direct paths for all four angles. Morphing into the sensor-pointing shape of Figure 7-5(a) uses a direct path for μ_4 and staggered paths for the remaining joints. The final shape change transforms the vehicle back into the launch configuration for a manually piloted recovery.

7.3 Summary

Morphing continues to be an attractive option for small aircraft designed to operate in urban environments. Shape change allows the vehicles to reconfigure for missions with disparate aerodynamic requirements, such as cruise, maneuvering, steep descent, and sensor-pointing. Biological design elements such as a shoulder and elbow joint are used

to vary the wing geometry in sweep and dihedral. Birds using such morphing are able to rapidly change direction, achieve high lift-to-drag ratios, descend at steep angles, and soar in updrafts during different phases of flight.

Simulations of a small UAV with avian-inspired morphology show that performance improvements are achieved for each task of an urban mission scenario. Optimizing the vehicle shape for each of these tasks often converges to the biological solution, matching observations made of gliding birds. The identified vehicle configurations also closely relate to findings in the literature regarding useful shapes for different flight tasks.

The shapes into which a vehicle may morph can be regulated by use of a stability criteria which sets an allowable range for the dynamic characteristics. Pilotability can be guaranteed for any configuration by requiring the morphed shapes to meet classical handling qualities. The vehicle then achieves versatile performance while allowing a human operator to manually control the flight path. Further improvements in performance are achieved by permitting any stable or even unstable configurations. The use of a controller is then required, but the vehicles may achieve task performance significantly higher than a fixed-geometry vehicle expected to perform all missions.

CHAPTER 8
CONCLUSIONS

Natural inspiration may transform aircraft design from fixed configurations to amorphous shapes that can reconfigure optimally for many disparate flight conditions. In-flight shape-change extends the design process to real-time, where a vehicle can undergo substantial variations in shape and change roles. Evidence from the gliding flight of seagulls, falcons, albatrosses, and other bird species suggests that such wing shape change can be used to control flight modes and maneuverability with improved performance over fixed aircraft. The potential areas for improvement in energy conservation, maneuverability, and versatility are significant and have justifiably received substantial research attention.

Avian skeletal structures are similar to those of humans in the joint and bone configuration. The shoulder, elbow, wrist, and digit joints of both allow a wide range of motions. Unlike a human arm, however, the avian wing is used as an aerodynamic surface rather than a serial manipulator. As such, the versatility of the skeleton and accompanying skin and feathers affords a variety of wing shapes for various flight tasks. Articulation of specific joints, such as sweep in the wrist joint, provide beneficial aerodynamic effects that are reported in the literature. Combined, complex articulation of the wing joints permit birds to achieve configurations that have favorable performance and dynamics. Quasi-static configurations are easily observed in species which spend large duration gliding in atmospheric currents.

The application of biological inspiration to aircraft design is arguably most relevant to vehicles that are dimensionally similar to the birds on which they are based. Micro air vehicles designed to reconnoiter in urban environments are ideal candidates for such design inspiration. Complicated maneuvers and varied missions envisioned for such aircraft will require a combination of performance and versatility not available with conventional, fixed-configuration designs. Morphing the shape of MAV wings will enable the same type of in-flight redesign versatility that are observed in birds. Multiple mission objectives,

such as endurance, pursuit, tracking, and maneuvering, can be achieved by morphing the aircraft into a shape appropriate for each task.

Quasi-static articulations of wing joints at the root and midboard positions of the wing permit a wide range of aerodynamic shapes. Aerodynamic modeling using vortex-lattice method predicts performance and dynamic characteristics for the morphed wings. Cost functions associated with each mission task are used to find optimal wing shapes in the configuration space. For several tasks, the optimal wing shape is similar to the natural solution. The performance of the adapted aircraft exceeds that of an aircraft with fixed configuration.

Morphing wing joints allows significant changes to the wing shape which subsequently cause large variations in the dynamic characteristics. Modeling these changes for any permissible wing configuration may be computationally prohibit. Reducing the allowable wing shapes to a subset of the configuration space retains the beneficial effects of the morphing while reducing the modeling burden.

Controlling the morphing aircraft requires some knowledge of the dynamic variation that occurs with shape change. With full knowledge of the dynamics, optimal LQR or robust H_∞ controllers can be designed for each configuration and switched or scheduled. Alternatively, the dynamics may be approximately modeled using linear interpolation between a set of design points. The linear interpolation reduces computational and storage burden considerably, although introduces modeling errors for nonlinear variation in the dynamic parameters. Adaptive control is used to allow the control to compensate for the modeling error. A reference model associated with each mission defines the expected response for the model and drives the controller adaptation.

REFERENCES

[1] M. Abdulrahim and R. Lind. Control and Simulation of a Multi-Role Morphing Micro Air Vehicle. AIAA-2005-6481, *AIAA Guidance, Navigation and Control Conference and Exhibit*, San Francisco, CA, 15-18 August, 2005.

[2] M. Abdulrahim, H. Garcia, and R. Lind. Flight Characteristics of Shaping the Membrane Wing of a Micro Air Vehicle. *Journal of Aircraft* 2005, 0021-8669, vol.42 no.1 pp 131-137.

[3] M. Abdulrahim. Flight Performance Characteristics of a Biologically-Inspired Morphing Aircraft. AIAA-2005-345, *43rd AIAA Aerospace Sciences Meeting and Exhibit*, Reno, NV, January 2005.

[4] M. Abdulrahim and R. Lind. Flight Testing and Response Characteristics of a Variable Gull-Wing Morphing Aircraft. AIAA-2004-5113, *AIAA Guidance, Navigation, and Control Conference and Exhibit*, Providence, RI, August 2004.

[5] AeroVironment, Inc. Special Ops Using 'Pointer' UAV for Vital Recon, Force Protection. July 2003, http://www.aerovironment.com/news /news-archive/pointsocom.html

[6] M. Allen. Autonomous Soaring for Improved Endurance of a Small Uninhabitated Air Vehicle. AIAA-2005-1025, *43rd AIAA Aerospace Sciences Meeting and Exhibit*, Reno, NV, Jan. 10-13, 2005.

[7] J.D. Anderson, Jr. *Aircraft Performance and Design*, WCB McGraw-Hill, Boston, MA. 1999.

[8] J.S. Bae, T.M. Seigler, D.J. Inman. Aerodynamic and Static Aeroelastic Characteristics of a Variable-Span Morphing Wing. *Journal of Aircraft*, Vol. 42, No.2, March-April 2005.

[9] R.H. Barnard and D.R. Philpott. *Aircraft Flight, Third Edition*. ISBN 81-297-0783-7, Pearson Education, Singapore, 2005.

[10] R. Bitten. Qualitative and Quantitative Comparison of Government and Industry Agility Metrics. *AIAA Journal of Aircraft*, Vol. 27, No.3, 1989.

[11] K. Boothe, K. Fitzpatrick, and R. Lind. Controls for Disturbance Rejcetion for a Linear Input-Varying Class of Morphing Aircraft. *46th AIAA Structures, Structural Dynamics and Materials Conference*, Austin, TX, 18-21 April 2005.

[12] K. Boothe. Dynamic Modeling and Flight Control of Morphing Air Vehicles. Masters thesis, University of Florida, December 2004.

[13] J. Bowman. Affordability Comparison of Current and Adaptive and Multifunctional Air Vehicle Systems. AIAA-2003-1713, *44th AIAA Structures, Structural Dynamics, and Materials Conference*, 7-10 April, 2003.

[14] J. Bowman, B. Sanders, and T. Weisshaar. Evaluating the Impact of Morphing Technologies on Aircraft Performance. AIAA-2002-1631, *43rd AIAA Structures, Structural Dynamics, and Materials Conference*, 22-25 April 2002.

[15] R.H. Cabell, N. Schiller, J.H. Mabe, R.T. Ruggeri, and G.W. Butler. Feedback Control of a Morphing Chevron for Takeoff and Cruise Noise Reduction. *ACTIVE 04*, Williamsburg, VA, 20-22 September 2004.

[16] D. Cadogan, T. Smith, F. Uhelsky, and M. MacKusick. Morphing Inflatable Wing Development for Compact Package Unmanned Aerial Vehicles. AIAA-2004-1807, *45th AIAA Structures, Structural Dynamics, and Materials Conference*, April 2004.

[17] D. Cadogan, W. Graham, and T. Smith. Inflatable and Rigidizable Wings for Unmanned Aerial Vehicles. AIAA-2003-6630, *AIAA Unmanned Unlimited Systesm*, San Diego, CA, September 2003.

[18] S.A. Cambone, K.J. Krieg, P. Pace and L. Well II. Unmanned Aircraft Systems Roadmap 2005-2030. *Office of the Secretary of Defense, United States of America Department of Defense*, August, 2005.

[19] C.E.S. Cesnik, H.R. Last, and C.A. Martin. A Framework for Morphing Capability Assessment. AIAA-2004-1654, *45th AIAA Structures, Structural Dynamics, and Materials Conference*, Palm Springs,CA, 19-22 April 2004.

[20] G.E. Cooper and R.P. Harper, Jr. The Use of Pilot Rating In the Evaluation of Aircraft Handling Qualities. NASA TN D-5133, *NASA Technical Note*, April 1969.

[21] C.D. Crane III and J. Duffy. Kinematic Analysis of Robot Manipulators, *Cambridge University Press*, 1998.

[22] J.B. Davidson, P. Chwalowski, B.S. Lazos. Flight Dynamic Simulation Assessment of a Morphable Hyper-Elliptic Cambered Span Winged Configuration. AIAA-2003-5301, *AIAA Atmospheric Flight Mechanics Conference and Exhibit*, 11-14 August 2003, Austin, TX.

[23] C. Dever, B. Mettler, E. Feron, J. Popovic, M. McConley. Trajectory Interpolation for Parameterized Maneuvering and Flexible Motion Planning of Autonomous Vehicles. AIAA-2004-5143, *AIAA Guidance, Navigation, and Control Conference and Exhibit*, August 16-19, 2004, Providence, RI.

[24] J. Doebbler, M.D. Tandale, J. Valasek, and A.J. Meade, Jr. Improved Adaptive-Reinforcement Learning Control for Morphing Unmanned Air Vehicles. AIAA-2005-7159, *AIAA Infotech@Aerospace* Arlington, VA, 26-29 September, 2005.

[25] M. Drela and H. Youngren AVL - Aerodynamic Analysis, Trim Calculation, Dynamic Stability Analysis, Aircraft Configuration Development. *Athena Vortex Lattice, v. 3.15* http://raphael.mit.edu/avl/

[26] C. Farivar. WHAT'S NEXT; A Flying Crime Fighter (Some Assembly Required). The New York Times - Technology, January 2005. http://tech2.nytimes.com/mem/technology /techreview.html ?res=9405E0DE1738F930A25752C0A9639C8B63

[27] J.B. Frommer and W.A. Crossley. Evaluating Morphing Aircraft in a Fleet Context Using Non-Deterministic Metrics. AIAA-2005-7460, *AIAA 5th Aviation, Technology, Integration, and Operations*, Arlington, VA, 26-28 September 2005.

[28] J.B. Frommer and W.A. Crossley. Enabling Continuous Optimization for Sizing Morphing Aircraft Concepts. AIAA-2005-816, *43rd AIAA Aerospace Sciences Meeting and Exhibit*, Reno, NV, 10-13 Janaury, 2005.

[29] S. Ganguli, A. Marcos, and G. Balas. Reconfigurable LPV Control Design for Boeing 747-100/200 Longitudinal Axis. *American Control Conference*, Anchorage, AK, May 8-10, 2002.

[30] S.E. Gano and J.E. Renaud. Optimized Unmanned Aerial Vehicle with Wing Morphing for Extended Range and Endurance. AIAA-2002-5668, *9th AIAA/ISSMO Symposium and Exhibit on Multidisciplinary Analysis and Optimization*, September 406, 2002, Atlanta, GA.

[31] V. Gavrilets, E. Frazzoli, B. Mettler, M. Piedmonte and E. Feron. Aggressive Maneuvering of Small Autonomous Helicopters: A Human-Centered Approach. *The International Journal of Robotics Research*, Sage Publications, Vol. 20, No.10, October 2001, pp. 795-807.

[32] V. Gavrilets, B. Mettler and E. Feron. Human-Inspired Control Logic for Automated Maneuvering of Miniature Helicopter. *AIAA Journal of Guidance, Control, and Dynamics*, Vol. 27, No.5 September-October 2004.

[33] J.H. Ginsberg. *Advanced Engineering Dynamics, Second Edition. Cambridge University Press*, 1995.

[34] G.C. Goodwin, S.F. Graebe, and M.E. Salgado, *Control System Design*, ISBN 81-203-2119-7, Prentice-Hall, New Jersey, 2001.

[35] D.T. Grant, M. Abdulrahim and R. Lind. Sensor Pointing using Biomimetic Joints and Structures on Morphing Micro Air Vehicles. *International Forum on Aeroelasticity and Structural Dynamics*, Stockholm, Sweden, June 2007.

[36] D.T. Grant, M. Abdulrahim and R. Lind. Flight Dynamics of a Morphing Aircraft Utilizing Independent Multiple-Joint Wing Sweep. AIAA-2006-6505, *AIAA Atmospheric Flight Mechanics Conference*, Keystone, CO, 21-24 August 2006.

[37] T.E. Goldbach. AVLab - Extended AVL Functionality in MATLAB. *University of Florida*, July 2005.

[38] M. Grady. UAVs Tested As Fire Spotters. *AVweb*, January 2005, http://www.avweb.com/ newswire/ 11_01a/ briefs/ 188894-1.html

[39] R. Guiler and W. Huebsch. Wind Tunnel Analysis of a Morphing Swept Wing Tailless Aircraft. AIAA-2005-4981, *23rd AIAA Applied Aerodynamics Conference*, Toronto, Ontario, Canada, 6-9 June 2005.

[40] S. Hall, C. Coleman, M. Drela, K. Lundqvist, M. Spearing, I. Waitz, and P. Young Unified Engineering: Unified Propulsion, Course 16.04. *MIT Open Coursewares*, http://ocw.mit.edu.

[41] C.R. Hargraves and S.W. Paris. Direct Trajectory Optimization Using Nonlinear Programming and Collocation. *Journal of Guidance, Dynamics, and Control*, Vol. 10, No.4, 1987.

[42] J.J. Henry, J.E. Blondeau, and D.J. Pines. Stability Analysis for UAVs with a Variable Aspect Ratio Wing. AIAA-2005-2044, *46th AIAA Structures, Structural Dynamics, and Materials Conference*, Austin, TX, 18-21 April 2005.

[43] J.J. Henry and D.J. Pines. A Mathematical Model for Roll Dynamics by Use of a Morphing-Span Wing. AIAA-2007-1708, *48th AIAA Structures, Structural Dynamics, and Materials Conference*, Honolulu, HI, 23-26 April 2007.

[44] R.A. Hyde, *H_∞ Aerospace Control Design: A VSTOL Flight Application*. Springer, New York, 1995.

[45] C.O. Johnston, D.A. Neal, L.D. Wiggins, H.H. Robertshaw, W.H. Mason, and D.J. Inman. A Model to Compare the Flight Control Energy Requirements of Morphing and Conventionally Actuated Wings. AIAA-2003-1716, *44th AIAA Structures, Structural Dynamics, and Materials Conference*, Norfolk, VA, 7-10 April 2003.

[46] S.P. Joshi, Z. Tidwell, W.A. Crossley and S. Ramikrashnan. Comparison of Morphing Wing Strategies Based Upon Aircraft Performance Impacts *AIAA/ASME/ASCE/AHS/ASC Structures, Structural Dynamics, and Materials Conference*, AIAA-2004-1722, April 2004, Palm Springs, CA

[47] T. Kailath. *Linear Systems*. Prentice Hall, Inc., New Jersey, 1980.

[48] H.K. Khalil. *Nonlinear Systems, Third Edition*. Prentice Hall, Inc., New Jersey, 2002.

[49] D.E. Kirk. *Optimal Control Theory - An Introduction*. Dover Publication, Inc, New York.

[50] M. Krstic, I. Kanellakopoulos, and P. Kokotovic. *Nonlinear and Adaptive Control Design*. John Wiley and Sons, Inc., New York, 1995.

[51] H-J. Lee and G. Song. Experimental and Analytical Studies of Smart Morphing Structures. *NASA Glenn Resarch Center*, June 2003.

[52] A. Lennon, *Basics of R/C Model Aircraft Design: Practical Techniques for Building Better Models*, ISBN 0911295402, Air Age Publishing, September 1996.

[53] R. Lind, M. Abdulrahim, K. Boothe and P. Ifju. Flight Characterization of Micro Air Vehicles Using Morphing for Agility and Maneuvering. SAE-2004-01-3138, *SAE World Aviation Congress and Exposition*, November 2004, Reno,NV

[54] T. Liu, K. Kuykendoll, R. Rhew, and S. Jones. Avian Wing Geometry and Kinematics. *AIAA Journal*, Vol. 44, No.5, May 2006.

[55] E. Livne and T.A. Weisshaar. Aeroelasticity of Nonconventional Airplane Configurations - Past and Future. *Journal of Aircraft*, Vol. 40, No. 6, November-December 2003.

[56] E. Livne. Future of Airplane Aeroelasticity. *Journal of Aircraft*, Vol. 40, No. 6, November-December 2003.

[57] M.H. Love, P.S. Zink, R.L. Stroud, D.R. Bye and C. Chase. Impact of Actuation Concepts on Morphing Aircraft Structures. AIAA-2004-1724, *45th AIAA/ASME/ASCE/AHS/ASC Structures, Structural Dynamics & Materials Conference*, April 19-22, 2004, Palm Springs, CA.

[58] P. Marks. Aviation - The Shape of Wings to Come. *New Scientist*, June 29, 2005.

[59] P. Marks. The next 100 years of flight - part two. *New Scientist*, December 2003, http://www.newscientist.com/article.ns?id=dn4484

[60] Unknown author. MATLAB Function Reference: Delaunay Triangulation. *The Mathworks* MATLAB 7.0.4, 2005.

[61] P.D. Mckeehen and T.J. Cord. Beck Maneuver Performance and Agility Metric Application to Simulation or Flight Data. AIAA-98-4144, *AIAA Atmospheric Flight Mechanics Conference and Exhibit*, Boston, MA, August 10-12, 1998.

[62] J.M. McMichael and Col. M.S. Francis. Micro Air Vehicles - Toward a New Dimension in Flight. August 1997. http://www.darpa.mil/tto /mav/mav_auvsi.html

[63] D.A. Neal, M.G. Good, C.O. Johnston, H.H. Robertshaw, W.H. Mason, and D.J. Inman. Design and Wind-Tunnel Analysis of a Fully Adaptive Aircraft Configuration. AIAA-2004-1727, *45th AIAA/ASME/ASCE/AHS/ASC Structures, Structural Dynamics & Materials Conference*, 19-22 April 2004, Palm Springs, CA.

[64] R.C. Nelson, *Flight Stability and Automatic Control*, McGraw Hill, Boston, MA, 1998.

[65] K. Ogata, *Modern Control Engineering*, Fourth Edition, ISBN 81-7808-579-8, Pearson Education, Singapore, 2005.

[66] I. Ordaz, K.H. Lee, D.M. Clark, and D.N. Mavris. Aerodynamic Optimization Using Physics-Based Response Surface Methodology for a Multi-Mission Morphing

Unmanned Combat Air Vehicle. AIAA-2004-6336, *AIAA 3rd Unmanned Unlimited Conference*, Chicago, IL, 20-23 September 2004.

[67] S.L. Padula, J.L. Rogers, and D.L. Raney. Multidisciplinary Techniques and Novel Aircraft Control Systems. AIAA-2000-4848.

[68] J. Perrin and J. Cluzaud. Winged Migration. DVD - ASIN B00000CGNEH, *Sony Pictures*, 2001.

[69] C. Peters, B. Roth, W.A. Crossley, and T.A. Weisshaar. Use of Design Methods to Generate and Develop Missions for Morphing Aircraft. AIAA-2002-5468, *9th AIAA Symposium on Multidisciplinary Analysis and Optimization*, Atlanta, GA, 4-6 September 2002.

[70] M. Piedmonte and E. Feron. Aggressive Maneuvering of Autonomous Aerial Vehicles: A Human-Centered Approach. *Robotics Research International Symposium*, 2000.

[71] J. Principe, N. Euliano and C. Lefebvre *Neural Systems: Fundamentals through Simulations*, John Wiley, 2000.

[72] D.S. Ramrakhyani, G.A. Lesieutre, M. Frecker, and Smita Bharti. Aircraft Structural Morphing Using Tendon-Actuated Compliant Cellular Trusses. *Journal of Aircraft*, Vol. 42, No. 6, November-December 2005.

[73] A. Rao. Optimal Control - Class Notes. April 2007.

[74] B. Roth, C. Peters, and W.A. Crossley. Aircraft Sizing With Morphing as an Independent Variable: Motivation, Strategies, and Investigations. AIAA-2002-5840, *AIAA Aircraft Technology, Integration, and Operations*, Los Angeles, CA, 1-3 October 2002.

[75] B.D. Roth and W.A. Crossley. Application of Optimization Techniques in the Conceptual Design of Morphing Aircraft. AIAA-2003-6733, *AIAA 3rd Annual Aviation Technology, Integration, and Operations Conference*, Denver, CO, 17-19 November 2003.

[76] M.T. Rusnell, S.E. Gano, V.M. Perez, J.E. Renaud, and S.M. Batill. Morphing UAV Pareto Curve Shift for Enhanced Performance. AIAA-2004-1682, *46th AIAA Structures, Structural Dynamics, and Materials Conference*, Palm Springs, CA, 19-22 April 2004.

[77] M.T. Rusnell. Morphing UAV Pareto Curve Shift for Enhanced Performance. Masters Thesis, University of Notre Dame, April 2004.

[78] G.W. Ryan III and D.R. Downing. Evaluation of Several Agility Metrics for Fighter Aircraft Using Optimal Trajectory Analysis. *Journal of Aircraft*, Vol. 32, No. 4, July-August 1995.

[79] J.A. Samareh. Multidisciplinary Aerodynamic-Structural Shape Optimization Using Deformation (MASSOUD). AIAA-2000-4911, *8th AIAA/USAF/NASA/ISSMO Symposium on Multidisciplinary Analysis and Optimization*, September 6-8, 2000.

[80] G. Sachs. Why Birds and Mini-Aircraft Need No Vertical Tail. AIAA-2005-5807, *AIAA Atmospheric Flight Mechanics Conference and Exhibit*, August 15-18, 2005, San Francisco, CA.

[81] G. Sachs. Yaw Stability in Gliding Birds. *Journal of Ornithology*, Vol. 146, 191-199, June 2005.

[82] B. Sanders, F.E. Eastep, E. Forster. Aerodynamic and Aeroelastic Characteristics of Wings with Conformal Control Surfaces for Morphing Aircraft. *Journal of Aircraft*, Vol. 40, No. 1, January-February 2003.

[83] A.G. Sparks. Linear Parameter Varying Control for a Tailless Aircraft. AIAA-97-3636, 1997.

[84] B. Stanford, M. Abdulrahim, R. Lind, and P. Ifju. Investigation of Membrane Actuation for Roll Control of a Micro Air Vehicle. *Journal of Aircraft*, Vol. 44, No. 3, May-June 2007.

[85] M.D. Tandale, J. Rong and J. Valasek. Preliminary Results of Adaptive-Reinforcement Learning Control for Morphing Aircraft. AIAA-2004-5358, *AIAA Guidance, Navigation, and Control Conference and Exhibit*, 16-19 August, 2004, Providence, RI.

[86] H. Tennekes, *The Simple Science of Flight: From Insects to Jumbo Jets*, ISBN 0-262-20105-4, MIT Press, Cambridge, MA, 1997.

[87] A.L.R. Thomas and G.K. Taylor. Animal Flight Dynamics I. Stability in Gliding Flight. *Journal of Theoretical Biology*, Vol. 212, pp. 399-424, 2001.

[88] V.A. Tucker and G.C. Parrott. Aerodynamics of Gliding Flight in a Falcon and Other Birds. *Journal of Experimental Biology*, Vol. 52, pp. 345-367, 1970, Great Britain.

[89] V.A. Tucker. Gliding Birds: The Effect of Variable Wing Span. *Journal of Experimental Biology*, Vol. 133, pp. 33-58, 1987.

[90] J. Valasek, M.D. Tandale, and J. Rong. A Reinforcement Learning-Adaptive Control Architecture for Morphing. *Journal of Aerospace Computing, Information, and Communication*, Vol. 2, April 2005.

[91] J.J Videler, *Avian Flight*, ISBN 0198566034, Oxford University Press, USA, October 20, 2005.

[92] T.A. Weisshaar. DARPA Morphing Aircraft Structures (MAS). http://www.darpa.mil/dso/thrust/matdev/mas.htm

[93] D.J. Wilson, D.R. Riley, and K.D. Citurs. Aircraft Maneuvers for the Evaluation of Flying Qualities and Agility - Vol 1: Maneuver Development Process and Initial Maneuver Set. WL-TR-93-3081, *Flight Dynamics Directorate, Wright Laboratory*, 1993.

[94] K.A. Wise and E. Lavretsky. Robust and Adaptive Control Workshop. University of Florida, Research Engineering Education Facility.

[95] R.W. Wlezien, G.C. Horner, A.R. McGowan, S.L. Padula, M.A. Scott, R.J. Silcox, and J.O. Simpson. The Aircraft Morphing Program. AIAA-1998-1927, *AIAA/ASME/ASCE/AHS/ASC Structures, Structural Dynamics, and Materials Conference and Exhibit, 39th, and AIAA/ASME/AHS Adaptive Structures Forum*, Long Beach, CA, Apr. 20-23, 1998

[96] T.R. Yechout with S.L. Morris, D.E. Bossert, and W.F. Hallgren *Introduction to Aircraft Flight Mechanics: Performance, Static Stability, Dynamic Stability, and Classical Feedback Control*, American Institute of Aeronautics and Astronautics, Reston, VA, 2003.

[97] K. Zhou and J.C. Doyle. *Essentials of Robust Control*. ISBN 0-13-525833-2, Prentice Hall, New Jersey, 1998.

BIOGRAPHICAL SKETCH

Mujahid Abdulrahim was born and raised among the rocky mountains of Calgary, Alberta, Canada. He proudly descends from a line of educators, nobles, and small-time inventors in his ethnic Syria, from the cities of Aleppo (Halab) and Al-Rahaab. His professional maturation began in the 2nd grade with his notable development of a Micro Machines stunt track from construction paper. He continued his interest in all things mechanical during his cross-continent move to Panama City, FL, where he firmly decided his career path as an aeronautical engineer by referencing an 8th-grade math-class poster. The poster listed various professions on the vertical axis with the corresponding math course requirement on the horizontal axis. Aeronautical engineering was one of the few careers that required virtually all the listed mathematics.

Since joining the University of Florida in 1999, Mujahid has been active in micro air vehicle, dynamics and control, and morphing research. He has also participated in numerous academic and sporting competitions including regional and national paper competitions, MAVs, cross-country bicycling, photography, autocross, drifting, and aerobatics. His success varied. Mujahid earned his aerospace engineering B.S. in 2003, his M.S. in 2004, and his Ph.D. in 2007. Noting, with some sadness, that the University of Florida offered no further relevant degrees, Mujahid promptly packed his belongings and headed west. At the time of this writing, he is driving in an RV, lost on a winding mountain road somewhere in Arizona. Someday, he hopes to get new batteries for his GPS and continue his trip to California, where he will start R&D work in UAV controls.